Monitoring ice-volcano interactions in Iceland using SAR and other remote sensing techniques

Dissertation
der Fakultät für Geowissenschaften
der Ludwig-Maximilians-Universität München

Kilian Scharrer
04. September 2007

Contents

Abstract

This thesis is an outcome of the European Space Agency (ESA) project on "Hazard Assessment and Prediction – Long-term Observation of Icelandic Volcanoes and Glaciers Using ENVISAT-ASAR and Other Radar Data" (ID 142, Principal Investigator U. Münzer). It comprises the results of five scientific papers (four published, one submitted) on several aspects of ice-volcano interactions in Iceland from an observational point of view.

This study was motivated by the lack of information on how remote sensing can actually contribute to monitoring and understanding subglacial volcanoes and their interaction with the overlying ice cover. For example, no continuous monitoring of the Icelandic subglacial volcanoes utilizing any kind of satellite images has been conducted so far. The ice cover across subglacial volcanoes is influenced by several processes of the underlying volcano. The increased geothermal heat flux leads to temperate conditions everywhere at the glacier bed. Therefore, sliding is an important mechanism in the glacier dynamics of these glaciers. Also, the generation of large amounts of subglacial melt water during volcanic activity is the reason for jökulhaups (glacial torrent) and evolution of extensive subglacial tunnel systems (melt water drainage). In case of subaerial eruptions, glaciers are influenced by ash fall, which reduces the albedo at their surface and thus control the mass balance of the ice cover. In addition, the variable loading controlled by glacier mass balance has an effect on the volcanic activity itself. In this thesis, several approaches are documented which analyse some of the important interactions between subglacial volcanoes and their ice cover by remote sensing techniques. It was found that glacier mass-balance parameters, ice-dynamics, and subglacial volcanic processes can be detected by remote sensing analysis.

One of the major problems for the investigation of temporal glacier development is the dectection of changes in extent and mass distribution. In this context, a combined analysis of optical (ASTER) and SAR (ENVISAT, ERS-2) data at Mýrdalsjökull test site was carried out which proved the potential to map the complete glacier outline and the temporal and spatial development of the transient snow line (TSL). Using this data, clear negative mass-balance conditions were determined for Mýrdalsjökull in 2004. Another approach for measuring accumulation rates was succesfully tested at the Vatnajökull test site. Using volcanic ash deposits of a subglacial eruption as time reference marker, it was possible to estimate accumulation rates by analysis of time sequential SAR (ENVISAT) backscatter data. In contrast to stake measurements, commonly used for accumulation measurements, this method provides areal coverage of the snow pack thickness.

Influences of jökulhlaups on ice dynamics and the propagation of such floodwaves draining subglacially are currently a highly discussed topic. The new theory of sheet flow or coupled sheet and tunnel flow leading to widespread basal lubrification resulting in increased ice flow velocities could be confirmed by a study at Skeidarárjökull, a major outlet glacier of Vatnajökull ice cap. For investigation of ice dynamics, image-to-image cross-correlation of optical ASTER images proved very useful in absence of suitable SAR images for interferometric analysis. By using that technique, a mean annual surface velocity of Skeidarárjökull could be derived for the period 2001 until 2005. Compared to these values, significantly increased surface velocity was derived over the whole width of the glacier from an additional ASTER pair covering a jökulhlaup which drained under Skeidarárjökull.

Knowledge about active subglacial geothermal areas and the subglacial tunnel system for melt water drainage is of great importance for hazard assessment purposes. Due to their characteristics, SAR data proved very useful for the study of the imprints of subglacial volcanic activity on a glacier surface. The ability to penetrate the upper layers of snow and firn enables the detection of buried topographic features of a glacier that are related to the underlying glacially- and fluvially-eroded bedrock or to subglacial volcanic activity. The analysis of a time series of SAR images (ERS-1/2, RADARSAT, JERS-1, ENVISAT) with special focus on identifying circular and linear depressions in the glacier surface of Mýrdalsjökull enabled the identification of subglacial geothermal heat sources and the connected subglacial drainage system. These data allowed a more precise identification of areas surrounding the glacier potentially endangered by a jökulhaup during a subglacial eruption and lead to a new, piecemeal caldera model of Katla volcano. This approach of investigating surface features by SAR time series analysis was transferred to Bardárbunga volcano under the northern parts of Vatnajökull, where seismic activity revealed unrest, to show its early-warning capabilities. The exact location of the corresponding active vent and therefore a potentially eruptive area could be detected in the SAR images leading to a precise prediction of surrounding regions prone to a jökulhlaup triggered by a possible future eruption at this location.

The results of all these studies proved specialised remote sensing techniques to be very useful to identify and quantify a number of important processes connected to the intercation between subglacial volcanoes and the overlying ice cover. A multisensor and multitemporal approach is necessary for the quantification of mass exchange and monitoring of potential hazard areas. Planned and already launched satellite missions will provide the necessary data basis for the development of an efficient monitoring system, aiming at the detection of mass changes and potential hazards by subglacial volcanoes.

1. Introduction

There is the general trend in Earth Sciences nowadays, to deal with highly interdisciplinary problems and the theme ice-volcano interactions is clearly one that spans disciplines. The timeliness of investigating the interactions and hazardous effects of subglacial volcanic eruptions is also demonstrated by the recent formation of the International Association of Volcanology and Chemistry of the Earth's Interior (IAVCEI) working group of Volcano-Ice interactions. On a global level, volcanoes covered by glacier represent a major hazard by threatening lives, destroying property, capital and the environment on an enormous scale. Besides the usual volcanic hazards (lava flows, pyroclastic clouds, tephra fall, lightning etc.), the volcano-ice interaction leads to enormous meltwater torrents (jökulhlaup) or mudflows (lahar) that devastate large areas in the surroundings of the affected glacier. These indirect dangers can occur long after the eruption and may reach very far from the eruptive centre devastating regions that were thought not to be in danger from an eruptive hazard. An example of such an event is the eruption of Nevado del Ruiz in 1985 produced a series of pyroclastic flows and surges melting parts of the summit ice cap triggering lahars with a total volume of about 9×10^7 m^3 (Pierson et al., 1990; Thouret, 1990). More than 20.000 people lost their lives in downstream areas up to 100 km away from the volcano summit.

This thesis is mainly an outcome of the European Space Agency (ESA) project on "Hazard Assessment and Prediction – Long-term Observation of Icelandic Volcanoes and Glaciers Using ENVISAT-ASAR and Other Radar Data (ID 142)", aiming to address questions relating to subglacial volcanic activity from an observational point of view. Direct observations of subglacial volcanoes are often difficult or even impossible to accomplish, therefore remote sensing seems a very promising tool allowing for the study of such large, remote and inaccessible areas. The use of remote sensing data enables a contribution to three crucial components in monitoring subglacial volcanoes: glaciology, volcanology, and hazard assessment.

Seated atop the volcano, a glacier interacts with the volcanic processes and is an essential element to understand the complex system. Thus, an essential part of this thesis deals with the determination of glaciological parameters using remote sensing data. Gathering knowledge about the seasonal variations of a glacier or gradual retreat driven by a changing climate is of special interest, considering that seismicity of subglacial volcanoes in Iceland appears to be influenced by glacier loading and de-loading throughout the year (Sigvaldason et al., 1992; Einarsson and Brandsdóttir, 2000).

Indicators of subglacial volcanic activity can be identified indirectly by remote sensing analysis due to the ice cover. For example crustal deformations caused by magma movements interfere with ice flow of the overlying glacier, preventing a distinct classification of the signal. Nevertheless depressions in the glacier surface develop above subglacier geothermal areas due to the volume loss at the glacier bottom, triggered by ice melting from geothermal activity (Björnsson, 1975; Björnsson, 1988; Benn and Evans, 1998). A continuous satellite-based monitoring of the glacier surface morphology allows for detection of variations in the heat flux of the volcanic system and a better forecast of potential eruption locations. Moreover, the arrangement of identified subglacial geothermal areas enables insights on the structure of the volcanic edifice covered by glacier.

Being the source for huge amounts of meltwater, the glacier further triggers the accompanying dangers (i.e., jökulhlaups, lahars) of subglacial volcanic eruptions and controls the flow direction of the flood likewise. In case of the thick Icelandic glaciers, meltwater produced by a subglacial eruption propagates subglacially from the eruption site to the glacier terminus (Björnsson, 1988). Therefore, exact knowledge about a potential eruption location and the origin of a floodwave is again crucial for the prediction of the potentially affected river catchment. It is possible to detect the pre-existing subglacial drainage system, at least for parts of a glacier, by remote sensing analysis. The course of subglacial meltwater tunnels is indicated by halfpipe-shaped sinks on the glacier surface due to the viscoplastic nature of the ice cover. Meltwater tunnels serve as the initial transport network for the basal passage of melt water during a catastrophic jökulhlaup (Björnsson et al., 2001; Björnsson, 2002; Roberts, 2005) and must be considered for hazard zonation purposes. With knowledge of potential eruption sites and the pre-existing drainage system a precise prediction of peri-glacial regions prone to a devastating outburst flood accompanying a future eruption becomes possible.

Iceland serves an ideal test area for investigating the potential and limits of monitoring ice-volcano interactions using remote sensing data. Approximately 11 % of the 103.000 km² volcanic island is glaciated, consisting mainly of the four large plateau glaciers Vatnajökull (8.100 km²), Langjökull (953 km²), Hofsjökull (925 km²) and Mýrdalsjökull (586 km²) (Björnsson, 1979; Saemundsson, 1979; Sigurdsson, 1998; Adalgeirsdóttir, 2003; Jaenicke et al., 2006). The huge ice masses of these glaciers cover several volcanic systems with central volcanoes, crater chains, and fissures (Björnsson and Einarsson, 1990; Thordarson and Larsen, 2007). The high activity and production rate of the Icelandic volcanoes results from superposition of the spreading plate boundary of the Mid Atlantic Ridge (MAR) over the Iceland mantle plume (e.g., Vink, 1984; Wolfe et al., 1997; Shen et al., 2002; Thordarson and Larsen, 2007). The so-called Neovolcanic Zone (NVZ), the surface expression of the active spreading and plate growth crosses Iceland roughly from Southwest to Northeast with different branches, indicated by the distribution and arrangement of the active volcanic centers (Fig. 1). This thesis focuses on the two test sites Mýrdalsjökull and western Vatnajökull, covering several of Iceland's most active volcanoes. These ice caps were continuously imaged by ENVISAT-ASAR acquisitions throughout this thesis. Furthermore a ground network of artificial corner reflectors installed at Mýrdalsjökull (1995) and Vatnajökull (1997) in the periglacial areas of the two test sites support SAR data processing.

The Katla volcanic system, overlain by Mýrdalsjökull ice cap, comprises an approximately 100 km² caldera, connected to an 80 km wide SW-NE trending fissure swarm (Jakobsson, 1979; Björnsson et al., 2000) (Fig. 1). The Katla volcanic rock series comprises two end-members which are Fe-Ti transitional-alkali basalts and mildly alkalic rhyolithes (Lacasse et al., 2006). On average two eruptions have occurred within the Katla system every century during the last 1100 years with minor subglacial events occurring in 1955 and 1999; whereas the peak rate of melt water discharge during the last major Katla eruption in 1918 was estimated as 300.000 m³/s (Tómasson, 1996; Larsen, 2000; Sigurdsson et al., 2000; Soosalu et al., 2006).

With an expanse of approximately 8.100 km² Vatnajökull is the largest Icelandic and even European glacier. Results of this thesis focus on the two subglacial volcanic systems under its western part, namely Grímsvötn and Bárdarbunga. The Grímsvötn volcanic system shows the highest eruption frequency of all subglacial volcanoes beneath Vatnajökull with about 70 eruptions in historical time (Thordarson and Larsen,

2007). The 62 km² caldera of the central volcano is situated in the central part of western Vatnajökull (Fig. 1). Due to ice cover, eruptions of Grímsvötn are phreato-magmatic and effects of the most recent Grímsvötn eruption which occurred from 1–6 November 2004, are presented here. The second most active volcano beneath Vatnajökull is the Bárdarbunga volcanic system. At least 23 eruptions are attributed to this system in historical time (Thordarson and Larsen, 2007). Bárdarbunga is a large volcanic edifice girding an 80 km^2 large caldera sited in the northern part of western Vatnajökull (Björnsson and Einarsson, 1990). Recent efforts have been directed to this area, as the northern flanks of Bárdarbunga show signs of unrest (i.e., increased seismic activity and sporadic heat flux) since end of 2004.
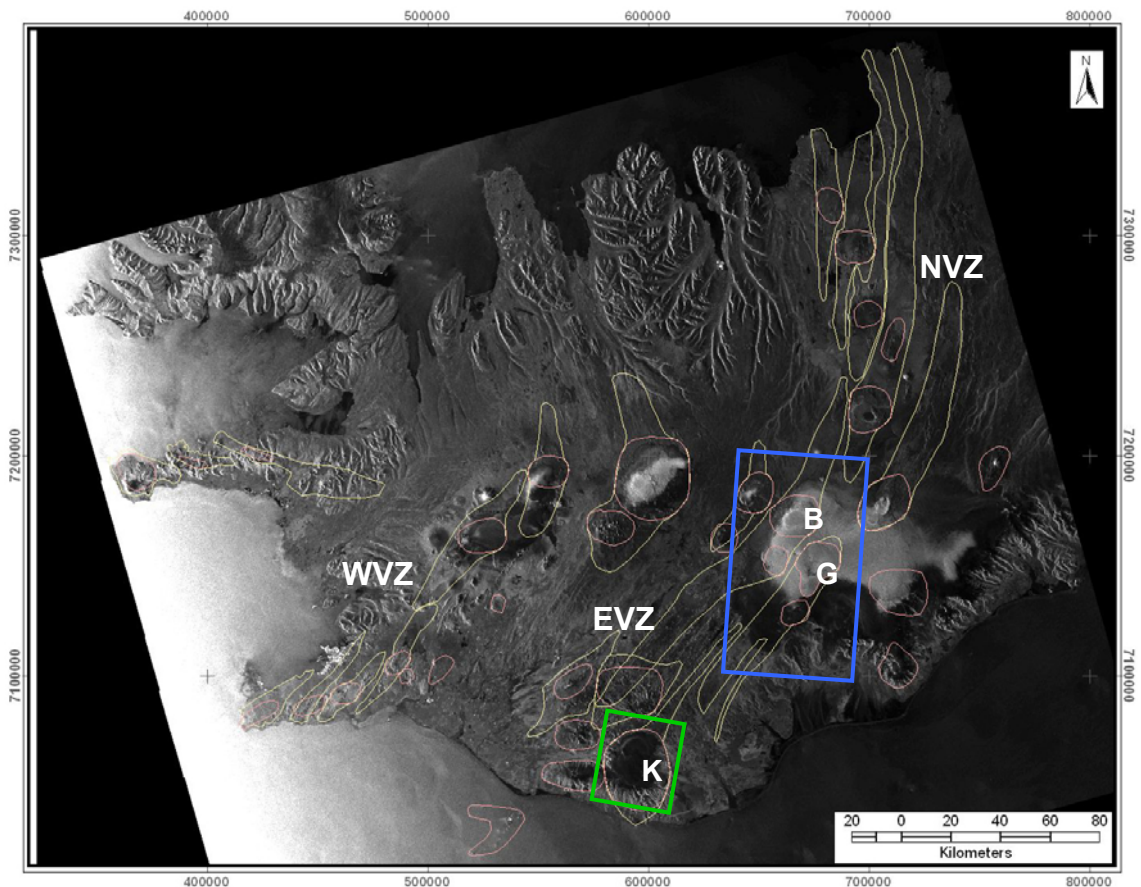
Figure 1: ENVISAT-ASAR wide swath image (30/12/2006) covering Iceland almost completely. Glaciated areas appear black (low backscatter intensity due to high water content of the snow cover at lower elevations) and light grey (dry snow cover at higher elevations leads to volume scattering and therefore high backscatter values). The course of the Neovolcanic Zone is indicated by the location of central volcanoes (reddish polygons) and their adjacent fissure swarms (yellow polygons). The different branches of the Neovolcanic Zone are the West Volcanic Zone (WVZ), the East Volcanic Zone (EVZ), and the North Volcanic Zone (NVZ). The green rectangle shows the Mýrdalsjökull test site with the Katla (K) volcano, the blue rectangle outlines the Vatnajökull test site with the volcanoes Bárdarbunga (B) and Grímsvötn (G).

2. Principles of SAR remote sensing

This section serves a short introduction to the remote sensing techniques utilised in this thesis. It is based on manuals and textbooks like Henderson and Lewis (1998), Lillesand and Kiefer (2004), and Ulaby et al. (1982) where additional and more technical information about SAR and optical remote sensing can be found. The main part of the results were achieved using Synthetic Aperture Radar (SAR) remote sensing, an important tool in light of the fact that Icelandic weather conditions and its proximity to the arctic circle hinder the use of other remote sensing tools. Radar is an acronym for Radio Detection and Ranging. It is an active sensor, transmitting a signal of electromagnetic energy, illuminating the terrain, and recording or measuring the response returned from the target or surface. Imaging radars are generally operating in the microwave region of the electromagnetic spectrum, including wavelengths from 1 mm to 1 meter (Fig. 2). Compared to passive optical sensors, mainly operating in the visible and infrared spectrum. Radar imaging has quite different characteristics due to the longer wavelength and active generation of microwave pulses illuminating the ground target. This enables continuous image acquisition independent from cloud cover and day light.
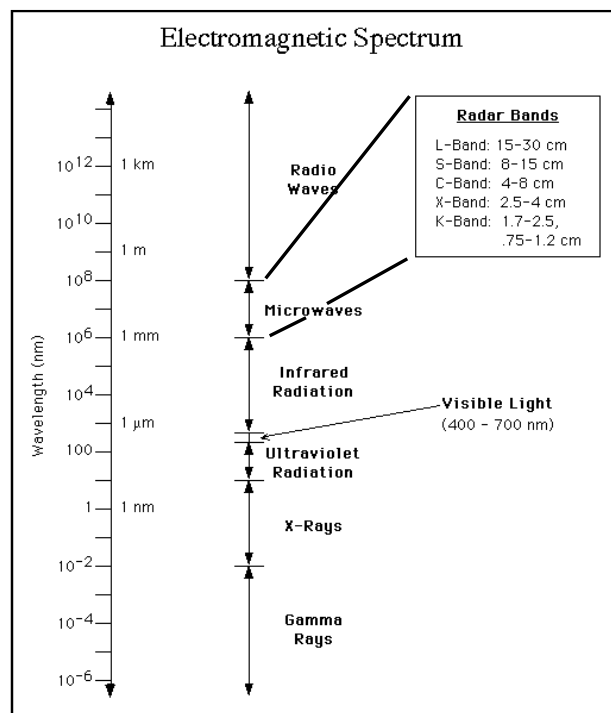

Figure 2: Electromagnetic spectrum showing the microwave range and the respective radar bands. (http://www.asf.alaska.edu/reference/html/7_4_3 _2.html).

2.1 SAR geometry

Radar is basically a distance measuring method, utilising the two-way travel time of an emitted microwave pulse between the antenna and various ground targets. Therefore radar has to be side-looking, otherwise objects with equal distance to the left and to the right of the sensor would give reflections at the same point in time and could not be distinguished. These SAR inherent recording parameters lead to some important terminologies and distortional effects which are described in the following.

Figure 3 illustrates a simplified geometry of a side-looking radar sensor. The footprint illuminated by the microwave pulse is called radar swath. The swath width is controlled by the look angle (θ). Azimuth direction refers to the along-track dimension parallel to the flight direction, whereas the range direction describes the dimension perpendicular to the sensor path. According to the

Figure 3: Simplified geometry of a side looking radar sensor.
(Roth, 2001)

distance from the flight path (nadir line) the radar swath is subdivided into near range and far range. As radar measures how far objects are from the sensor, distances are recorded in slant range along an imaginary line between the radar antenna and the target. Ground range is the perpendicular distance from the platform ground track to an illuminated object. Another important factor is the incidence angle which describes the angle between the incident radar beam and the ground surface assuming no topography. The term local incidence angle is used for the angle between the radar beam and the normal to the surface at a particular point. Incidence angle and local incidence angle are only equal over flat terrain respectively.
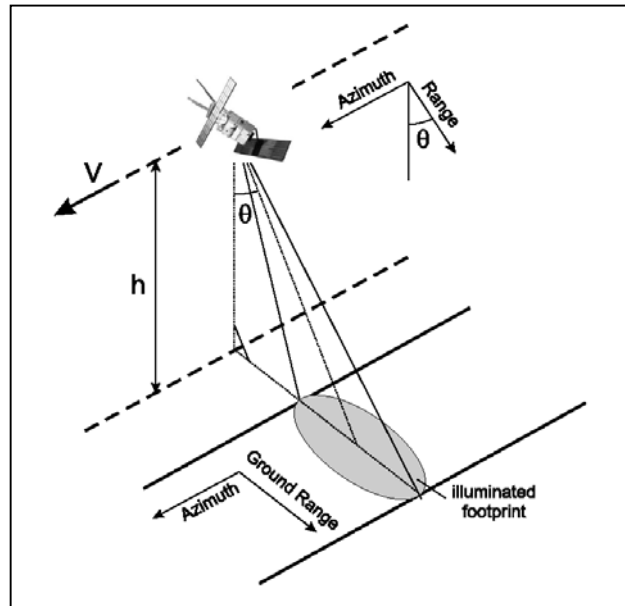
The side-looking geometry also causes some distortions in radar images especially in mountainous areas known as layover, foreshortening, and shadow. These geometric distortions depend mainly on the relation between terrain slope and the look angle of the radar beam. Since the radar pulse is emitted radially, equal travel times to ground objects are located on a circle centred at the sensor. As a result, objects with different distances on the ground may have the same distance from the satellite sensor.
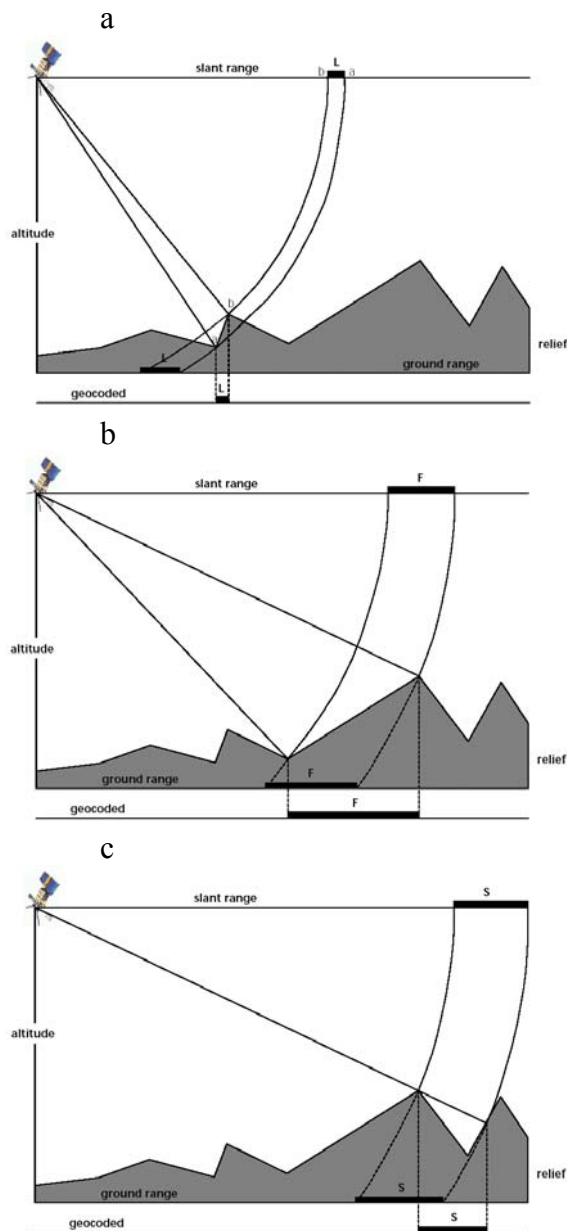
Figure 4: Distortions caused by the radar inherent side-looking geometry. Layover (a) results in a reversion of the terrain geometry. Foreshortening (b) causes compression of slopes facing towards the sensor. Points in the shadow (c) of an object are not visible in the radar image.
(Roth, 2001)

Figure 4a illustrates the layover effect. The mountain top (b) is closer to the sensor than the foot of the mountain (a). Therefore the signal of the mountain top (b) reaches the sensor before the reflection of the foot of the mountain resulting in layover of the terrain geometry in the slant range image. Generally, layover zones, facing radar illumination, appear as bright features in the image. The ambiguities in these zones can not be resolved due to the representation of several points on the ground by one single point in the image.

In figure 4b the ground distance of the mountain slope is much larger than the recorded distance in the slant range geometry, because the top of the mountain is again relatively close to the sensor. This effect is called foreshortening. Foreshortening is obvious in radar images of mountainous areas, where the mountains seem to lean towards the sensor. The ambiguities of this range compression of the radiometric information backscattered from foreslope areas can be corrected by means of rectification procedures which use topographic information.

The shadow effect (Fig. 4c) is caused by slopes facing away from the sensor with an angle that is steeper than the sensor look angle. Therefore such areas cannot be reached by the

radar signal and appear dark (zero signal) in the image. Further, the radar shadows of two objects of the same height are longer in the far range than in the near range of an image.

2.2 SAR resolution

A radar imaging system is characterised by its resolution in azimuth (along-track) and range (across-track) direction. Range resolution in a radar image is mainly controlled by the bandwidth of the emitted microwave pulse. To improve range resolution, pulse duration (τ) should be as short as possible. This would lead to a higher pulse repetition frequency allowing for distinction between more closely spaced objects. However, it is also crucial to transmit enough energy in a pulse to enable the detection of the reflected signals. If the pulse is shortened, its amplitude must be increased to keep the same total energy in the pulse. Technically this is achieved by frequency modulation of the emitted pulses (chirped pulse). Instead of a short pulse with a constant frequency, a long pulse is emitted with a modulated frequency. The frequency modulation must be processed after reception to focus the pulse to a much shorter value. The slant range resolution (r_r) of a radar system and the ground range resolution (r_g), which is the projection of the former to the ground is given by:

$$r_r = \frac{c\tau}{2}$$

and

$$r_g = \frac{c\tau}{2\sin\theta}$$

c = propagation velocity
θ = look angle

The azimuth resolution describes the ability of an imaging radar to separate two closely spaced targets in the direction parallel to the motion of the sensor. For a real aperture radar the resolution along track (azimuth resolution r_a) depends on the antenna beamwidth and the distance between the sensor and the observed surface and is given by:

$$r_a = r * \frac{\lambda}{L}$$

r = distance between antenna and target
λ = wavelength
L = antenna length

As height and therefore the distance to the target is fixed for satellite based imaging radars, a better resolution can only be achieved by increasing the antenna length. However, assuming a satellite height of about 800 km (like ENVISAT) equipped with a c-band radar ($\lambda = 5.6$ cm), an antenna length of 3 km would be required to obtain a 10 m azimuth resolution. Obviously this limits the usability of conventional radar and is overcome by a synthetic array approach. A Synthetic Aperture Radar (SAR) utilizes the motion of the sensor to simulate a long antenna (Fig. 5). The received signals from subsequent antenna positions are coherently recorded and then added in a processor,

using the Doppler principle, to synthesize a long antenna array. With this technique, the 10 meter long ASAR antenna onboard the ENVISAT satellite achieves an azimuth resolution (single look) of about 4.8 m (Rosich et al. 2003).
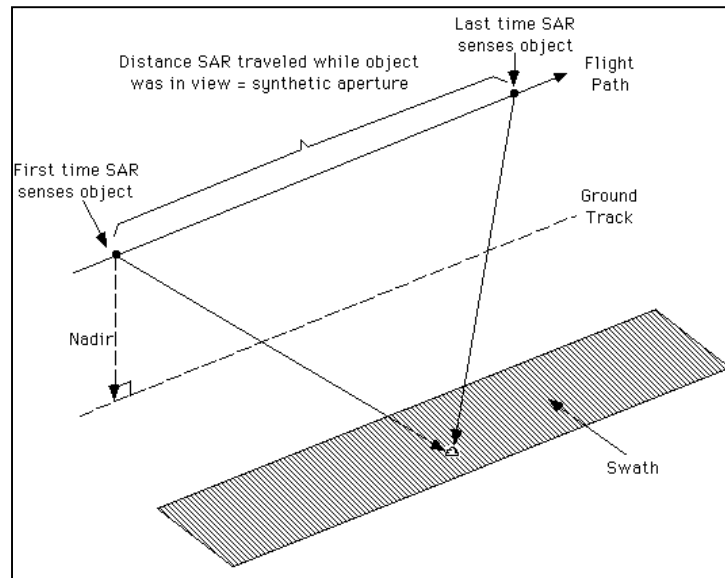
Figure 5: Simplified sketch of the SAR principle. (http://envisat.esa.int/object/index.cfm?fobjectid=3772& contentid=3829)

2.3 Interaction with target

The SAR amplitude image provides information on the portion of the transmitted energy that is reflected back to the antenna from the illuminated surface. Darker areas in an amplitude image represent low backscatter, brighter areas indicate high backscatter. Generally two types of scattering mechanisms are possible: reflection at the surface which is called surface scattering while scattering inside the illuminated medium is called volume scattering. The main factors controlling the microwave interaction with the surface are roughness, geometric shape and dielectric properties of the target.
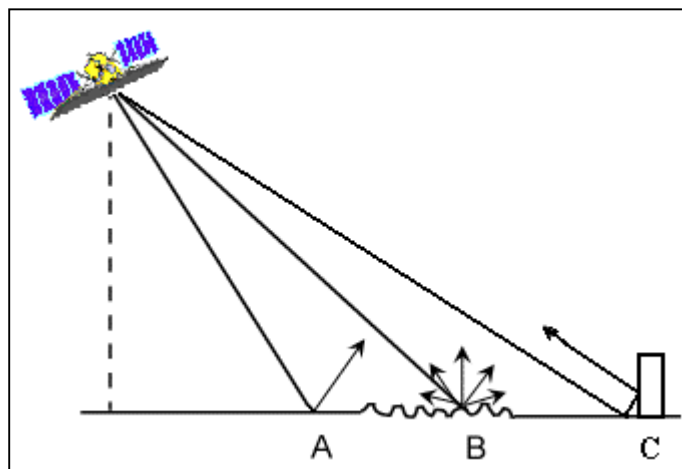
Figure 6: Reflections from three different surface characteristics. (http://www.asf.alaska.edu/reference/general/SciSARu serGuide.pdf)

Surface roughness is considered the main factor affecting radar backscattering. A rough surface (Fig. 6 B) will create much more backscatter to the sensor than a smooth surface which acts like a specular reflector (Fig. 6 A). There most of the energy is reflected away from the incoming direction. The Rayleigh criterion defines the classification of a surface depending on the wavelength of the sensor and is written as:

$$h > \frac{\lambda}{8\cos\theta} \quad \text{for a rough surface}$$

and

$$h < \frac{\lambda}{8\cos\theta} \quad \text{for a smooth surface}$$

> h = mean height of surface variations
> λ = wavelength of the sensor
> θ = incidence angle

Objects with a special shape can act like corner reflectors (Fig. 6 C) creating a double bounce reflection. This leads to punctually very high backscatter values in the image making such points easily identifiable. Artificial corner reflectors taking advantage of this principle. For example the two test sites of this thesis Mýrdals- and Vatnajökull were equipped with a network of artificial corner reflectors in the 1990's (10 around each glacier, 5 oriented towards ascending and 5 oriented towards descending orbits respectively) to enable a fast and accurate geocoding of acquired SAR images.

Another important factor controlling radar backscatter is the dielectric properties of the illuminated material. The complex dielectric constant (ε) is the principal description of the material's response to an electric field. It consists of two parts (permittivity and conductivity) that are both highly dependent on the moisture content of the illuminated material. In the microwave region, most natural materials have a dielectric constant between 3 and 8, under dry conditions, whereas water has a high dielectric constant of 80. As a result, a change in moisture content generally produces a significant change of the dielectric properties of natural materials. This means, that increasing moisture is associated with an increased radar reflectivity. In contrast to that, the penetration depth of electromagnetic waves in an object is an inverse function of water content. This means that dry materials tend to act as volume scatterers, while materials with increased moisture content acts as a surface scatterer.

The amount of reflectivity recorded in a SAR image is also dependent on the sensor parameters (e.g. radar wavelength, viewing geometry, polarisation). As the sensor characteristics are known values, SAR amplitude images can be corrected to give the average reflectivity induced only by the properties of the scatterer. These calibrated images therefore denote the radar backscattering coefficient (σ_0) expressed in the logarithmic unit decibels.

For snow and glacier ice which are mainly observed in this thesis the main factors controlling backscattering at SAR frequencies are:

- the liquid water content,
- the surface roughness (wet snow and glacier ice),
- internal interfaces, ice inclusions and grain size (dry or refrozen snow)

Generally these factors are strongly influenced by seasonal variations. During the winter half, when the glacier is covered by dry snow, the SAR signal penetrates into this layer due to its small dielectric constant. Frozen ice pipes, ice lenses and internal interfaces in the snowpack result in high backscatter from the volume and therefore a bright appearance in the SAR image. When the snow gets wet in spring, σ_0 drops significantly. Surface scattering at the air/snow boundary is the dominant scattering mechanism where most of the incoming signal is reflected away from the sensor leading to dark appearance in the SAR image. In areas where bare ice is exposed on a glacier σ_0 is affected by the roughness and melting condition of the ice surface. In spring, when wet snow covers the ice, the signal originates again from the snow surface and σ_0 is low. The maximum of σ_0 on the ice surfaces in summer can be explained by the increased roughness during the melt period caused by crevasses or incised meltwater channels. Several examples and explanations of the different scattering mechanisms and, therefore, changing appearance of the test sites Mýrdals- and Vatnajökull can be found in paper 1, 2 and 4 of this thesis.

3. Principles of optical remote sensing

In contrast to the active microwave sensors, passive optical sensors rely on electromagnetic energy emitted from natural sources in the visible, near infrared and short-wave infrared spectrum (0.3 to approximately 14 μm). This could be solar irradiation reflected from the earth's surface or thermal radiation emitted directly from objects on the earth. The sensors are measuring the spectral radiance expressed in watts per steradian per unit area per wavelength interval. Before arriving at the sensor, all radiation has to travel through the atmosphere where it interacts with the atmosphere molecules leading to absorption or scattering processes. Atmospheric scattering is the unpredictable diffusion of radiation by particles in the atmosphere, whereas atmospheric absorption results in the effective loss of energy at a defined wavelength, the so-called absorption bands of the electromagnetic spectrum (Fig. 7). Therefore only the wavelength regions outside the main absorption bands of the atmospheric gases can be used for remote sensing. These regions are known as the Atmospheric Transmission Windows and remote sensing systems are usually designed to fall within these windows to minimize the atmospheric absorption effects. These windows are found in the visible (0.4-0.7 μm), near-infrared (0.7-2.5 μm) and certain bands in the middle (3-5 μm) and thermal infrared (8-14 μm) regions.
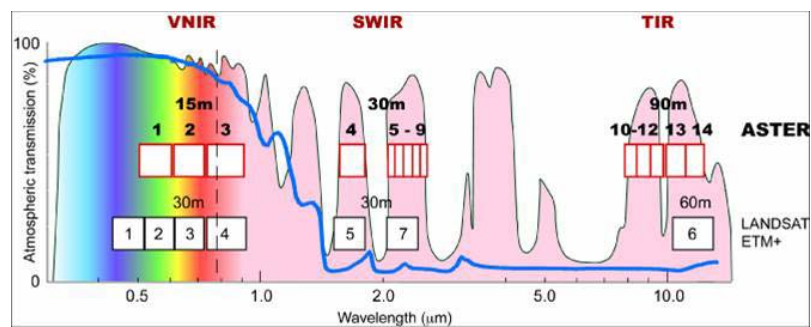
Figure 7: Transmission windows in the visible, near, middle and thermal infrared regions superimposed by the spectral bands of the ASTER and LANDSAT satellites. (http://asterweb.jpl.nasa.gov/characteristics.asp).

However, the presence of clouds strongly limits the application of optical sensors especially in regions with frequent cloudiness like Iceland. Furthermore, in such high latitude areas, optical remote sensing is hindered during the winter month (in Iceland from November until February) due to the polar night. For example only 7 useful i.e. cloudfree images of the ASTER sensor were available from the launch of the satellite in December 1999 until spring 2007 for the Mýrdalsjökull test site. Optical remote sensing systems are characterised by the following attributes:

- Spectral resolution: The spectral resolution describes the ability of a sensor to resolve fine wavelength intervals by the number of spectral bands and the bandwidth of the respective band. The finer the spectral resolution, the narrower the wavelength range for a particular channel or band.

- Spatial resolution: The spatial resolution refers to the size of the smallest possible feature that can be detected by the sensor. It depends mainly on the Instantaneous Field of View (IFOV) of the sensor which describes the resolution

cell and therefore the pixel size of the corresponding image. An enhanced spatial resolution causes a smaller IFOV of the sensor, which means that less total ground area can be seen.

▪ Radiometric resolution: The radiometric resolution refers to the amount of radiometric information which can be differentiated in a certain spectral band, i.e., the number of grey values (or digital numbers, DN) in this band. The finer the radiometric resolution of a sensor, the more sensitive it is to detecting small differences in reflected or emitted energy.

▪ Temporal resolution: The temporal resolution describes the revisiting period of a satellite sensor, i.e. the time separation between imaging exact the same area at the same viewing angle. Roughly speaking, the spatial and temporal resolution is inversely proportional for most space-borne sensors. Systems with very high temporal resolution offer only a coarse spatial resolution (e.g., Meteosat, NOAA-AVHRR), whereas for example the ASTER sensor with a better spatial resolution has a repeat cycle of 16 days.

3.1 Scanning geometries

Optical remote sensing systems acquire two dimensional images of the terrain for a swath beneath the sensor. Most commonly multispectral scanners are used which collect data over a variety of different wavelength ranges. There are two different modes how this can be done: across-track scanning (whiskbroom) or along-track (pushbroom) scanning.
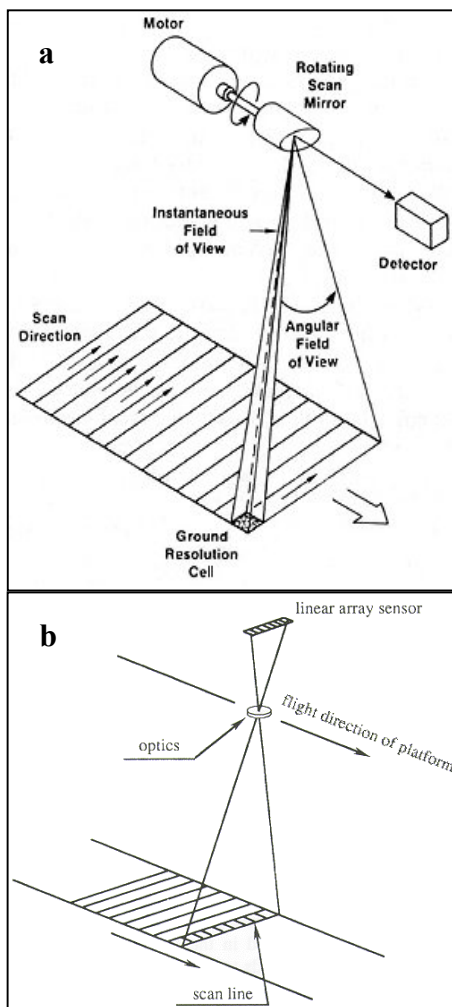
Across-track or whiskbroom scanners scan the surface in a series of lines, whereas these lines are oriented perpendicular to the motion of the sensor platform. By using an oscillating or rotating mirror each line is scanned from one side of the platform to the other. The length of a scan line, i.e. the angular field of view, typically ranges between 10°-20° for satellite systems. The forward motion of the platform is utilised to generate a two-dimensional image of the surface by stringing together the subsequent scan lines. As the distance from the sensor to the target increases symmetrically on each side of the nadir, the ground resolution cells also become larger and geometric distortions are introduced to the images.

Figure 8: Schematic diagram of data acquisition by a whiskbroom scanner (a, http://www.fas.org/irp/imint/docs/rst/Intro/Part2_5a.html) and a pushbroom scanner. (b, http://www.profc.udec.cl/~gabriel/tutoriales/rsnote/cp2/2-11-1.gif).

Along track or pushbroom scanners also record multispectral image data along a swath beneath the sensor. Further, pushbroom scanners also use the forward motion of the platform to build up a two-dimensional image, perpendicular to the flight direction by recording subsequent scan lines. No scanning mirror is used to record a scan line. Instead, a linear array of detectors consisting of numerous charge-coupled devices (CCDs) is arranged perpendicular to the direction of sensor motion. Linear array CCDs are designed to be very small, as each spectral band of sensing requires its own linear array. The arrays are located in the focal plane formed by the lens system of the scanner such that each scan line is viewed by all arrays simultaneously.

The ASTER sensor which is the only source of optical data used in this thesis consists of three separate instrument subsystems: The visible and near infrared (VNIR), as well as the Shortwave Infrared (SWIR) scanners are operating in the pushbroom mode, whereas the thermal infrared (TIR) radiation is sensed with a whiskbroom scanner.

4. Results (Abstracts of manuscripts)

4.1 Glaciology

4.1.1 The use of remote sensing data for mass balance studies at Mýrdalsjökull ice cap, Iceland

A series of satellite images of Mýrdalsjökull, Iceland, was analyzed in view of their value for mass-balance investigations. A combination of optical satellite images from the ASTER sensor and synthetic aperture radar data from ERS-2 and Envisat ASAR proved very useful. The glacier margin of Mýrdalsjökull was delineated on ASTER images from summer and winter 2004. With a time series of summer ASAR images it was possible to monitor the temporal and spatial development of the transient snowline (TSL) throughout the year 2004, as well as the firn line (FL) at the end of the balance year. An 'inverse' function was applied to visually enhance detail in the radar imagery. Winter radar images were not useful for mass-balance observations because of frequent surface melting, which prevented the transparency of the snow cover for C-band microwaves. Interannual mass-balance fluctuations were observed by comparing three radar images acquired in late summer 1998, 1999 and 2004 respectively. These fluctuations follow the same trend as the annual mean air temperature which shows a strong increasing trend between 1999 and 2004. An accumulation-area ratio of <0.43 was determined for 2004, indicating clear negative mass-balance conditions. Monitoring the TSL–FL with radar summer images for mass-balance studies, rather than the equilibrium line (EL), is suggested for large ice caps in maritime climates.

4.1.2 Effects of ash-layers of the 2004 Grímsvötn eruption on SAR backscatter in the accumulation area of Vatnajökull

The usability of volcanic ash deposits on Vatnajökull ice cap (Iceland) as a time reference marker for measuring accumulation by the analysis of time sequential SAR backscatter data was investigated. A volcanic eruption at Grímsvötn caldera, a subglacial volcanic system beneath Vatnajökull, in early November 2004 produced an ash layer, which was deposited north of the vent, covering a V-shaped area of approx. 88 km² on the glacier surface. The ash fall, which was subsequently buried by snow, reveals a distinct backscatter signal in SAR images. In total, the σ^0 backscatter values of 40 ENVISAT-ASAR images were analysed, covering two post-eruption accumulation periods (4 November 2004 until 31 March 2005 and 25 October 2006 until 14 March 2006). Significant differences over time were observed in the SAR backscatter signals over the deposited ash, that appear to be related to the snow accumulation history. The backscatter signals were compared to meteorological conditions at the time of SAR acquisition and to accumulation data derived from two snow pits, one of them located within the ash fall. A linear regression analysis between the accumulation data and the SAR backscattering coefficient result in high R^2 confidence values (> 0.8), indicating that the SAR data can be used for estimation of the areal accumulation distribution in areas with an existing ash layer.

4.1.3 Influences of the 2004 jökulhlaup on ice dynamics of Skeidarárjökull, Iceland, using Terra-ASTER imagery

On 01–06 November 2004 a volcanic eruption occurred at the subglacial Grímsvötn caldera sited under the western part of Vatnajökull ice cap. The accompanying jökulhlaup travelled subglacially over a distance of 50 km under the Skeiðarárjökull outlet and finally flooded huge areas of the Skeiðarársandur plain in the south. Meltwater discharge peaked on 2 November and finally ended in early December, having released a total volume of ~0.8 km³ from Grímsvötn. The influences of this jökulhlaup on the ice dynamics of Skeiðarárjökull were investigated applying image cross-correlation on five optical images pairs (October 2001 to July 2005) of the Advanced Spaceborne Thermal Emission and Reflection Radiometer (ASTER) aboard the EOS Terra satellite. The average horizontal surface displacement of nearly annual periods (2001-2002, 2002-2003, 2003-2004, 2004-2005) were compared to the velocity obtained from a 64 day image pair covering the period of the jökulhlaup. A considerable acceleration of up to 0.4 m d^{-1} over nearly the whole width of the glacier appeared during the jökulhlaup in contrast to the annual velocities. This extensive increase of surface velocity is only hardly explainable by the classical jökulhlaup theory of floodwater drainage in a single subglacial conduit. Considering the results, a sheet flow or coupled sheet and tunnel flow leading to a widespread basal lubrification seems more likely.

4.2 Glaciovolcanism

4.2.1 Imprints of subglacial volcanic activity on a glacier surface – SAR study of Katla volcano (Iceland)

The Katla central volcano, covered by the fourth largest Icelandic glacier Mýrdalsjökull, is among the most dangerous and active volcanoes in Iceland. Due to the ice cover, several indicators of its volcanic activity can only be identified indirectly. We analysed a total of 30 Synthetic Aperture Radar (SAR) images, with special focus on identifying circular and linear depressions in the glacier surface. Such features are indicative of subglacial geothermal heat sources and the adjacent subglacial tunnel (melt water drainage) system. The time series comprises images from five different SAR sensors (ERS-1, ERS-2, JERS-1/SAR, RADARSAT and ENVISAT-ASAR) covering a time period of 12 years, starting in 1994. Individual SAR scenes only partly map the glacier surface morphology, due to the environmental influences on the SAR backscatter intensity. Thus, only surface features detectable in several SAR scenes at the same location were considered and merged to form an overall picture of the surface morphology of Mýrdalsjökull and its modification by subglacial volcanic activity between 1994 and 2006. Twenty permanent and 4 semi-permanent ice cauldrons could be identified on the surface of Mýrdalsjökull indicating geothermally active areas in the underlying caldera. An analysis of their size was not possible, due to the indistinct outline in the SAR images. The spatial distribution of the geothermally active areas led to a new, piecemeal caldera model of Katla volcano. All cauldrons are connected to tunnel systems for meltwater drainage. More than 100 km of the subglacial drainage system could be identified under the Mýrdalsjökull in the SAR time series. It has been found, that the tunnel systems are not in agreement with estimated water divides.

According to our results allow improved assessment of areas of potential jökulhlaup hazard accompanying a subglacial eruption.

4.3 Hazard assessment

4.3.1 Combination of SAR remote sensing and GIS for monitoring subglacial volcanic activtiy – Recent results from Vatnajökull ice cap (Iceland)

This paper presents latest results from the combined use of SAR (Synthetic Aperture Radar) remote sensing and GIS providing detailed insights into recent volcanic activity under Vatnajökull ice cap (Iceland). Glaciers atop active volcanoes pose a constant potential danger to adjacent inhabited regions and infrastructure. Besides the usual volcanic hazards (lava flows, pyroclastic clouds, tephra falls, etc.), the volcano-ice interaction leads to enormous meltwater torrents [icelandic: jökulhlaup], devastating large areas in the surroundings of the affected glacier. The presented monitoring strategy addresses the three crucial questions: When will an eruption occur, where is the eruption site and which area is endangered by the accompanying jökulhlaup. Therefore, sufficient early-warning and hazard zonation for future subglacial volcanic eruptions becomes possible, as demonstrated for the Bardárbunga volcano under the northern parts of Vatnajökull. Seismic activity revealed unrest at the northern flanks of Bardárbunga caldera at the end of September 2006. The exact location of the corresponding active vent and therefore a potentially eruptive area could be detected by continuous ENVISAT-ASAR monitoring. With this knowledge a precise prediction of peri-glacial regions prone to a devastating outburst flood accompanying a possible future eruption is possible.

5. Conclusions and outlook

The results of this thesis prove that the application of remote sensing on ice-volcano interactions in Iceland is a powerful tool to investigate various aspects of the complex phenomenon of glacier-clad volcanoes. The use of Synthetic Aperture Radar (SAR) is very advantageous, due to the largely independence of meteorological conditions and the potential to study subsurface features and processes on a glacier. However, the 35 day repeat pass of ENVISAT restricted interferometric analysis of current processes, due to total decorrelation of the glaciated areas within this time period. Therefore, image-to-image cross-correlation of optical ASTER images was applied successfully to study glacier motion. This method is limited of course by the availability of cloud-free images and to lower elevations of a glacier tongue where the bare ice is exposed during the ablation period. Data from the next generation of SAR satellites, including ALOS and TerraSAR-X, will guarantee continuity in SAR monitoring of Icelandic subglacial volcanoes. As such radar performance has not been previously available, especially the high-quality images of TerraSAR-X (ground resolution up to 1 m), will open new possibilities. The proposed TANDEM-X mission, operating a second satellite on a one day repeat pass compared to TerraSAR-X has the potential to push such monitoring to a new level by deriving digital elevation models and deformation maps on a regular basis. Further, the potentials of very-high resolution optical data such as IKONOS (1 m ground resolution) and QuickBird (0.6 m ground resolution) have not yet been evaluated, probably due to the high product price.

In Paper 1 of this thesis it is demonstrated, that remote sensing data are of great use for continuous mass-balance monitoring at Mýrdalsjökull test site. Combined analysis of optical (ASTER) and SAR (ENVISAT, ERS-2) data allowed the determination of the total area of the glacier in 2004 and the gradual retreat of the snow/firn line during the ablation period of the same year. Relative mass-balance fluctuations could be measured by comparison of three radar images acquired in late summer 1998, 1999 and 2004. An accumulation-area ratio (AAR) of < 0.43 was determined for 2004, indicating clear negative mass-balance conditions. The proposed methodological approach is transferable to other glaciers worldwide enabling at least quantitative estimates of mass-balance fluctuations. Considering the effects of de-loading due to glacier retreat on subglacial volcanoes, monitoring of mass balance parameters is of great importance not only at Mýrdalsjökull and should be continued and expanded. Comparing future changes in internal volcanic processes such as seismic activity, gas content, etc. with the mass-balance data could help to understand the mechanisms of their interactions.

In Paper 2, the tephra deposits of the 2004 Grímsvötn eruption on the surface of Vatnajökull were used as a time reference marker for measuring accumulation rates by the analysis of time sequential SAR backscatter data. Backscatter values over the tephra deposits were significantly reduced compared to the undisturbed snow pack outside the tehpra fans. A temporal reduction of this difference indicated a relation to the increasing snow depth over the tephra. A linear regression analysis between accumulation data and the SAR backscattering coefficient resulted in high R^2 confidence values (> 0.8), indicating that the SAR data could be used for the estimation of the areal accumulation distribution in areas with an existing ash layer. This totally new approach enables as well the determination of the penetration depth of the SAR signal into the snow pack and therefore a clearer picture of what a SAR sensor is actually detecting on Icelandic

glaciers. For future research a comparison with ALOS-PALSAR, operating at L-band, would be very interesting. The longer wavelength will allow a prolongated detection of the 2004 tephra fans and therefore the areal reconstruction of accumulation rates over an extended period. When the signal will show no more difference to the undisturbed snow pack outside the tehpra fans, the maximum penetration depth of L-band SAR can be determined likewise.

Paper 3 also deals with effects of the 2004 Grímsvötn eruption. An acceleration of Skeidarárjökull was investigated by cross-correlation of several ASTER image pairs. The speed up of the outlet was triggered by a jökulhlaup accompanying the eruption in autumn 2004. An extensive acceleration over nearly the whole width of the glacier could be observed suggesting a sheet like distribution or coupled sheet and tunnel flow of the subglacial meltwater flood. Cross-correlation of optical images is a valuable method to study glacier motion from space, especially when interferometric analysis is not possible due to whatever reason. By using a high number of ASTER images it should be possible to inventory annual surface velocities of all Icelandic glaciers, what is already aimed within the Global Land Ice Measurement from Space (GLIMS) project. As information content of images increases with spatial resolution, it would further be of great interest to find out, how cross-correlation works with very-high resolution data.

In Paper 4, the imprints of subglacial volcanic activity on the surface of Mýrdalsjökull are monitored. The viscous behaviour of ice causes circular depressions on the glacier surface (ice cauldrons) where active geothermal zones melt the bottom of the glacier. The adjacent basal system of meltwater drainage tunnels is manifested by halfpipe-shaped surface depressions likewise. Therefore it was possible to detect the geothermal active areas under Mýrdalsjökull as well as large parts of the basal network of meltwater tunnels by SAR time series analysis. The spatial distribution of the geothermally active areas led to a new, piecemeal caldera model for Katla volcanic edifice. As the detected basal meltwater tunnels transcend estimated water divides, they must be taken into consideration for a new hazard zonation of areas surrounding the glacier, potentially affected by a jökulhlaup during a future subglacial eruption. Considering the eruption cycle of Katla and the seismic activity in this area, this should be realized as soon as possible. Continuous monitoring of the ice cauldrons with the new high resolution TerraSAR-X data would lead to detailed information about their dimensions and temporal variations. Therefore, the cauldrons could be used as natural calorimeters quantifying the heat flux of the underlying geothermal active areas. Furthermore, it is of great interest to find out if SAR time series analysis of glacier surface morphology can be used to detect geothermally active areas and/or the basal drainage system in other regions as well; especially if glaciers are smaller and not forming a plateau like in Iceland. Probably the most interesting future project would be drilling to the bottom of one or even several of the ice cauldrons at Mýrdalsjökull, conducting various measurements and dye-tracing experiments.

Paper 5 presents a monitoring strategy for hazard assessment of subglacial volcanic activity based on SAR remote sensing. Continuous ENVISAT-ASAR monitoring enabled the identification of recently active vents or fissures under Vatnajökull at the northern flanks of Bardárbunga volcano leading to an improved hazard zonation of areas endangered by a jökulhlaup accompanying a future subglacial eruption at this location. It was found that the combination of SAR and seismic monitoring has the potential for a reliable forecasting system of subglacial volcanic activity and accompanying dangers. It is of course crucial to push this monitoring to a

real time service. Therefore, a future task would be automation of SAR processing, whereas first steps were already made by the implementation of an automated terrain correction based on the artificial corner reflectors at the test sites in Iceland. The significantly improved near real-time capabilities of TerraSAR-X (data delivery up to 1 hour after acquisition) should also be utilized for timely analysis of the behaviour of subglacial volcanoes not only in Iceland.

Finally, it should be mentioned that several important contributions could be made within this thesis to the complex problems arising with subglacial volcanism. A multisensor and multitemporal approach is a prerequisite for quantification of glacier mass changes and monitoring of potential hazard areas. The high number of planned and already launched satellite missions will provide a unique chance to establish an operational and reliable early-warning system for subglacial volcanoes worldwide. Nevertheless, these data sets should only serve as a valuable basis for further cross-disciplinary investigations primarily in terms of material-specific, experimentally-based studies and modeling of processes involved in subglacial volcanic systems.

References

Adalgeirsdóttir G (2003) Flow dynamics of Vatnajökull ice cap, Iceland. Ph. D. thesis, ETH Zürich

Benn DJ, Evans DJA (1998) Glaciers & Glaciation. Arnold, London

Björnsson H (1975) Subglacial water reservoirs, jökulhlaups and volcanic eruptions. Jökull 25:1-15

Björnsson H (1979) Glaciers in Iceland. Jökull 29:74-81

Björnsson H (1988) Hydrology of ice caps in volcanic regions. Soc Sci Isl 45, Reykjavík

Björnsson H (2002) Subglacial lakes and jökulhlaups in Iceland. Global and Planetary Change 35:255-271

Björnsson H, Einarsson P (1990) Volcanoes beneath Vatnajökull, Iceland: Evidence from radio echo-sounding, earthquakes and jökulhlaups. Jökull 40:147-169

Björnsson H, Pálsson F, Gudmundsson MT (2000) Surface and bedrock topography of the Mýrdalsjökull ice cap, Iceland: The Katla caldera, eruption sites and routes of jökulhlaups. Jökull 49:29-46

Björnsson H, Rott H, Gudmundsson S, Fischer A, Siegel A, Gudmundsson MT (2001) Glacier-volcano interaction deduced by SAR interferometry. J Glaciol 47:58-70

Einarsson P, Brandsdóttir B (2000) Earthquakes in the Mýrdalsjökull area, Iceland, 1978-1985: Seasonal correlation and connection with volcanoes. Jökull 49:59-74

Henderson FM, Lewis AJ (eds) (1998) Manual of remote sensing: Principles and Application of Imaging Radar, 3rd edition. John Wiley & Sons, New York

Jaenicke J, Mayer Ch, Scharrer K, Münzer U, Gudmundsson Á (2006): The use of remote sensing data for mass balance studies at Mýrdalsjökull ice cap, Iceland. J Glaciol 52:565-573

Jakobsson SP (1979) Outline of the Petrology of Iceland. Jökull 29:57-73

Lacasse C, Sigurdsson H, Carey SN, Jóhannesson H, Thomas LE, Rogers NW (2006) Bimodal volcanism at the Katla subglacial caldera, Iceland: insight into the geochemistry and petrogenesis of rhyolitic magmas. Bull Volcanol 69:373-399. DOI 10.1007/s00445-006-0082-5

Larsen G (2000) Holocene eruptions within the Katla volcanic system, south Iceland: Characteristics and environmental impact. Jökull 49:1-28

Lillesand TM, Kiefer RW, Chipman JW (2004) Remote Sensing and Image Interpretation, 5th edition. John Wiley & Sons, New York

Pierson TC, Janda RJ, Thouret JC, Borrero CA (1990) Perturbation and melting of snow and ice by the 13 November 1985 eruption of Nevado del Ruiz, Colombia, and consequent mobilization, flow and deposition of lahars. J Volcanol Geotherm Res 41:17-66

Roberts MJ (2005) Jökulhlaups: A reassessment of floodwater flow through glaciers. Rev Geophys 43:RG1002. DOI 10.1029/2003RG000147

Rosich B, Zink M, Torres R, Closa J, Buck C (2003) ASAR instrument performance and product quality status. IGARSS 2003 Proceedings IEEE International 2:1109-1111. DOI 10.1109/IGARSS.2003.1294027

Roth A (2001) SAR Interferometrie: DHM Generierung. Münchner Sommerschule 2001

Saemundsson K (1979) Outline of the Geology of Iceland. Jökull 29:7-28

Shen Y, Solomon SC, Bjarnason IT, Nolet G, Morgan WJ, Allen RM, Vogfjörd K, Jakobsdóttir S, Stefánsson R, Julian BR, Foulger GR (2002) Seismic evidence for a tiled mantle plume and north-south mantle flow beneath Iceland. Earth and Planetary Science Letters 197:261-272

Sigurdsson O (1998) Glacier variations in Iceland 1930-1995. Jökull 45:3-25

Sigurdsson O, Zóphoníasson S, Ísleifsson E (2000) The jökulhlaup from Sólheimajökull, July18th 1999. Jökull 49:60-75

Sigvaldason GE, Annertz K, Nilsson M (1992) Effect of glacier loading/deloading on volcanism: postglacial volcanic production rate of the Dyngjufjöll area, central Iceland. Bull Volcanol 54:385-392

Soosalu H, Jónsdóttir K, Einarsson P (2006) Seismicity crisis at the Katla volcano, Iceland – signs of a cryptodome?. J Volcanol Geotherm Res 153:177-186

Thordarson T, Larsen G (2007), Volcanism in Iceland in historical time: Volcano types, eruption styles and eruptive history. Journal of Geodynamics 43:118-152

Thouret JC (1990) Effects of the November 13, 1985 eruption on the snow pack and ice cap of Nevado del Ruiz volcano, Colombia. J Volcanol Geotherm Res 41:177-201

Tómasson H (1996) The jökulhlaup from Katla in 1918. Ann Glaciol 22:249-254

Ulaby FT, Moore RK, Fung AK (1982) Microwave Remote Sensing: Active and Passive, Vol. II: Radar Remote Sensing and Surface Scattering and Emission Theory. Addison-Wesley, Massachusetts

Vink GE (1984) A Hotspot model for Iceland and the Vöring Plateau. J Geophys Res 89:9949-9959

Wolfe CJ, Bjarnason IT, VanDecar JC, Solomon SC (1997) Seismic structure of the Iceland mantle plume. Nature 385:245-247

Appendix

Paper 1

Jaenicke J, Mayer Ch, Scharrer K, Münzer U, Gudmundsson Á (2006) The use of remote sensing data for mass balance studies at Mýrdalsjökull ice cap, Iceland.- J Glaciol, 52, 179, 565-573.

Reprinted from the Journal of Glaciology with permission of the International Glaciological Society.

The use of remote-sensing data for mass-balance studies at Mýrdalsjökull ice cap, Iceland

Julia JAENICKE,[1] Christoph MAYER,[2] Kilian SCHARRER,[1] Ulrich MÜNZER,[1] Ágúst GUDMUNDSSON[3]

[1]*Department of Earth and Environmental Sciences, Ludwig-Maximilians University, Luisenstrasse 37, D-80333 Munich, Germany*
E-mail: julia.jaenicke@gmx.de
[2]*Commission for Glaciology, Bavarian Academy of Sciences, Alfons-Goppel-Strasse 11, D-80539 Munich, Germany*
[3]*Fjarkönnun ehf., Furugrund 46, IS-200 Kópavogur, Iceland*

ABSTRACT. A series of satellite images of Mýrdalsjökull, Iceland, was analyzed in view of their value for mass-balance investigations. A combination of optical satellite images from the ASTER sensor and synthetic aperture radar data from ERS-2 and Envisat ASAR proved very useful. The glacier margin of Mýrdalsjökull was delineated on ASTER images from summer and winter 2004. With a time series of summer ASAR images it was possible to monitor the temporal and spatial development of the transient snowline (TSL) throughout the year 2004, as well as the firn line (FL) at the end of the balance year. An 'inverse' function was applied to visually enhance detail in the radar imagery. Winter radar images were not useful for mass-balance observations because of frequent surface melting, which prevented the transparency of the snow cover for C-band microwaves. Interannual mass-balance fluctuations were observed by comparing three radar images acquired in late summer 1998, 1999 and 2004 respectively. These fluctuations follow the same trend as the annual mean air temperature which shows a strong increasing trend between 1999 and 2004. An accumulation-area ratio of <0.43 was determined for 2004, indicating clear negative mass-balance conditions. Monitoring the TSL–FL with radar summer images for mass-balance studies, rather than the equilibrium line (EL), is suggested for large ice caps in maritime climates.

1. INTRODUCTION

Global warming has accelerated noticeably in the past 25 years. Model simulations indicate a rise in mean global surface air temperature by about 0.18–0.35°C per decade during the next 100 years due to increasing concentrations of CO_2 and other greenhouse gases in the atmosphere (Houghton and others, 2001). One of the most visible consequences of climate warming is the retreat of glaciers. Monitoring the mass balance of the temperate glaciers in Iceland is interesting. These glaciers are very sensitive to climatic changes due to marine conditions in Iceland. Most of the Icelandic glaciers have been retreating since about 1995, following a continuous warming since the mid-1980s (Jóhannesson and Sigurðsson, 1998). The Icelandic climate is very sensitive to changes in atmospheric circulation and ocean currents in the North Atlantic (Mackintosh and others, 2002). Consequently, glacier reactions in Iceland could indicate changes of these circulation patterns which are linked to global climate variations. Furthermore, the mass-balance status and the glacier runoff are important to the management and planning of hydropower, which is of great economic value to Iceland.

The aim of this study is to investigate the feasibility of using remote-sensing data (space-borne optical and radar) for continuous glacier mass-balance monitoring in south Iceland. Satellite imagery enables continuous monitoring of large, remote areas. An advantage of radar over optical data is the independence from cloud cover and daylight. Synthetic aperture radar (SAR) microwaves can penetrate through clouds and also dry snow. However, on SAR images

it is often difficult to delineate the glacier margin because of poor backscatter contrast between the glacier terminus and the surrounding moraine. In this case, optical imagery proves very useful, as was shown by Hall and others (2000) for Hofsjökull ice cap, Iceland. On the other hand, glacier ice and wet snow or firn can be discriminated on radar images. Thus, the annual evolution of the transient snowline (TSL) and the firn line (FL), if exposed in summer, can be monitored (e.g. Rott and Mätzler, 1987; König and others, 2001; de Ruyter de Wildt and Oerlemans, 2003). Most of the preceding work relating radar backscatter to glacier surface and near-surface characteristics analyzed σ^0 backscatter images (dB values) in order to separate the glacier into different zones. For example, Forster and others (1996) concluded from investigating Hielo Patagónico Sur (HPS; the South Patagonia Icefield) with shuttle imaging radar (SIR-C/X-SAR) imagery that σ^0 changes are closely linked to elevation and air temperature. Hall and others (2000) showed the same for Hofsjökull ice cap by analyzing a European Remote-sensing Satellite (ERS) SAR time series. In addition, they investigated the late-summer FL. Fahnestock and others (1993) found distinct glacier surface boundaries on the Greenland ice sheet with ERS-1 SAR data and suggested that monitoring the location of the boundaries can reveal changes in local climate conditions long before they result in a change in the ice-sheet geometry or dynamic. A few studies utilized a combination of optical and radar imagery for glacier investigations (e.g. Hall and others, 2000; de Ruyter de Wildt and Oerlemans, 2003).

This study uses optical data from the Advanced Space-borne Thermal Emission and Reflection Radiometer (ASTER)
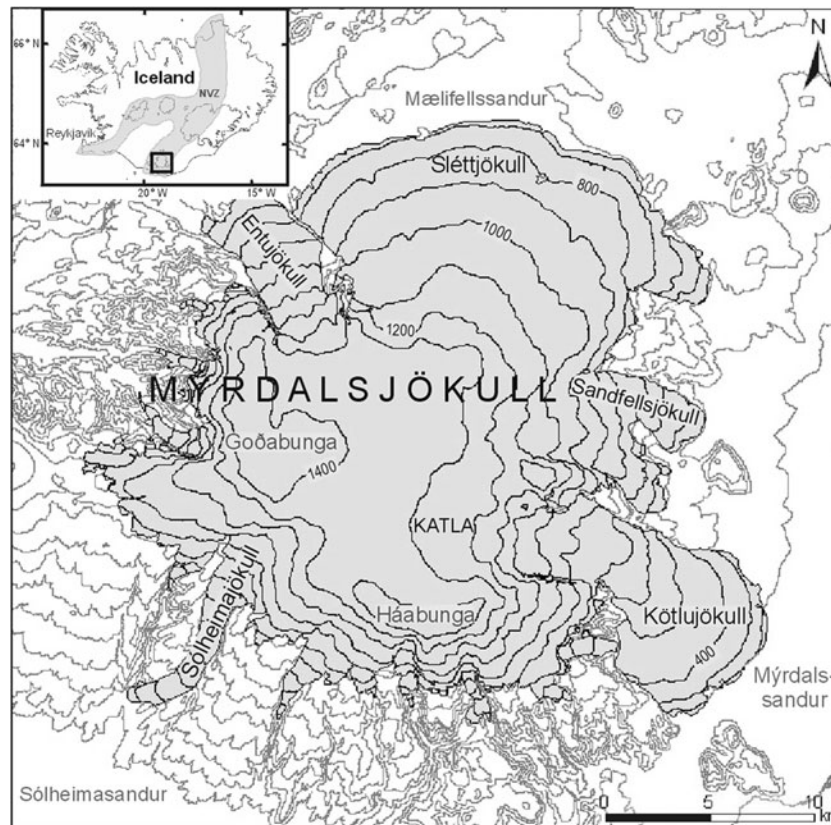
Fig. 1. The location of Mýrdalsjökull on the south coast of Iceland and in the southeastern part of the neovolcanic zone. The ice cap is characterized by a high, flat central part surrounded by a radial system of outlet glaciers. The margin is delineated from 2004 ASTER images; height contours from a DEM based on DMA (1990).

to delineate the glacier margin and determine the area extent of Mýrdalsjökull ice cap, Iceland. Furthermore, Envisat Advanced SAR (ASAR) data from 2004 and ERS-2 SAR data from earlier years are visually analyzed for snow- and firn-line monitoring. For this we used the findings of previous work regarding the radar-backscatter/glacier–surface interaction and then concentrated on the digital mapping of the detectable glacier zones. These data were implemented in a Geographical Information System (GIS) for further analysis and comparison. Thus, mass-balance conditions could be investigated qualitatively and then linked to weather data from nearby stations.

2. STUDY AREA

Mýrdalsjökull, the fourth largest ice cap in Iceland, has an area of about 590 km^2 (Fig. 1). It is located on the south coast of the island (63°40′ N, 19°05′ W) and at the southeastern end of the neovolcanic zone. The glacier ice covers the active volcano Katla which last erupted in 1918. Two eruptions have occurred within the Katla system every century on average during the last 1100 years (Larsen, 2000). Therefore, an eruption is expected in the near future. In addition, deloading due to a glacier mass loss induced by climate warming is also considered as a possible triggering mechanism for a future eruption (Sigvaldason and others, 1992).

This study visually analyzes the entire Mýrdalsjökull ice cap. Morphologically the ice cap can be divided into a plateau, where the ice forms a contiguous cover down to about 1300–1000 m a.s.l., and the peripheral zone below, where the ice cap splits into separate outlet glaciers (Fig. 1).

Ice lobes exist in the east and the north, such as Sléttjökull with a slope of <5°. Outlet glaciers on the western and southern side are much steeper. Sólheimajökull in the southwest shows typical characteristics of the tongue of a valley glacier. It terminates at 120 m a.s.l., the lowest point of Mýrdalsjökull, while the highest point is at about 1500 m a.s.l. (Goðabunga). Orographic effects are important due to the mountainous topography. The windward south-eastern slopes receive more snowfall than the northwestern slopes in the lee of the ice cap itself. This affects the position of the snow-/firn line. Temperature is mild for the latitude, due to the moderating influence of North Atlantic Drift waters that extend around the south coast of Iceland (warm Irminger current). The combination of warm ocean waters and a general southeasterly wind direction leads to a very high annual precipitation of >4000 mm on the southeastern slopes of Mýrdalsjökull and at least 2000 mm on the northwestern side (Mackintosh, 2000). More than 80% of the annual precipitation falls between September and May (Björnsson, 1979).

There are no in situ mass-balance data available for Mýrdalsjökull, and very few remote-sensing data of the ice cap have been analyzed so far (two ERTS-1 (Landsat) images from 1973 by Crabtree (1976); one Multispectral Scanner Landsat image from 1973 by R.S. Williams in Björnsson (1978); and one ERS-2 image from 1996 by Brown (1998), used for glacier extent and surface studies). Terminus fluctuations of Sólheimajökull have been manually measured since 1930. A retreat of 342 m between 1996 and 2004 has been recorded, with the largest annual retreat, 92 m, in 2003 (Sigurðsson, 1998, 1999, 2000a, b, 2001, 2002,

2003a, b, 2004, 2005). Due to the large size and inaccessibility of Mýrdalsjökull, the use of remote-sensing methods for investigating the whole ice cap is recommended.

3. DATA

3.1. Satellite images

Of all recorded ASTER images of Mýrdalsjökull from the launch of the Terra satellite in December 1999 until the end of 2004, there are only five useful, i.e. cloud-free, scenes. The resolution of the ASTER images is 15 m in the visible and very near-infrared spectrum (bands 1–3). These three bands were used to determine the glacier margin.

Due to frequent cloudiness in Iceland, radar imagery is very valuable for continuous monitoring of Mýrdalsjökull ice cap. The Envisat satellite, launched in March 2002, carries the ASAR sensor in continuation of the ERS-2 SAR mission. Data from these two radar sensors were used for this study. In total, 25 images of Mýrdalsjökull, most of them from 2004, were available (Table 1). The ERS-2 SAR and Envisat ASAR data were ordered as single look complex (SLC) images and processed to a pixel size of 12 m. Both radar sensors operate in C-band at a wavelength of 5.6 cm. All radar images used were acquired with vertical transmit-and-receive (VV) polarization. While ERS-2 scenes are imaged with a mean look angle of 23°, the ASAR antenna is steerable and seven different look angles (IS1–IS7, 14–45°) can be chosen by the user. The ASAR images of Mýrdalsjökull were ordered in image modes IS2 (23°) and IS5 (38°). Thus, a continuous ASAR data series for the year 2004 was built up with a temporal resolution of up to 9 days, including ascending (asc.) and descending (desc.) orbits (Table 1). The series was used for monitoring dynamic surface changes over 2004. In addition, two ERS-2 images from the end of mass-balance years 1997/98 and 1998/99, respectively, were used for investigating longer-term mass-balance fluctuations. For this study, there was no further SAR imagery available that could have been used to investigate other mass-balance years.

3.2. Additional data and image processing

Topographic maps from 1990 (DMA, 1990) were used to generate a digital elevation model (DEM) and for subsequent orthoprojection of all available satellite imagery, based on a common map projection (Universal Transverse Mercator, WGS84 zone 28). For the ASTER images a horizontal and vertical referencing accuracy of <15 m (1 pixel), i.e. displacement between image and reference map, was achieved. In order to optimize geocoding of the radar images, ten corner reflectors were used. These corner reflectors were installed in 1995 on five positions around Mýrdalsjökull. At each location, one reflector was orientated towards the ascending orbit and another towards the descending orbit. The corner reflectors are clearly identifiable points on the ERS-2 and ASAR images and therefore serve as high-quality ground-control points (GCPs). Due to the lack of infrastructure in the area surrounding the glacier (resulting in no easily identifiable features for GCPs), geocoding without corner reflectors would be difficult, time-consuming and imprecise. However, an accuracy of less than 1 pixel, i.e. 12 m, was achieved with the help of corner reflectors. The geocoding of some winter images required the use of topographic maps in addition to corner

Table 1. ERS-2 SAR, Envisat ASAR and Terra ASTER images of Mýrdalsjökull used in this study

Year	Date	Sensor
1998	21 August	SAR
1999	22 August	SAR
2003	4 February	ASTER
2004	9 January*	ASAR IS5 desc.*
	17 March	ASTER
	11 April	ASAR IS5 asc.
	23 April	ASAR IS5 desc.
	2 May	ASAR IS2 desc.
	16 May	ASAR IS5 asc.
	28 May	ASAR IS5 desc.
	6 June	ASAR IS2 desc.
	20 June	ASAR IS5 asc.
	21 June	ASTER
	6 August	ASAR IS5 desc.
	29 August	ASAR IS5 asc.
	10 September	ASAR IS5 desc.
	19 September	ASAR IS2 desc.
	23 September	ASTER
	15 October	ASAR IS5 desc.
	24 October*	ASAR IS2 desc.*
	25 October	ASTER
	7 November	ASAR IS5 asc.
	19 November*	ASAR IS5 desc.*
	28 November*	ASAR IS2 desc.*
	24 December*	ASAR IS5 desc.*

Note: ASAR images acquired during freezing conditions over the high, flat central part of Mýrdalsjökull are marked *.

reflectors, as some of the reflectors were not visible, possibly because they were filled with wet or heavily metamorphosed snow, preventing sufficient backscatter.

After the geocoding, a few satellite images had to be co-registered, i.e. made to conform to each other to remove slight displacements between the images. This is very important for boundary delineation and comparison. It has to be mentioned that the radar images were not radiometrically corrected, and thus no σ^0 backscatter images (dB values) were generated. This processing step is only necessary for quantitative, not for visual, image analyses.

In addition to the satellite imagery, oblique photography from an aerial survey in 2004 and local knowledge was helpful for delineating the glacier margin in questionable regions on the ASTER images. Weather data from eight nearby weather stations, of which seven are located south and one east of Mýrdalsjökull, were obtained from the Icelandic Meteorological Office. For the year 2004, hourly and daily data of different meteorological parameters (e.g. temperature, precipitation and wind) were available. Monthly mean values of temperature and precipitation, recorded since 1961 at two nearby weather stations (Vatnsskarðshólar and Vík), were downloaded from the Internet (http://www.vedur.is).

4. RADAR IMAGE ENHANCEMENT

After geocoding and co-registration, an image enhancement operation was applied to the summer radar scenes. Various techniques were tested in order to optimize the contrast between wet snow and glacier ice for visual boundary detection. The following three-step method was found to be
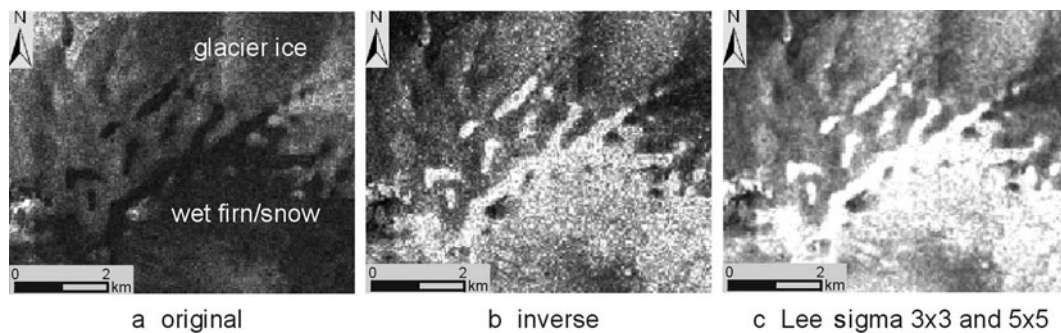
Fig. 2. (a) A 6 × 7.5 km detail of an ASAR image of Sléttjökull, acquired on 10 September 2004. (b, c) Image enhancement for the boundary detection between wet firn/snow and glacier ice on Mýrdalsjökull by first generating an 'inverse' image (b) and then running a Lee sigma filter with a 3×3 and 5×5 window (c). © European Space Agency 2004.

the best: First, an 'inverse' image is generated (default function available in ERDAS Imagine), then a Lee sigma filter is applied twice, using a 3×3 window, followed by a 5×5 window. 'Inverse' is a brightness inversion function which emphasizes detail that would otherwise be lost in the low-digital-number (low-DN) (dark) pixels. In addition, the input data range (DN 0–255) is scaled to 0–1.0. The Lee sigma filter reduces the radar speckle, i.e. areas become more homogeneous and boundaries are sharpened. The result of these image enhancement steps is illustrated in Figure 2.

5. IMAGE ANALYSIS

After image processing, boundaries were manually digitized on the satellite images in ESRI's ArcGIS environment. While the ASTER images were used for delineating the glacier margin, the glacier surface changes were monitored using the radar images.

5.1. Glacier margin

To delineate the whole glacier margin of Mýrdalsjökull ice cap, four ASTER images from 2004 were necessary (Table 1). Most of the glacier margin was detected on the image acquired on 23 September 2004. However, additional data were needed because of clouds over the southern outlet glaciers on that scene and due to debris cover on the glacier front of Sléttjökull in the north and Kötlujökull in the southeast. Debris cover is not distinguishable from the glacier forefield on summer images. However, the debris-covered glacier margins were clearly detectable on the winter images because the two outlet glaciers terminate on a sandur plain, forming a distinct topographic edge. It is assumed that the regional-margin changes within the observation period (March–October) are not considerably larger than the ASTER image resolution, which allows us to produce a continuous glacier margin for 2004.

5.2. Snow-/firn-line monitoring

In late summer, only two glacier facies can be observed on Mýrdalsjökull: the wet-snow facies and the ablation facies (classification according to Benson, 1962; Williams and others, 1991). This is typical for temperate glaciers (Paterson, 1981). The wet-snow facies consists of melting snow and/or melting firn. Firn is defined as snow that is at least 1 year old, to distinguish it from snow fallen in the mass-balance year under consideration (Oerlemans, 2001). At the end of a mass-balance year, the wet-snow facies and the ablation

facies, i.e. the bare glacier ice, are separated either by the TSL or, if firn is exposed, by the FL, depending on the weather conditions during the ablation season. The discrimination of snow and firn is important for the detection of the equilibrium line (EL). The EL equals the TSL at the end of a balance year, and its position contains information about the mass balance.

The boundary between the wet-snow facies and the ablation facies is detectable on radar images (e.g. Rott and Mätzler, 1987; Hall and others, 1995). The discrimination of wet-snow facies and glacier ice is based on the difference in their backscatter intensity: wet snow absorbs the radar signal, while glacier ice shows strong backscattering due to surface roughness. However, it is not possible to discriminate snow and firn on single-polarized C-band radar images due to similar backscatter values (e.g. König and others, 2001; de Ruyter de Wildt and others, 2002). Consequently, the TSL or EL at the end of the mass-balance year is only visible on radar images if no firn is exposed at the glacier surface. Nevertheless, the temporal and spatial evolution of the TSL, which varies each year, also contains information about the mass balance of a glacier. De Ruyter de Wildt and Oerlemans (2003) explain that the TSL or FL on a glacier separates the area of high albedo (snow/firn) and relatively low albedo (ice) which strongly determines the amount of surface melt and hence the mass balance. In addition, the evolution of the TSL reflects the accumulation history of the preceding winter. As the TSL position affects the amount and timing of seasonal melt discharge, its evolution yields interesting information for hydrologic research.

Since the boundary between wet snow and bare ice on radar summer images is either the TSL or the FL, it is abbreviated to TSL–FL (first used by de Ruyter de Wildt and Oerlemans, 2003) in this study. Furthermore, the term 'radar glacier zones', introduced by Forster and others (1996) and also used by other authors (e.g. Forster and others, 1997; Smith and others, 1997; Ramage and others, 2000), was found to be more appropriate than using the glaciological facies definition. In contrast to the glacier facies, which imply an annual timescale, the radar glacier zones develop on a timescale of days and weeks. Forster and others (1996) define four radar glacier zones which they found on the temperate HPS by comparing C- and L-band imagery from the space-shuttle missions in 1994: a relatively dry-snow zone, a moderately wet-snow zone, a wet-snow zone (with weak returns in both bands) and a bare-ice zone (with strong returns in both bands). Analyzing C-band data, on

Mýrdalsjökull only a wet-snow zone and a bare-ice zone can be observed. At the end of the melt season, these zones equal Benson's wet-snow and ablation facies, respectively. Smith and others (1997) show for the Stikine icefields, British Columbia, Canada, that meltwater production is affected by the development of these radar glacier zones.

In this study, the TSL–FL, separating the wet-snow zone and the bare-ice zone, was manually delineated on seven ASAR summer images of Mýrdalsjökull, acquired between 11 April and 10 September 2004. The latter image marks the end of mass-balance year 2003/04 due to snowfall on 16 and 17 September below the FL and a consecutive snow cover throughout the winter. The TSL–FL was also clearly detectable on the ERS-2 images from the end of August 1998 and 1999. It was found that ASAR IS5 descending images are preferable over ascending and IS2 images for TSL–FL digitizing due to the topography of Mýrdalsjökull with its steep western outlet glaciers. These cause sensor over-saturation due to topographic foreshortening and layover.

On three summer images, acquired during the 2004 melt season, the TSL–FL could not be detected due to areas within the wet-snow zone that show unusually high back-scatter values, similar to those of the glacier ice. Bright areas within the otherwise dark wet-snow zone are also visible on other summer images, but there they do not disturb the course of the TSL–FL. De Ruyter de Wildt and Oerlemans (2003) found similar bright backscatter areas within the wet-snow zone on 5 out of 43 ERS-1/-2 SAR summer images of Vatnajökull ice cap, located northeast of Mýrdalsjökull (see Fig. 1). Analyzing the weather data from stations close to Mýrdalsjökull, the isolated high backscatter values seem to be caused by increased surface roughness or a decrease in snow wetness due to special weather conditions such as a rainstorm, a strong temperature drop (refreezing), or a dust storm from the sandur plains. These are only short-term events and therefore alter the radar glacier zones only for a few hours or days. In the case of a rainstorm and a sharp temperature decrease, this is confirmed by Forster and others (1997) using sub-daily space-shuttle SAR imagery for investigating HPS. Due to the isolated bright areas within the wet-snow zone on Mýrdalsjökull, automatic zone detection with a *k*-means algorithm could not be success-fully applied over the glacier surface.

Since the C-band SAR signal is able to transmit through dry snow, often winter images are used to detect the position of the EL or FL from the end of the mass-balance year (e.g. König and others, 2001; Engeset and others, 2002; Storvold and others, 2005). In the case of Mýrdalsjökull, however, winter radar images are not useful for mass-balance obser-vations because melting conditions also occur frequently in the winter (see Table 1). Thus, the winter snow cover is no longer transparent for C-band radar.

6. RESULTS

6.1. Estimation of errors

All processing steps introduce some uncertainty in the area measurements. However, all area uncertainties are small compared to the large area of Mýrdalsjökull and its wet-snow zone. Two kinds of errors can be discriminated: systematic and random errors. The latter are introduced by the analyst during the mapping of glacier boundaries on the satellite images. Systematic errors result from the spatial

resolution of the satellite data, the DEM resolution and generation as well as the geocoding of the imagery. There is a maximum displacement error of ± 12 m for ERS-2 SAR and Envisat-ASAR data and ± 15 m for ASTER data. The displace-ment error introduced by the DEM resolution is ± 20 m in the vertical and ± 12 m in the horizontal direction. From the DEM generation an error of ± 2.6 m in height (from digitizing contour lines) plus an unknown interpolation error has to be added. The geocoding accuracy is ± 1 pixel for all used imagery. After orthoprojection the accuracy must be reduced to less than 1 pixel.

Thus, delineation of the glacier margin on 15 m resolution ASTER images results in an error of ± 4 km^2 for the glacier area. The DEM used in this study is the largest source of error for the calculation of glacier areas. This is due to elevation changes of the ice cap in recent years. A maximum error of 1.5% is estimated for the whole glacier area. The relative accuracy of the results, however, is very high due to the use of corner reflectors for radar image geocoding, which allows a highly precise (sub-pixel) co-referencing of the individual radar images.

6.2. Area of Mýrdalsjökull

It is important to know the present area of a glacier for a quantitative mass-balance comparison with past and future years which can then be related to a climatic change. The glacier area is needed for determining the accumulation-area ratio (AAR), a characteristic of glacier mass balance (see section 6.4). By delineating the glacier margin of Mýrdals-jökull on ASTER images and combining it with the existing DEM, a total glacier area of 586 ± 13 km^2 was determined for 2004. At the beginning of the 20th century, the area was about 700 km^2, measured from topographic maps (Björns-son, 1978). The extent of the glacier then shrank to about 596 km^2 in 1973, as determined from a Landsat satellite image (80 m resolution) by R.S. Williams (in Björnsson, 1978) (the error margin is estimated to be ± 22 km^2, resulting from the coarse image resolution). The area reduction of Mýrdalsjökull in the second half of the 20th century, compared to the first half, corresponds to in situ measure-ments of the Sólheimajökull terminus (Sigurðsson, 1998). Such long-term glacier variations can be investigated by monitoring the glacier area. However, for short- and medium-term reactions of a glacier to changes in climatic conditions, it is necessary to measure the mean specific mass balance (B_m). Without having in situ B_m data, as in the case of Mýrdalsjökull, the AAR is a suitable parameter for describing the state of a glacier. The AAR, determined from the calculated equilibrium-line altitude (ELA), and B_m correlate significantly (Oerlemans, 2001). The use of SAR data for AAR determination is discussed in section 6.4. The next subsection shows the results of the radar glacier zone analysis by comparing snow- and firn lines as well as investigating their position and evolution within a Geo-graphical Information System (ArcGIS by ESRI).

6.3. The snow- and firn lines in 2004

Figure 3 shows the result of the ASAR 2004 summer image analysis as described above. On six summer images, the boundary between the wet-snow zone and the glacier ice zone was digitized to monitor the spatial and temporal evolution of the TSL–FL. During the melt period, a reduction of the wet-snow zone by 335 km^2 was measured, with the largest daily area loss in June (see Table 2), even though the
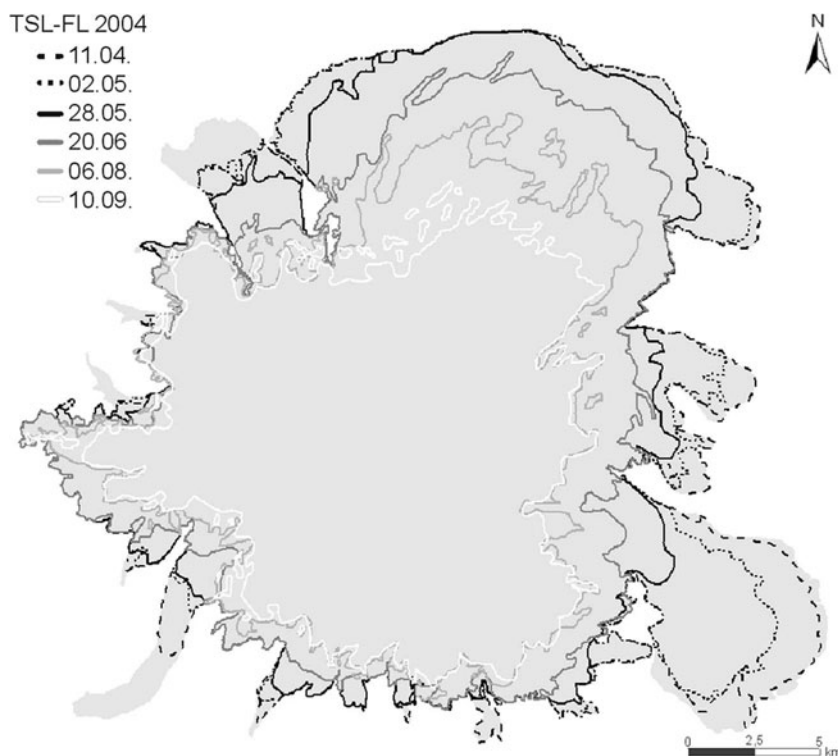
Fig. 3. Retreat of the TSL–FL on Mýrdalsjökull, 11 April–10 September 2004 (boundaries delineated on ASAR images). Dates are dd/mm.

highest air temperatures were reached in August. This indicates that firn was exposed on the glacier surface in summer 2004. In general, the FL maintains a more stable position than the TSL, because of higher densification of the snowpack and thus lower melt rates. Furthermore, 2004 was an unusually warm year. Therefore, the boundary of the wet-snow zone, as determined from the 10 September 2004 radar image (white in Fig. 3), is assumed to be the late-summer FL. For this situation, the FL represents the theoretical maximum extent of the accumulation area. A more accurate position of the EL cannot be derived from the analysis of the 2004 ASAR single-polarized C-band imagery. The altitude of the FL varies over the large ice cap due to orographic effects. In 2004, its lowest position, 1020 m a.s.l., is on Kötlujökull outlet glacier, which is located on the
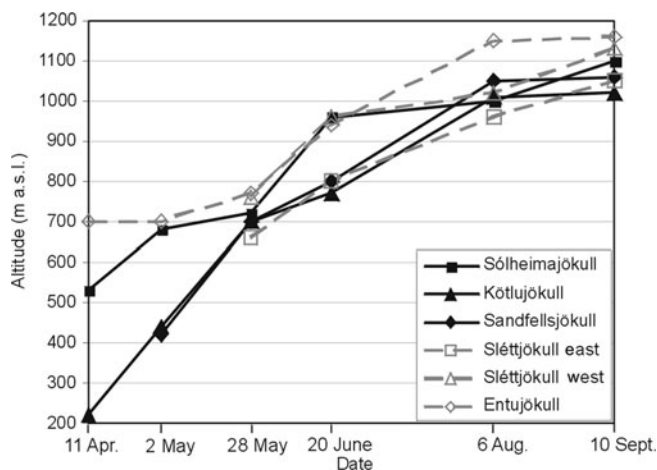
maritime and windward eastern side of Mýrdalsjökull. It reaches a maximum of 1160 m a.s.l. on Entujökull, located on the more continental and drier northwestern side. On Sléttjökull the transition between the windward and the lee exposition of the glacier is visible, where the FL gradually decreases in altitude from west to east (Fig. 3). The position of the FL, influenced by the mountainous topography of the ice cap, can best be investigated when overlain on the DEM and displayed in three dimensions (e.g. using the program ArcScene within ArcGIS).

Figure 4 illustrates the development of the TSL–FL altitude during the 2004 melt season on six outlet glaciers of Mýrdalsjökull. Due to the different topographic influences on Sléttjökull, the glacier has been separated into an eastern and western part. Figure 4 demonstrates that changes in the TSL–FL altitude are in general reduced between 6 August and 10 September. It is assumed that in late July the TSL reaches the FL. Afterwards the wet-snow zone consists of snow and firn which cannot be distinguished. Figure 4 also shows that for most of the melt season the TSL–FL is at higher altitudes on Sólheimajökull than on the other windward outlet glaciers (Kötlujökull, Sandfellsjökull, Sléttjökull east). This is probably due to higher direct and indirect sun irradiance because of its south-facing slopes and the proximity of the ocean.

As already mentioned, the TSL–FL contains information about the mass balance of a glacier since it separates high- and low-albedo zones and shows an annual evolution characteristic of the balance year under investigation. Many glaciological studies use the ELA to infer the mean specific mass balance. However, de Ruyter de Wildt and Oerlemans (2003) have successfully correlated the average altitude of the TSL–FL, derived from ERS SAR images, during the second half of the melt season with in situ mean specific mass-balance (B_m) values for some drainage basins of

Fig. 4. Development of the TSL–FL altitude on various outlet glaciers of Mýrdalsjökull in 2004 (for glacier location see Fig. 1).
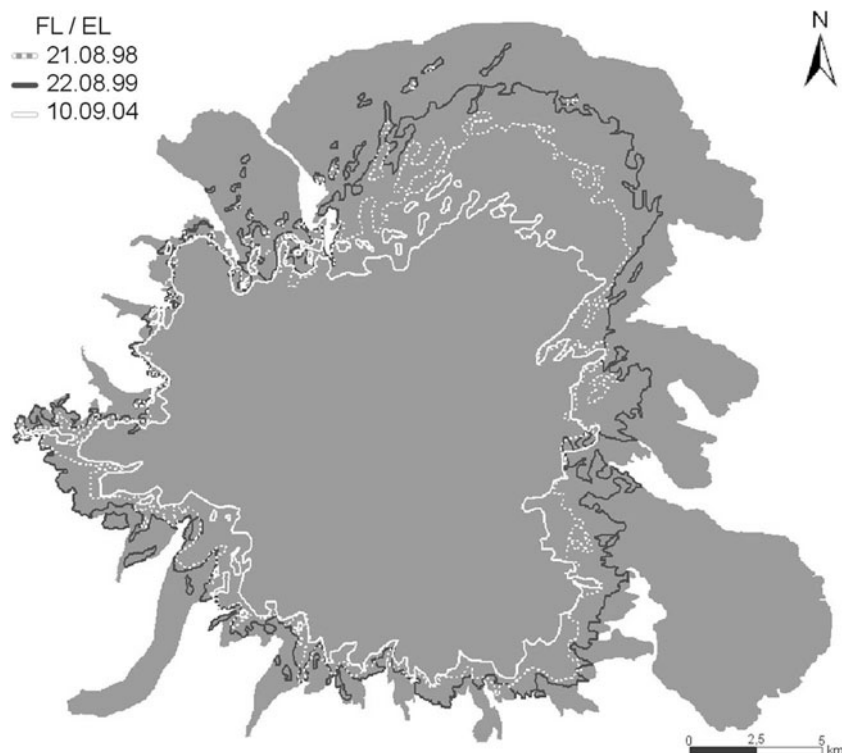
Fig. 5. Three different mass-balance situations of Mýrdalsjökull at the end of melt seasons 1998, 1999 and 2004. There is a clear difference in the position of the FL/EL between the individual years, and thus in the glacier mass balance. Boundaries delineated on two ERS-2 images and one ASAR 2004 image. Dates are dd.mm.yy.

Vatnajökull. For this study, it would be interesting to test the relationship between B_m and the temporal evolution of the wet-snow zone. In this case, no smoothing of the TSL–FL altitude would be necessary, and the method could be applied to large entire ice caps like Mýrdalsjökull. However, this method requires in situ B_m values which are not available for Mýrdalsjökull.

6.4. Mass-balance fluctuations

In Figure 5, the wet-snow/bare-ice zone boundaries delineated on the late-summer radar images from 10 September 2004, 21 August 1998 and 22 August 1999 are displayed together for relative mass-balance investigations. Snowfall on Mýrdalsjökull occurs mainly between September and April, i.e. the mass-balance year generally ends in early September. From analyzing the evolution of the 2004 radar glacier zones (see section 5.2), it is obvious that the melt season ended at the beginning of September 2004 at the latest. A comparison of all available summer radar images shows that in early August 2004 the TSL–FL had already reached a higher elevation than in the late-August images of 1998 and 1999. Moreover, the air temperatures recorded at Vatnsskarðshólar station, located 13 km south of the Mýrdalsjökull glacier margin, show significantly lower August temperatures in 1998 and 1999 compared with 2004 (mean temperature difference of 3.5–4.0°C). Due to the comparatively cold late-summer temperatures, it is assumed that the two late-August images from 1998 and 1999 represent the end of the ablation seasons. Thus, the TSL–FL of these images can be interpreted as the FL or EL of mass-balance years 1997/98 and 1998/99. In Figure 5, a large displacement between the three snow-/firn lines is especially recognizable on the flat and extended Sléttjökull.

The considerable distance between these late-summer snow-/firn lines indicates a distinct mass-balance difference between the three balance years. Given the proximity of the warm ocean and the low altitude of Mýrdalsjökull, high annual mass-balance fluctuations are not surprising.

The late-summer radar imagery of Mýrdalsjökull enables a relative mass-balance comparison without the need for in situ data. The FL in late summer 2004 is clearly located above the other boundaries in Figure 5, i.e. the mass-balance year 2003/04 is highly negative compared to 1998 and 1999. Area measurements show that at the end of summer 2004, 124 km² more glacier ice was exposed to melting than in 1999. The boundary in 1999 is located at a lower elevation than at the end of the previous balance year. Thus, the delineated boundary must be the snowline and represents the EL for the 1998/99 mass-balance year.

Table 2. Areal reduction of the wet-snow zone on Mýrdalsjökull in 2004 as measured on six ASAR images (total glacier area 586 km²)

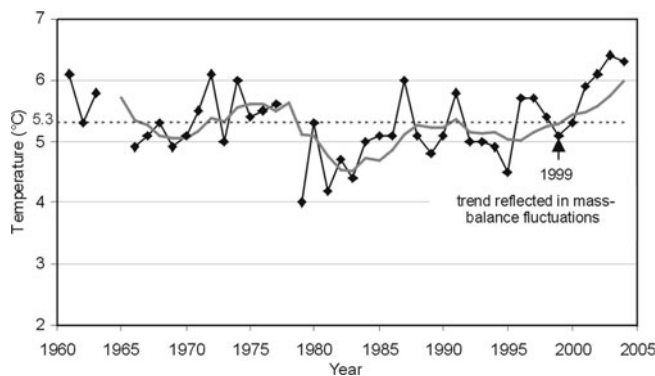| Date (2004)	Radar wet-snow zone	Daily area loss between image dates
	km²	km² d⁻¹
11 April	564	
2 May	539	1.2
28 May	482	2.2
20 June	409	3.2
6 August	305	2.2
10 September	251	1.5

Fig. 6. The annual mean air temperature recorded at Vatnsskarð-shólar weather station, 1961–2004 (black lines and symbols). The solid grey line is the running mean over 5 years. The dashed line marks the 5.3°C mean of the years 1961–2004. Data source: Icelandic Meteorological Office.

Compared to the previous year, the balance year 1998/99 is positive, and an AAR of about 0.64 was determined. For 1998 it is not possible to decide whether the detected boundary is the EL or the FL since no further radar imagery from 1998 or 1997 was available for this study. For mass-balance year 2003/04 the AAR can only be estimated since the wet-snow zone, as determined from radar image analysis, includes snow from the balance year under investigation and firn from the previous year/s. In 2004 the EL is located somewhere above the FL, so the AAR is somewhat smaller than the 'wet-snow zone divided by glacier area'. Since radar imagery can often only detect the FL and not the EL, the term firn-area ratio (FAR) is introduced:

FAR = wet-snow zone (including snow and firn)/glacier area.

This parameter can be applied to mass-balance investigations by means of radar imagery when the mass-balance year under investigation is negative compared to the previous year. At present, this is frequently the case for many glaciers due to the warming climate. In general, the FAR will show smaller annual changes than the AAR since the FL is usually more stable than the EL. At Mýrdalsjökull the FAR for mass-balance year 2003/04 is 0.43. So far, this is the only available FAR value for Mýrdalsjökull. Therefore, it has to be compared with the AAR which is <0.43. This suggests that 2003/04 was a negative mass-balance year since the AAR for zero mass balance is generally 0.5–0.8 for temperate mountain glaciers (Meier and Post, 1962). As a comparison, the trend of B_m values measured at Vatnajökull is similar to the mass-balance observations at Mýrdalsjökull. B_m values of Vatnajökull were measured from 1993 to 1999 (de Ruyter de Wildt and Oerlemans, 2003). Since 1995, negative values have been recorded. The year 1999, with a value of –0.26 m w.e., was less negative than 1998 (–0.77 m w.e.), which is in agreement with our observations.

The mass-balance situation of the three investigated years at Mýrdalsjökull is well reflected in the annual mean air temperatures measured at Vatnsskarðshólar weather station (cf. Figs 5 and 6). The mean temperature in 2004 was 1.2°C higher than in 1999, but 1999 was 0.2°C colder than 1998. The mean winter temperatures (November–March) are low enough in all years to prevent considerable

runoff from the glacier, and the annual precipitation does not show significant variation. This suggests that the summer temperatures are the driving factor for mass-balance fluctuations at Mýrdalsjökull ice cap. This is in agreement with Jóhannesson and Sigurðsson (1998) who also found a general relation between summer temperatures and glacier fluctuations in Iceland. Furthermore, the duration of the melt season at Mýrdalsjökull has increased in recent years due to increasing mean temperatures in April and September.

7. CONCLUSIONS

This study shows that remote-sensing data are of great use for continuous mass-balance monitoring of Mýrdalsjökull. The investigation of this large ice cap (586 ±13 km^2), which is located in a sparsely populated area, would not be possible without the use of remote-sensing data.

Analysis was carried out on several ASTER images, a time series of Envisat ASAR images for the year 2004 and two ERS-2 SAR images, acquired at the end of mass-balance years 1997/98 and 1998/99, respectively. This combination of optical and radar satellite data proved to be very useful for mass-balance investigations. The sensors acquire different characteristics of the glacier surface and subsurface and thus yield complementary information when combined. With four ASTER images from 2004, the whole glacier margin was delineated and the area of Mýrdalsjökull determined. For glacier margin detection, summer as well as winter optical images are required. It was found that winter SAR images are not useful for mass-balance studies at Mýrdalsjökull because of frequent surface melt conditions even during wintertime. However, with summer SAR images the dynamic glacier surface changes during the ablation season can be continuously monitored. The TSL is detectable as long as no firn is exposed. It is known that wet snow and wet firn cannot be discriminated on single-polarized C-band SAR imagery. Consequently, the EL is often not detectable because most mass-balance years have been negative for the last decade. Therefore, we suggest mass-balance investigations by monitoring temporal and spatial fluctuations of the snow- and firn line rather than the EL. We propose a SAR image enhancement method which improves the contrast between glacier ice and wet snow/firn, allowing better manual delineation of the snow- or firn line. Furthermore, we introduce the term FAR (firn-area ratio) in addition to the known AAR (accumulation-area ratio). The FAR can be used for mass-balance investigations if the radar imagery reveals the FL and not the EL.

Quantitative mass-balance measurements still require in situ data besides remote-sensing data. With this study, conclusions of relative mass-balance fluctuations of Mýrdalsjökull between 1998 and 2004 could be made. In cases where the vertical balance profile is known (e.g. from field measurements), the relative position of the EL allows quantification of the mass-balance conditions. For years where only the FL can be detected, at least a quantitative estimate of the mass balance can be made. The mass-balance fluctuations of Mýrdalsjökull are reflected in the change in annual mean air temperatures recorded at nearby weather stations, with the summer temperatures the driving factor. With a mean temperature of 6.3°C, the year 2004 was unusually warm and shows, with a FAR of 0.43, a highly negative mass balance.

REFERENCES

Benson, C.S. 1962. Stratigraphic studies in the snow and firn of the Greenland ice sheet. *SIPRE Res. Rep.* 70.

Björnsson, H. 1978. The surface area of glaciers in Iceland. *Jökull,* **28**, 31.

Björnsson, H. 1979. Glaciers in Iceland. *Jökull,* **29**, 74–80.

Brown, I.A. 1998. The analysis of glacier firn lines and the firn dynamics of Icelandic ice caps using remote sensing and other data. (PhD thesis, University of Dundee.)

Crabtree, R.D. 1976. Changes in Mýrdalsjökull ice cap, south Iceland: possible uses of satellite imagery. *Polar Rec.,* **18**(112), 73–76.

Defense Mapping Agency (DMA). 1990. *Topographic map of Iceland, 1 : 50 000. Sheets 1812-II, 1912-I, 1912-III, 1912-IV.* Washington DC, Defense Mapping Agency.

de Ruyter de Wildt, M.S., J. Oerlemans and H. Björnsson. 2002. A method for monitoring glacier mass balance using satellite albedo measurements: application to Vatnajökull, Iceland. *J. Glaciol.,* **48**(161), 267–278.

de Ruyter de Wildt, M.S. and J. Oerlemans. 2003. Satellite retrieval of mass balance: comparing SAR images with albedo images and in situ mass-balance observations. *J. Glaciol.,* **49**(166), 437–448.

Engeset, R.V., J. Kohler, K. Melvold and B. Lundén. 2002. Change detection and monitoring of glacier mass balance and facies using ERS SAR winter images over Svalbard. *Int. J. Remote Sens.,* **23**(10), 2023–2050.

Fahnestock, M., R. Bindschadler, R. Kwok and K. Jezek. 1993. Greenland ice sheet surface properties and ice dynamics from ERS-1 SAR imagery. *Science,* **262**(5139), 1530–1534.

Forster, R.R., B.L. Isacks and S.B. Das. 1996. Shuttle imaging radar (SIR-C/X-SAR) reveals near-surface properties of the South Patagonian icefield. *J. Geophys. Res.,* **101**(E10), 23,169–23,180.

Forster, R.R., L.C. Smith and B.L. Isacks. 1997. Effects of weather events on X-SAR returns from ice fields: case-study of Hielo Patagónico Sur, South America. *Ann. Glaciol.,* **24**, 367–374.

Hall, D.K., R.S. Williams, Jr and O. Sigurðsson. 1995. Glaciological observations of Brúarjökull, Iceland, using synthetic aperture radar and thematic mapper satellite data. *Ann. Glaciol.,* **21**, 271–276.

Hall, D.K., R.S. Williams, Jr, J.S. Barton, L.C. Smith and J.B. Garvin. 2000. Evaluation of remote-sensing techniques to measure decadal-scale changes of Hofsjökull ice cap, Iceland. *J. Glaciol.,* **46**(154), 375–388.

Houghton, J.T. and 7 others. 2001. *Climate change 2001: the scientific basis. Contribution of Working Group I to the Third Assessment Report of the Intergovernmental Panel on Climate Change.* Cambridge, etc., Cambridge University Press.

Jóhannesson, T. and O. Sigurðsson. 1998. Interpretation of glacier variations in Iceland 1930–1995. *Jökull,* **45**, 27–33.

König, M., J.G. Winther, N.T. Knudsen and T. Guneriussen. 2001. Firn-line detection on Austre Okstindbreen, Norway, with airborne multipolarization SAR. *J. Glaciol.,* **47**(157), 251–257.

Larsen, G. 2000. Holocene eruptions within the Katla volcanic system, south Iceland: characteristics and environmental impact. *Jökull,* **49**, 1–28.

Mackintosh, A. 2000. Glacier fluctuations and climate change in Iceland. (PhD thesis, University of Edinburgh.)

Mackintosh, A.N., A.J. Dugmore and A.L. Hubbard. 2002. Holocene climatic changes in Iceland: evidence from modelling glacier length fluctuations at Sólheimajökull. *Quat. Int.,* **91**(1), 39–52.

Meier, M.F. and A.S.Post. 1962. Recent variations in mass net budgets of glaciers in western North America. *IASH Publ.* 58 (Symposium at Obergurgl 1962 – *Variations of the Regime of Existing Glaciers*), 63–77.

Oerlemans, J. 2001. *Glaciers and climate change.* Lisse, etc., A.A. Balkema.

Paterson, W.S.B. 1981. *The physics of glaciers. Second edition.* Oxford, etc., Pergamon Press.

Ramage, J.M., B.L. Isacks and M.M. Miller. 2000. Radar glacier zones in southeast Alaska, U.S.A.: field and satellite observations. *J. Glaciol.,* **46**(153), 287–296.

Rott, H. and C. Mätzler. 1987. Possibilities and limits of synthetic aperture radar for snow and glacier surveying. *Ann. Glaciol.,* **9**, 195–199.

Sigurðsson, O. 1998. Glacier variations in Iceland 1930–1995. From the database of the Iceland Glaciological Society. *Jökull,* **45**, 3–25.

Sigurðsson, O. 1999. Jöklabreytingar 1930–1960, 1960–1990 og 1995–1996. *Jökull,* **47**, 101–107.

Sigurðsson, O. 2000a. Jöklabreytingar 1930–1960, 1960–1990 og 1996–1997. *Jökull,* **48**, 63–69.

Sigurðsson, O. 2000b. Jöklabreytingar 1930–1960, 1960–1990 og 1997–1998. *Jökull,* **49**, 83–90.

Sigurðsson, O. 2001. Jöklabreytingar 1930–1960, 1960–1990 og 1998–1999 (glacier variations). *Jökull,* **50**, 129–136.

Sigurðsson, O. 2002. Jöklabreytingar 1930–1960, 1960–1990 og 1999–2000 (glacier variations). *Jökull,* **51**, 79–86.

Sigurðsson, O. 2003a. Jöklabreytingar 1930–1960, 1960–1990 og 2000–2001 (glacier variations). *Jökull,* **52**, 61–67.

Sigurðsson, O. 2003b. Jöklabreytingar 1930–1960, 1960–1990 og 2001–2002 (glacier variations). *Jökull,* **53**, 55–62.

Sigurðsson, O. 2004. Jöklabreytingar 1930–1960, 1960–1990 og 2002–2003 (glacier variations). *Jökull,* **54**, 75–83.

Sigurðsson, O. 2005. Jöklabreytingar 1930–1960, 1960–1990 og 2003–2004 (glacier variations). *Jökull,* **55**, 163–170.

Sigvaldason, G.E., K. Annertz and M. Nilsson. 1992. Effect of glacier loading/deloading on volcanism: postglacial volcanic production rate of the Dyngjufjöll area, central Iceland. *Bull. Volcanol.,* **54**(5), 385–392.

Smith, L.C., R.R. Forster, B.L. Isacks and D.K. Hall. 1997. Seasonal climatic forcing of alpine glaciers revealed with orbital synthetic aperture radar. *J. Glaciol.,* **43**(145), 480–488.

Storvold, R., K.A. Høgda, E. Malnes and I. Lauknes. 2005. SAR firn line detection and correlation to glacial mass balance; Svartisen Glacier, Northern Norway. *In* Lacoste, H. and L. Ouwehand, eds. *Proceedings of the 2004 Envisat & ERS Symposium, 6–10 September 2004, Salzburg, Austria (ESA SP-572).* Noordwijk, European Space Agency.

Williams, R.S., Jr, D.K. Hall and C.S. Benson. 1991. Analysis of glacier facies using satellite techniques. *J. Glaciol.,* **37**(125), 120–128.

Paper 2

Scharrer K, Mayer Ch, Nagler T, Münzer U, Gudmundsson Á (2007) Effects of ash-layers of the 2004 Grímsvötn eruption on SAR backscatter in the accumulation area of Vatnajökull. Annals of Glaciology, 45, 189-196.

Reprinted from the Annals of Glaciology with permission of the International Glaciological Society.

Effects of ash layers of the 2004 Grímsvötn eruption on SAR backscatter in the accumulation area of Vatnajökull

K. SCHARRER,[1] C. MAYER,[2] T. NAGLER,[3] U. MÜNZER,[1] Á. GUÐMUNDSSON[4]

[1]Ludwig-Maximilians-University, Department of Earth and Environmental Sciences, Section Geology, Luisenstr. 37, 80333 Munich, Germany
Email: k.scharrer@iaag.geo.uni-muenchen.de
[2]Bavarian Academy of Sciences and Humanities, Commission for Glaciology, Alfons-Goppel Str. 11, 80539 Munich, Germany
[3]ENVEO IT GmbH, Technikerstr. 21a, A-6020 Innsbruck, Austria
[4]Fjarkönnun ehf, Furugrund 46, 200 K'pavogur, Iceland

ABSTRACT. The applicability of volcanic ash deposits on Vatnajökull ice cap, Iceland, as a time reference marker for measuring accumulation by the analysis of time sequential SAR backscatter data was investigated. A volcanic eruption at Grímsvötn caldera, a subglacial volcanic system beneath Vatnajökull, deposited an ash layer north of the vent in early November 2004. This ash layer covered a V-shaped area of ~88 km^2 on the glacier surface. The ash fall, which was subsequently buried by snow, reveals a distinct backscatter signal in SAR images. In total, the σ^0 backscatter values of 40 ENVISAT-ASAR images were analyzed, covering two post-eruption accumulation periods (4 November 2004 to 31 March 2005 and 25 October 2006 to 14 March 2006). Significant differences over time were observed in the SAR backscatter signals over the deposited ash, which appear to be related to the snow accumulation history. The backscatter signals were compared to meteorological conditions at the time of SAR acquisition and to accumulation data derived from two snow pits, one located within the ash fall. A linear regression analysis between the accumulation data and the SAR backscattering coefficient results in high R^2 confidence values (>0.8), indicating that the SAR data can be used for estimating the areal accumulation distribution in areas with an existing ash layer.

INTRODUCTION

Due to its climatic and physical conditions, Iceland presents an ideal test site to monitor various geo-dynamic processes. At present, ~11% of the 103 000 km^2 volcanic island is covered by glacier, represented mainly by four large ice caps: Vatnajökull (8100 km^2); Langjökull (953 km^2); Hofsjökull (925 km^2); and Mýrdalsjökull (596 km^2) (Björnsson, 1978). The huge ice masses of these glaciers cover several volcanic systems with central volcanoes, crater chains and fissures (Björnsson and Einarsson, 1990). The rift zone of the Mid-Atlantic ridge, which superficially crosses the island, is responsible for the high seismic and volcanic activity.

The southern part of this highly active Neovolcanic Zone, underlying the ice caps of Mýrdals- and Vatnajökull, has been the focus of several ESA earth observation projects since 1995. At present, ENVISAT-ASAR collects SAR data on a regular basis within the project 'Hazard Assessment and Prediction – Long-term Observation of Icelandic Volcanoes and Glaciers Using ENVISAT-ASAR and Other Radar Data' (ESA, ID142). The ASAR instrument is a side-looking C-band SAR antenna operating at a wavelength of 5.6 cm, where the image swaths IS2 (incidence angle 21.5°) and IS5 (incidence angle 37.5°) are continuously acquired over Vatnajökull ice cap for monitoring the subglacial volcanic activities.

On 1 November 2004 (ca. 22:00 GMT) a 6 day eruption at Grímsvötn caldera (a subglacial volcanic system beneath the western part of Vatnajökull) began, resulting in a tephra fall over part of the ice cap. This tephra layer was subsequently buried by snow during the following winter season.

Visual inspection of the SAR data acquired after the 2004 Grímsvötn eruption showed a distinct backscatter signal over the area where the ash was deposited. Further,

significant temporal differences were observed in the SAR backscatter signals over the ash fan. These differences appear to be related to the snow accumulation history and suggest that the ash deposits can be used as a time reference marker for estimating accumulation rates by the analysis of time sequential SAR backscatter data. Due to the continuous SAR acquisition, the available data series provide a very valuable data basis for the investigation of snow accumulation history using the 2004 ash layer as a time reference marker. Given that the tephra layer does not change during time after becoming covered by snow, the observed changes in the backscatter signal should be predominantly related to changing backscatter conditions in the overlying snow pack. Apart from melt effects, which were excluded from the analysis, accumulation is the major parameter changing the conditions of the snow pack. The relation between SAR backscatter values and accumulation rates was determined by linear regression analysis between ground truth accumulation data and the temporal evolution of the SAR backscattering coefficient (σ^0) at the locations of two snow pits. With this approach it should be possible to estimate the accumulation distribution over large areas with a high temporal resolution for all regions where such reference horizons exist.

TEST SITE

Vatnajökull is a temperate ice cap located on the southeast coast of Iceland (Fig. 1). The glacier extends 150 km from west to east and 100 km from south to north. The entire ice cap is highly dynamic and ice surface velocities of 60–80 m a^{-1} at outlet glaciers are typical (Adalgeirsdóttir, 2003).
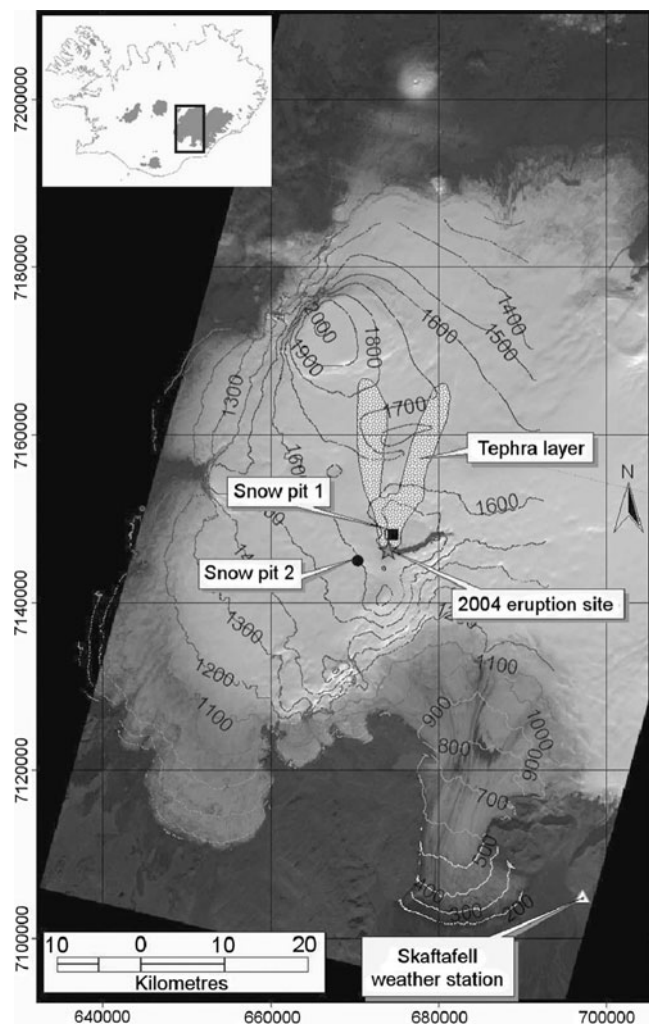
Fig. 1. ASTER-Mosaic (27 September 2004) of the western part of Vatnajökull, showing the location of the 2004 eruption vent, the extent of ash deposits, pit locations and Skaftafell weather station. The coverage is shown on the insert map (top left). Map projection: UTM, WGS 84° N, Zone 27.

The maritime climate in South Iceland is strongly influenced by the warm North Atlantic current, passing the south and east coast of the island. Due to relatively low summer temperatures and heavy winter precipitation, Vatnajökull shows high rates of surface mass exchange (Adalgeirsdóttir, 2003). Melting occurs in the accumulation area even during winter, which also influences the quality of SAR data acquired during these periods.

Our investigations focus on the larger region of Grímsvötn caldera, situated in the central part of western Vatnajökull. The southern rim of the caldera protrudes through the ice cover at an elevation of 1722 m a.s.l., whereas the rest of the crater rim is covered by the ice cap. The caldera itself (~1450 m a.s.l.) is filled by the geothermally-fed subglacial lake Grimsvötn, which itself is overlain by glacier ice up to 250 m thick, forming the inner surface at ~1450 m a.s.l. (Björnsson and Einarsson, 1990).

Continuous mass balance observations have been carried out on the western and northern outlets surrounding the Grímsvötn caldera since 1991 (Adalgeirsdóttir, 2003). On the western part of Vatnajökull, the equilibrum line altitude (ELA) is located at 1200–1400 m a.s.l. (Björnsson and others, 2005).
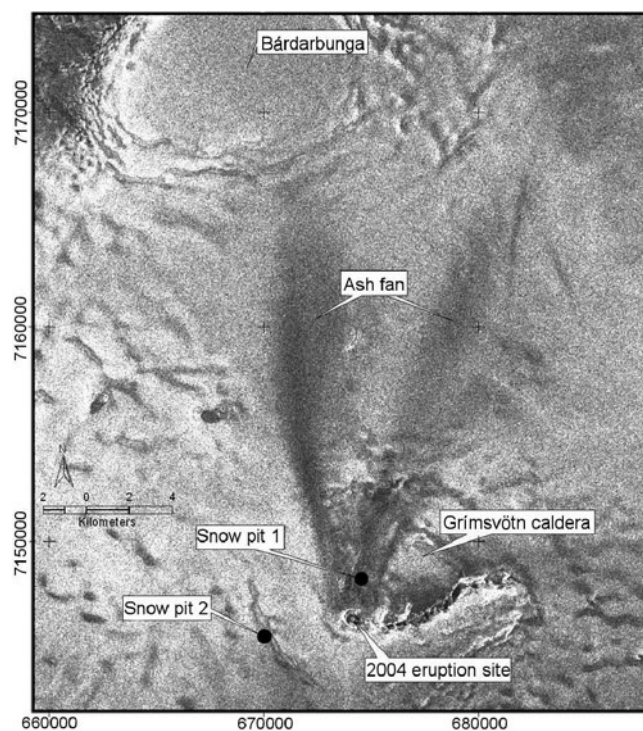

Fig. 2. Section of ENVISAT-ASAR image (13 November 2004) over the test site showing the extent of the V-shaped ash fan 7 days after the eruption. Even at a larger distance from the eruption site, where the ash layer becomes thinner, the ASAR backscatter values are reduced significantly. Locations of the two snow pits are marked with dots. Map projection: UTM, WGS 84° N, Zone 27.

During the last several hundred years, Grímsvötn was the most active volcano beneath Vatnajökull (Guðmundsson and Björnsson, 1991). Due to the ice cover, eruptions of Grímsvötn are phreato-magmatic. The most recent eruption occurred between 1–6 November 2004, after a dormant phase of only 6 years (Sigmundsson and Guðmundsson, 2004). The eruption site was located at the southwest flank of the Grímsvötn caldera. Analysis of the ENVISAT-ASAR data acquired during and shortly after the event showed that the magma–ice interaction melted an area of ~0.4 km^2 of the glacier ice, ~150 m thick, around the eruption vent. The meltwater drained subglacially via the Grímsvötn caldera and Skeidarárjökull to the Skeidarársandur outwash plain (Hardardóttir and others, 2005). No lava was formed during the eruption and all magma fragmented into pyroclasts that accumulated at the eruptive site or were carried by the eruption plume as tephra (Sigmundsson and Guðmundsson, 2004). The prevailing southerly and southeast winds during the outbreak led to the deposition of a V-shaped ash layer north of the eruption site (Figs 1 and 2). In the ENVISAT-ASAR scene acquired on 13 November 2004, about one week after the eruption, the extension of the ash fan could be delineated. The fan comprises two branches that extend ~19 km towards the Bárdarbunga caldera and cover an area of ~88 km^2 on the glacier surface.

DATA AND METHODS

A fieldtrip was conducted about 6 months after the Grímsvötn eruption (6–13 April 2005) in order to investigate the structure of the snow layer which had accumulated in
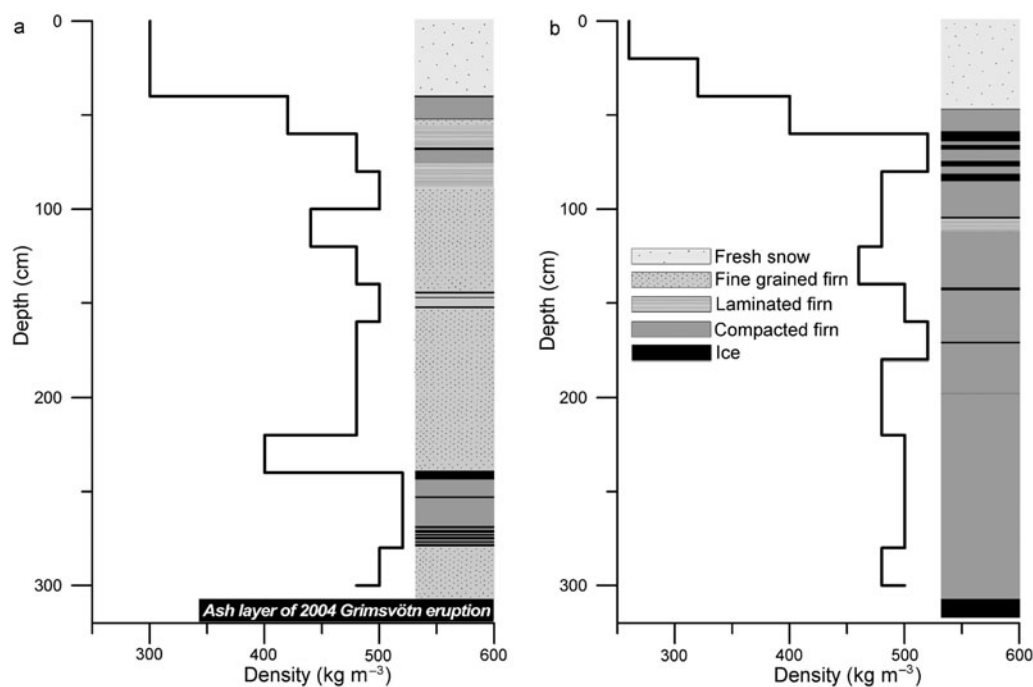
Fig. 3. Density profile and stratigraphy of (a) snow pit 1 and (b) snow pit 2, dug during the field campaign in April 2005. The ash layer was found at a depth of 3.2 m in pit 1. The thickness of the ash layer could not be determined, due to hard frozen conditions of the material (≥50 cm).

the Grímsvötn area. Two snow pits were dug and five shallow firn cores were drilled in the accumulation zone. In this study, the snow deposition history constructed from the two snow pits is used for interpretation of the radar signatures.

Snow pit 1 is located in the Grímsvötn caldera at a height of ~1450 m a.s.l. and about 1.8 km north of the eruption site (Fig. 2). The ash layer was found at a depth of 3.2 m. In the area around the snow pit, the ash accumulated continuously during the eruption, resulting in a thick tephra layer not penetrable by the SAR signal. An exact determination of the layer thickness was not possible due to the hard frozen conditions of the material (the thickness is at least 50 cm at pit 1, which corresponds to the maximum depth reached). Snow pit 2 is situated about 4 km southwest of the vent, at a height of ~1564 m a.s.l. outside the caldera (Fig. 2). At this location, no ash was deposited during the eruption. Therefore, this pit serves as an undisturbed reference for a SAR backscatter comparison. For quantification of precipitation, the water equivalent was determined by density measurements of snow samples on a vertical profile in both pits (Fig. 3). In addition, visual stratigraphy and the vertical temperature distribution were determined for identification of the deposition history (Fig. 3).

The remote sensing data used in this analysis are recorded by the ASAR instrument, a side looking C-band SAR antenna operating at a wavelength of 5.6 cm. ASAR is part of the payload of ENVISAT, successfully launched in March 2002. The satellite is on a 35 day repeat pass, providing images of the same ground target from the same orbit position every 35 days. Due to its beam steering capability the ASAR instrument can acquire images in seven different swaths, within the incidence angle range 15–45°. By acquiring all swaths, both on ascending and descending orbit, it is theoretically possible to image the same ground target with a mean repetition cycle of 2.5 days. Basically, different polarizations can be chosen, whereas all images used in this study are acquired with vertical transmit and receive polarization (VV). The ground resolution of the scenes is ~20 m and the swath width about 100 km.

Due to frequent SAR acquisition, a total amount of 40 ASAR scenes could be analyzed in this study (Table 1). The study area was imaged during the period from the eruption in November 2004 until the field trip in April 2005 no less than 27 times by the ASAR instrument, from both ascending and descending orbits. For this period, data of the ASAR swaths IS1, IS2, IS5 and IS6 were available, covering an incidence angle range 14.1–42.8°. Furthermore, 13 scenes (IS2 descending, IS5 ascending, IS5 descending) acquired during winter 2005/06 were investigated in order to analyze the temporal development of the local SAR backscatter conditions over an extended period.

For the quantitative backscatter comparison at the location of the two snow pits, precise absolute image calibration was performed for all ASAR images. The different error contributions of the SAR system (e.g. side looking geometry, antenna pattern) had to be removed in order to convert the image information to physical values. To obtain the radar backscattering coefficient σ^0, the individual calibration constant of every ASAR scene, included in the corresponding header file, was used (Rosich and Meadows, 2004). The local slope (i.e. local incidence angle) derived from a Digital Elevation Model (DEM) based on 1:50 000 topographic maps produced in the 1990s, was also considered in the corrections. The change in surface slope since the map production is thought to be negligible, as the two snow pits are situated in rather flat terrain. Finally, σ^0 values were converted to decibels (dB).

Individual radar pixels are not representative of the local backscatter value due to radar inherent speckle (Lopes and

Table 1. Specifications of all 40 analyzed ASAR scenes

Date	Track	Swath	Orbit	Local incidence angle	
				Pit 1	Pit 2
04/11/04	5445	IS5	A	38.27	37.99
09/11/04	2009	IS2	D	23.04	25.22
11/11/04	2044	IS2	A	23.54	23.15
12/11/04	1052	IS1	D	18.24	19.65
13/11/04	6066	IS6	D	42.57	43.00
27/11/04	1273	IS1	A	21.35	20.90
28/11/04	2281	IS2	D	20.66	22.05
05/12/04	5381	IS5	D	36.00	37.42
09/12/04	5445	IS5	A	38.24	27.99
14/12/04	2009	IS2	D	23.04	24.44
16/12/04	2044	IS2	A	23.51	23.11
02/01/05	2281	IS2	D	20.63	22.02
04/01/05	2316	IS2	A	26.10	25.68
09/01/05	5381	IS5	D	36.07	37.48
13/01/05	5445	IS5	A	38.31	38.03
18/01/05	2009	IS2	D	23.09	24.49
20/01/05	2044	IS2	A	23.61	23.21
06/02/05	2281	IS2	D	20.69	22.09
13/02/05	5381	IS5	D	36.02	37.44
17/02/05	5445	IS5	A	38.23	37.96
22/02/05	2009	IS2	D	23.06	24.47
24/02/05	2044	IS2	A	23.52	23.13
13/03/05	2281	IS2	D	20.62	22.02
20/03/05	5381	IS5	D	36.06	37.48
24/03/05	5445	IS5	A	38.30	38.01
29/03/05	2009	IS2	D	23.11	24.51
31/03/05	2044	IS2	A	23.59	23.20
25/10/05	2009	IS2	D	23.03	24.14
20/11/05	5381	IS5	D	35.99	37.08
24/11/05	5445	IS5	A	38.18	37.92
29/11/05	2009	IS2	D	23.05	24.39
25/12/05	5381	IS5	D	35.98	37.26
29/12/05	5445	IS5	A	38.29	38.01
03/01/06	2009	IS2	D	23.01	23.87
29/01/06	5381	IS5	D	36.05	37.11
02/02/06	5445	IS5	A	38.24	37.97
07/02/06	2009	IS2	D	23.08	24.18
05/03/06	5381	IS5	D	35.98	37.07
09/03/06	5445	IS5	A	38.30	38.02
14/03/06	2009	IS2	D	23.11	24.03

Note: A, D refer to ascending, descending orbits respectively.

others, 1990). In order to derive representative values, mean σ^0 (dB) was calculated for image windows of 20×20 multi-looked (5 in azimuth, 1 in range) pixels, centred at the coordinates of snow pits 1 and 2. Taking the ASAR ground resolution into consideration, these image chips correspond to an area of $\sim 16\,000\,m^2$ on the glacier surface. The mean local incidence angles were calculated for the same image windows from the incidence angle maps, corresponding to the different ASAR swaths (Table 1).

In order to relate the snow pit measurements to meteorological events, data from the nearby Skaftafell weather station were provided by the Icelandic Meteorological Office for the period under investigation. Skaftafell station is located on the southern sandur plain at the terminus of the Skeidarárjokull outlet, at a height of $\sim 100\,m\,a.s.l.$ The distance between the station and the test sites is $\sim 55\,km$. Daily mean values of temperature and precipitation were used for the interpretation of the SAR backscatter signals (Fig. 4).

ANALYSIS
Backscatter analysis

In the following section the biennial time series of the 40 ASAR scenes at the two snow pits are discussed. No summer scenes are included, as surface scattering at the wet/melting snow surface is the dominant scattering mechanism during this season. No differences between the two pits can be observed during this period.

Visual inspection of the scenes shows that the ash fan is detectable on all 40 ASAR images. This was true even for the most recent scene in March 2006, ~ 16 months after the eruption occurred. This indicates that the radar signal penetrates to the ash layer even after a second accumulation season.

The local incidence angles differ only slightly at the two snow pits (Table 1). At the undisturbed pit (pit 2), the σ^0 values remain stable (low variance) for the whole time series (if melt events are excluded) (Fig. 5b). At lower incidence angles the variability is somewhat higher. Images from different swaths show characteristic σ^0 values during the two years of observations. The IS2 descending scenes reveal a mean value of $\sim 0\,dB$, IS5 descending $\sim -6\,dB$ and IS5 ascending varies around $-5\,dB$ at pit 2. Volume scattering of dry snow is expected to be the dominant scattering mechanism in this area, indicating more or less temporally stable snow cover characteristics. On a few dates, namely at the onset of the time series in November 2004 (all swaths), on 20 March 2005 (IS5 descending) and on 25 October 2005 (IS2 descending) the σ^0 values are reduced significantly (Fig. 5). These sudden changes in backscatter intensity are related to a change of the scattering mechanism from volume to surface scattering caused by surface melt. On all these acquisition dates, higher temperatures and considerable amounts of precipitation were recorded at the Skaftafell weather station, providing a layer of wet snow in the region of pit 2. Consequences of these conditions for SAR backscatter are demonstrated in Figure 6.

At pit 1, an increase in value of σ^0 is found in all time series of the different antenna swaths, whereas IS2 and IS5 show a rather similar behaviour. During the second winter after the eruption, the σ^0 values also increase with time (Fig. 5a). This suggests an increasing volume scattering contribution by the snow layer accumulating above the ice surface of the ash horizon. In the first 6 months after the eruption the values increase from $-8.9\,dB$ (11 November 2004) to $-4.0\,dB$ (31 March 2005) in the IS2 ascending scenes. In IS2 descending scenes, backscatter values increase from $-9.8\,dB$ (9 November 2004) to $-4.1\,dB$ (29 March 2005). Due to the higher incidence angle, the level of the IS5 values is generally lower, but the temporal increase is still pronounced. Values of IS5 ascending scenes rise from $-13.9\,dB$ (4 November 2004) to $-10.7\,dB$ (24 March 2005). In the IS5 descending series an increase is observed for the first three acquisition dates: $-13.9\,dB$ (5 December 2004) to $-13.0\,dB$ (13 February 2005). The last scene in the first winter period, however, gives a lower value: $-14.4\,dB$ (20 March 2005). This value is connected to the weather situation mentioned before.

Even in the second winter, the temporal increase of backscatter is maintained although it begins at a higher level. In the IS2 descending series the values increase from $-5.3\,dB$ (25 October 2005) to $-2.6\,dB$ (14 March 2006), in IS5 ascending images from $-13.7\,dB$ (24 November 2005) to
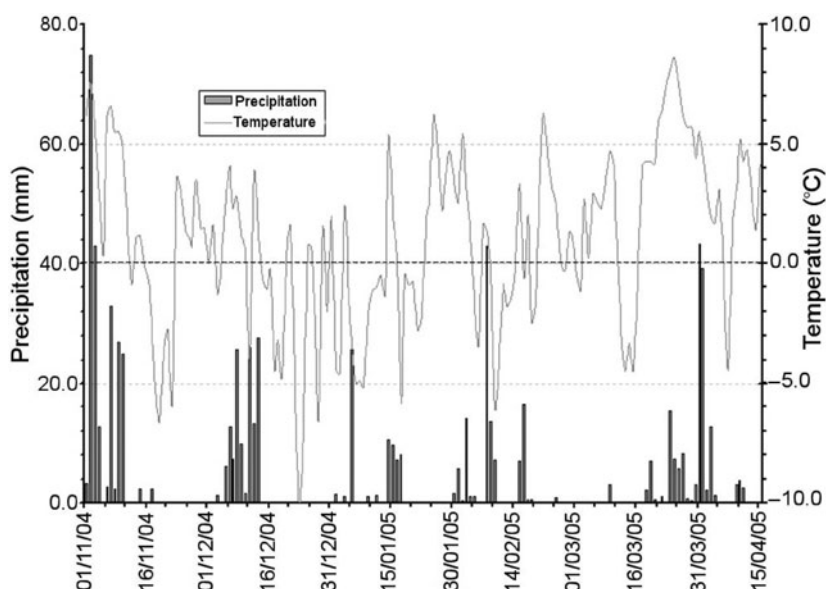
Fig. 4. Daily mean temperature and precipitation for the period 1 November 2004 to 15 April 2005 recorded at the Skaftafell weather station. These data were used for reconstructing the accumulation history at the two snow pits and for inspecting the weather conditions at the ASAR acquisition dates (only SAR images under cold and dry conditions were chosen).

–11.0 dB (9 March 2006) and in IS5 descending images from –12.6 dB (20 November 2005) to –10.7 dB (5 March 2006) (Fig. 5).

To conclude, the σ^0 values increase during the first accumulation period (winter) by 4.8 dB in IS2 ascending scenes, by 5.6 dB in IS2 descending scenes, 3.0 dB in IS5 ascending scenes and 0.9 dB in IS5 descending scenes for the first three acquisition dates. In the second accumulation period (winter) after the eruption the IS2 descending series increases by 2.8 dB, IS5 ascending images by 2.7 dB and IS5 descending images by 1.9 dB. Comparing the two pits, the σ^0 values of IS2 swaths are generally lower by about 5 dB and about 7 dB lower for IS5 swaths at pit 1, while the only considerable difference between the two locations is the existence of the ash layer at pit 1.

Accumulation history

In both snow pits, close to the eruption site (pit 1) and outside the crater (pit 2), vertical density profiles and stratigraphy were measured. The ash layer in pit 1 is a clear time marker, representing the eruption of 1–6 November 2004. A total water equivalent of 702 mm was derived from the density measurements in pit 1 for the time between 6 November 2004 and 9 April 2005 (Fig. 7). The stratigraphic comparison between the two pits resulted in assigning the same date to a thick ice lens in 3.20 m depth in pit 2. The total water equivalent for the same period at pit 2 corresponds to 736 mm which leaves a difference of 34 mm between the two pits 5.5 km apart.

Using temperature and precipitation information from the Skaftafell station, the deposition history was reconstructed for both pits. Since both pits are situated well within the accumulation zone, it is assumed that no runoff took place even for the warmest periods during the winter 2004/05 and that potential rainfall was refrozen in the snow layer. Ice lenses and compact, laminated firn layers were associated with warm periods. Certain precipitation events recorded at the weather station, as well as strong melt events could be identified in the pits. Hence, due to the elevation difference,
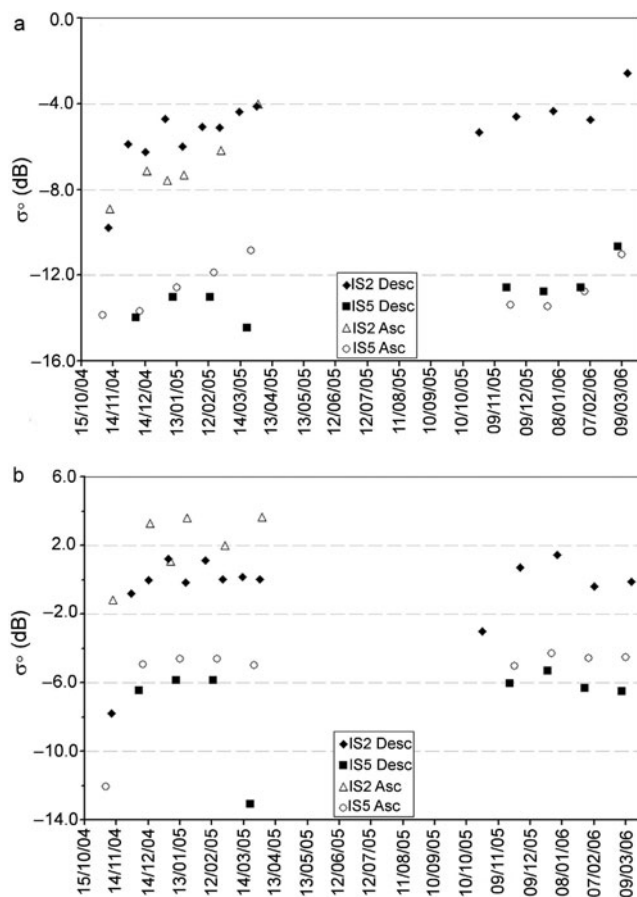

Fig. 5. Plots of the ENVISAT-ASAR backscatter time series at (a) snow pit 1 and (b) snow pit 2. Outliers, where the σ^0 backscatter values are reduced significantly, are included. In contrast to pit 2 (b), where values remain stable, a temporal increase in σ^0 is found at pit 1 in all ASAR swaths. Comparing pit 1 and pit 2, the σ^0 values of IS2 are generally lower by about 5 dB, and about 7 dB for IS5 at pit 1, due to the ash layer.
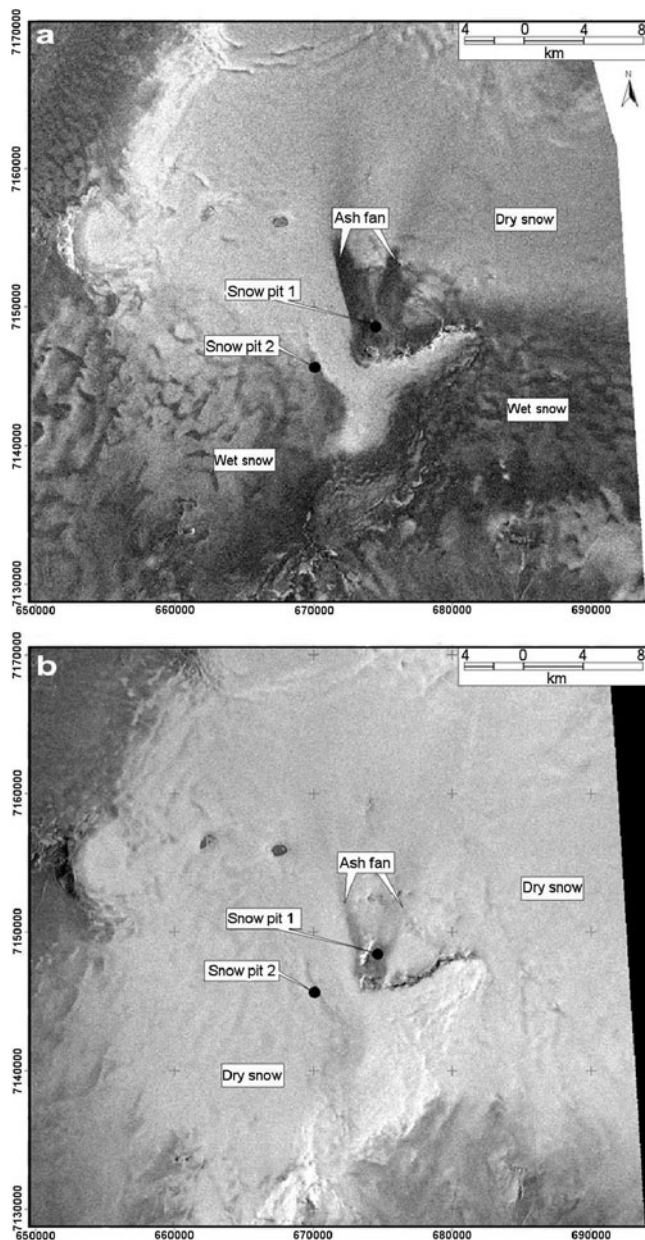
Fig. 6. ENVISAT-ASAR scenes showing the difference between (a) wet, 4 November 2004 and (b) dry, 18 January 2005 conditions at acquisition. In (a), the σ^0 backscatter values are reduced significantly over the southern part of the glacier. Map projection: UTM, WGS 84° N, Zone 27.

the mean density below the new snow of pit 2 is slightly higher than the density of pit 1. The total precipitation at Skaftafell for the period of investigation is 561 mm, which is about 80% of the mean precipitation at Grímsvötn. A comparison of the accumulation history for the two pits and the accumulated precipitation at Skaftafell shows good agreement (mean $R^2_{(\text{Pit 1, Pit 2})} = 0.84$, see also Fig. 7).

DISCUSSION

The radar backscatter data for the two locations on the glacier were compared with the derived accumulation history. The remarkable increase of the backscatter values at pit 1 in contrast to the lack of backscatter variation at pit 2 implied a direct connection between the accumulation above the ash layer and the backscatter conditions (Fig. 5).

The radar signal is able to penetrate into a dry snow layer, where the amplitude of the received backscatter signal mainly depends on volume scattering within the snow pack (Henderson and Lewis, 1998). In the case of pit 1, the radar backscatter signal is still affected by the existence of the ash layer even after more than a year, which indicates a penetration depth of at least several metres. Compared with scattering in the undisturbed snow pack of pit 2, the mean σ^0 values are about 5 dB lower for IS2 and 7 dB lower for IS5, respectively. For our purpose it is important to assume temporally stable backscatter conditions of the ash layer. Because of the continuously frozen conditions after the first snowfall events it is very likely that the ash layer is unchanged since. The individual scattering properties of the ash layer, such as its surface roughness, permittivity and inner structure (grain size) can then be neglected in this study. It is also assumed that the ash layer functions as a surface scatterer, as indicated by the strong reduction of backscatter values even over a thin ash layer at the larger distance of the eruption site (Fig. 2). The fraction of volume scattering in the overlying snow pack could therefore be calculated from differences in σ^0 values at the two snow pit locations. It is anticipated that the ash layer can thus be used as a reference horizon with a known age in accumulation studies, calculating snow accumulation from the σ^0 differences.

In order to investigate the relation between snow accumulation and the differences between σ^0 values of the two pits ($\Delta\sigma^0$), a linear regression analysis was carried out (Fig. 7). For this study, only SAR images with cold and dry conditions on the glacier surface were chosen. In the case of wet conditions, scattering occurs at the surface and the underlying snow volume has no influence on the measurements. Due to the strong correlation between the measured accumulation in the snow pits and the precipitation data at Skaftafell weather station, the latter have been used for the analysis.

Introducing a linear relation between reduction in $\Delta\sigma^0$ values and increasing snow pack results in a high correlation between the two variables for the period between the date of eruption and the field trip. Only the IS2 descending and IS5 ascending series have been used, due to good temporal coverage for these swaths in this observation period. The analysis shows rather high R^2 confidence values of 0.81 for IS2 descending and 0.86 for IS5 ascending. For an increase in snow thickness of 100 mm w.e., $\Delta\sigma^0$ decreases by about 0.94 dB for IS5 and 0.97 dB for IS2, respectively. This relation between snow depth above the ash layer and reduction in $\Delta\sigma^0$ can be used to determine accumulation rates between individual SAR image acquisitions for dry snow conditions.

A similar investigation was made for the winter of 2005/06 where no in situ accumulation data are available for the glacier (Fig. 7). The comparison of the Skaftafell precipitation data and the radar data show a similar relation. However, the slope of the regression line is steeper for both swaths. This indicates that for this year the ash layer can still be used as a reference horizon for accumulation studies, but a new calibration is required for each accumulation period.

CONCLUSIONS

Results presented in this paper demonstrate that volcanic ash deposits on a glacier can be used as a time reference marker for measuring accumulation rates by the analysis of time

sequential SAR backscatter data. The change in SAR backscatter values (σ^0) for a cold snow pack is strongly linked to the accumulation history above the reference horizon. In the absence of such a horizon (e.g. at pit 2) the snow pack shows a temporally uniform backscatter behaviour, indicating a more or less stable composition in time. Therefore, the gradient in temporally distributed σ^0 values over the reference layer provides a tool for the reconstruction of accumulation rates during an accumulation period.

Even after two seasons the ash layer from the 2004 Grímsvötn eruption can be used as such a reference layer for the determination of the increase in snow depth. The nearby undisturbed snow pack at pit 2 provides a control, in order to eliminate other factors influencing the backscatter coefficient. So far, the relation has only been tested for one accumulation period and a thorough investigation of the backscattering theory is required to quantify the method. However, comparison with weather data from a nearby station allows an approximate reconstruction of the accumulation history during the winter season. A new calibration for each accumulation period would increase the accuracy significantly.

One of the main advantages of our approach is its applicability to raster data in contrast to point measurements from conventional field investigations, which allows the computation of areal distributions of accumulation rates calibrated by known local data. The necessary existence of a reference horizon so far is a strongly limiting factor. The characteristics required to make such internal layers (e.g. ash or dust) usable as reference layers need to be determined. Such a study might prove that the frequent dust-fall events on alpine and Asian glaciers could be utilized for widespread accumulation investigations. For Vatnajökull, further monitoring of SAR backscatter and analysis of its spatial variations will provide an interesting insight into the areal accumulation distribution in the central part of the ice cap by investigating the signals over the recent and future ash layers. The analysis of multiple years of ENVISAT-ASAR data will allow development of annually calibrated accumulation retrieval algorithms. For this purpose, the establishment of several control sites over the ash layer and in adjacent regions is planned for future field activities. Data from these control sites will improve the quantification of the accumulation/backscatter relation considerably.

Even for a snow depth of 3.2 m, the analyzed SAR data reveal a difference in backscatter from 5–7 dB for the two pits. After the following winter season (2005/06), with additional snow accumulation, a difference in backscatter was still detectable. Observation of future differences between the two sites will provide more information on the penetration depth of the SAR signal under dry conditions on Icelandic glaciers, which is at least more than the observed 3.2 m (700 mm w.e.) in 2004/05 plus the ~950 mm w.e. in 2005/06.
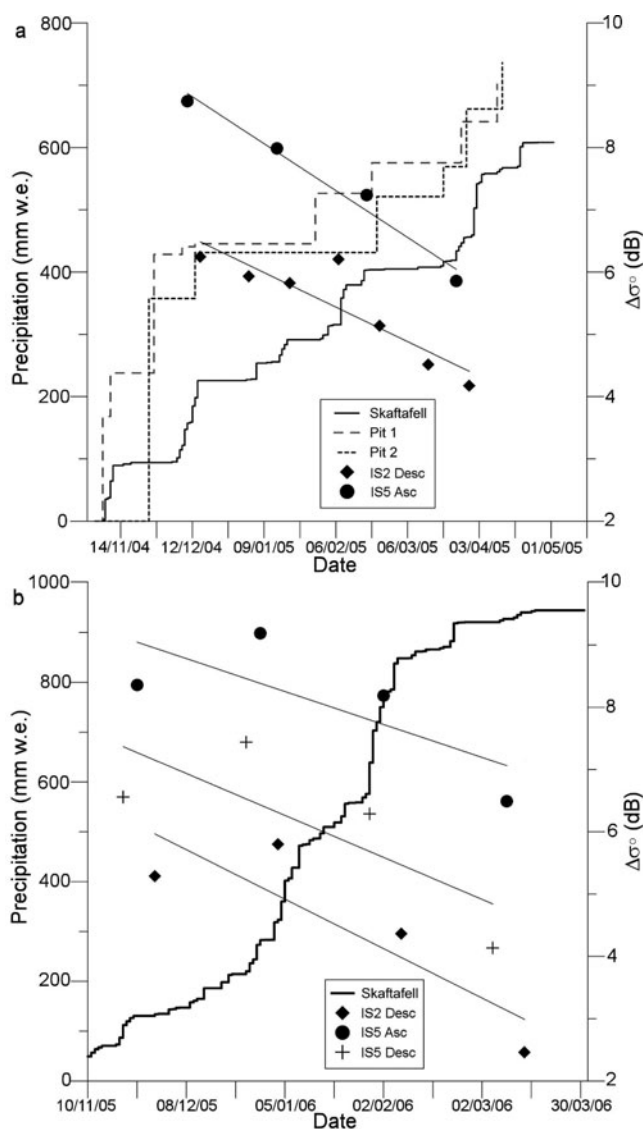
Fig. 7. Comparison of the accumulation history during the winter season and the $\Delta\sigma^0$ backscatter values (pit 2 minus pit 1) of different ENVISAT swaths. (a) Accumulated precipitation measurements from the snow pits and recordings from Skaftafell station for the period 2004/05. (b) Skaftafell station only for the period 2005/06. The lines represent the regression lines of the corresponding ASAR swaths, providing high (>0.8) R^2 confidence values.

REFERENCES

Adalgeirsdóttir, G. 2003. Flow dynamics of Vatnajökull ice cap, Iceland. (PhD thesis, ETH-VAW Zürich.)

Björnsson, H. 1978. The surface area of glaciers in Iceland. *Jökull*, **28**, 31.

Björnsson, H. and P. Einarsson. 1990. Volcanoes beneath Vatnajökull, Iceland: evidence from radio echo-sounding, earthquakes and jökulhlaups. *Jökull*, **40**, 147–168.

Björnsson, H., F. Palsson, G. Adalgeirsdóttir and S. Guðmundsson. 2005. Mass balance of Vatnajökull (1991–2004) and Langjökull (1996–2004) ice caps, Iceland. *Geoph. Res. Abs.*, **7**, 06485.

Guðmundsson, M.T. and H. Björnsson. 1993. Eruptions in Gríms-vötn, Vatnajökull Iceland 1934–1991. *Jökull,* **41**, 21–45.

Hardardóttir, J., P. Jonsson, G. Sigurdsson, S.O. Elefsen, B. Sigfusson and S. Gislason. 2005. Discharge and sediment monitoring of the 2004 glacial outburst flood event (jökulhlaup) on Skeidara sandur plain south Iceland. *Geoph. Res. Abs.,* **7**, 08854.

Henderson, F.M. and A.J. Lewis, eds. 1998. Manual of remote sensing: principles and application of imaging radar. Third edition. 2. New York, NY, John Wiley & Sons.

Lopes, A., T. Ridha and E. Nezry. 1990. Adaptive filters and scene heterogeneity. *IEEE Trans. Geosci. Remote Sens.,* **28**(6), 992–1000.

Rosich, B. and P. Meadows. 2004. Absolute calibration of ASAR level 1 products generated with PF-ASAR. ESA-ESRIN Technical Note, ENVI-CLVL-EOPG-TN-03-0010.

Sigmundsson, F. and M.T. Guðmundsson. 2004. Eldgosið í Grímsvötnum í nóvember 2004 – the Grímsvötnum eruption, November 2004. *Jökull,* **54**, 139–143.

Paper 3

Martinis S, Scharrer K, Münzer U, Mayer Ch, Gudmundsson Á (2007) Influences of the 2004 jökulhlaup on ice dynamics of Skeidarárjökull, Iceland, using Terra-ASTER imagery. PFG, 2007 (5), 337-349.

Reprinted with permission of Deutsche Gesellschaft für Photogrammetrie und Fernerkundung (DGPF)

Influences of the 2004 jökulhlaup on ice dynamics of Skeiðarárjökull, Iceland, using Terra-ASTER imagery

[1] Sandro Martinis, [1] Kilian Scharrer, [1] Ulrich Münzer, [2] Christoph Mayer, [3] Ágúst Gudmundsson

[1] Department of Earth- and Environmental Sciences, Section Geology, Ludwig-Maximilians-University Munich
[2] Bavarian Academy of Sciences and Humanities, Commission for Glaciology
[3] Fjarkönnun ehf., Kópavogur, Iceland

Summary: On 01–06 November 2004 a volcanic eruption occurred at the subglacial Grímsvötn caldera sited under the western part of Vatnajökull ice cap. The accompanying jökulhlaup travelled subglacially over a distance of 50 km under the Skeiðarárjökull outlet and finally flooded huge areas of the Skeiðarársandur plain in the south. Meltwater discharge peaked on 2 November and finally ended in early December, having released a total volume of ~0.8 km³ from Grímsvötn. The influences of this jökulhlaup on the ice dynamics of Skeiðarárjökull were investigated applying image cross-correlation on five optical images pairs (October 2001 to July 2005) of the Advanced Spaceborne Thermal Emission and Reflection Radiometer (ASTER) aboard the EOS Terra satellite. The average horizontal surface displacement of nearly annual periods (2001-2002, 2002-2003, 2003-2004, 2004-2005) were compared to the velocity obtained from a 64 day image pair covering the period of the jökulhlaup. A considerable acceleration of up to 0.4 m d^{-1} over nearly the whole width of the glacier appeared during the jökulhlaup in contrast to the annual velocities. This extensive increase of surface velocity is only hardly explainable by the classical jökulhlaup theory of floodwater drainage in a single subglacial conduit. Considering the results, a sheet flow or coupled sheet and tunnel flow leading to a widespread basal lubrification seems more likely.

Zusammenfassung: *Der Einfluss des Jökulhlaup im Jahr 2004 auf die Eisdynamik des Skeiðarárjökull, Island, unter Verwendung von Terra-ASTER Daten.* Zwischen dem 01.11.2004 und 06.11.2004 ereignete sich eine Vulkaneruption am südwestlichen Rand der Grímsvötn-Caldera unter dem westlichen Vatnajökull. Der begleitende Jökulhlaup floss subglazial über ca. 50 km unter dem Auslassgletscher Skeiðarárjökull ab und überflutete schließlich weite Bereiche des im Süden gelegenen Skeiðarársandur. Der Jökulhlaup erreichte seinen Spitzenabfluss am 02.11.2004 und endete Anfang Dezember. Insgesamt wurde ein Schmelzwasservolumen von ca. 0,8 km³ freigesetzt. Ziel dieser Studie ist die Untersuchung des Einflusses dieses Gletscherlaufs auf die Eisdynamik des Skeiðarárjökull. Dabei wurde Kreuzkorrelation zwischen fünf optischen Datenpaaren (Zeitraum Oktober 2001 – Juli 2005) des Advanced Spaceborne Thermal Emission and Reflection Radiometer (ASTER) durchgeführt. Die durchschnittliche horizontale Oberflächengeschwindigkeit nahezu einjähriger Zeitabschnitte (2001-2002, 2002-2003, 2003-2004, 2004-2005) wurde den Korrelationsergebnissen eines Datenpaares mit 64tägigem Abstand zur Zeit des Jökulhlaup gegenübergestellt. Die Resultate zeigen während des Jökulhlaup eine im Verhältnis zu den einjährigen Datenpaaren bis zu 0,4 m/Tag erhöhte Oberflächengeschwindigkeit des Skeiðarárjökull über dessen nahezu gesamte Breite. Dieser flächenhafte Geschwindigkeitsanstieg kann nur schwer mit der klassischen Jökulhlaup-Theorie in Einklang gebracht werden, die den subglazialen Abfluss der Wassermassen über einen einzigen Schmelzwassertunnel beschreibt. Die Ergebnisse zeigen, dass Blockschollenbewegung oder eine Kombination aus Blockschollenbewegung und Tunnelabfluss, die zu einem großflächig basalen Gleitfilm führt, wahrscheinlicher ist.

1 Introduction

The objective of this study is the determination of two-dimensional ice-surface velocity fields of the Skeiðarárjökull, a southward trending outlet of the Vatnajökull ice cap, by cross-correlation of ASTER image pairs.

Due to its climatic and physical conditions Iceland presents an ideal test site for monitoring glacier dynamics. At present approx. 11 % of the 103,000 km² of the volcanic island is ice-covered, represented mainly by the four large ice caps Vatnajökull (8,100 km²), Langjökull (925 km²), Hofsjökull (900 km²)

and Mýrdalsjökull (600 km²) (BJÖRNSSON et al. 2004).

The large ice masses cover several active volcanic systems with central volcanoes, crater chains, and fissures (BJÖRNSSON & EINARSSON 1990).

Besides the usual volcanic hazards (lava flows, pyroclastic clouds, tephra fall, etc.), the volcano-ice interaction leads to enormous melt water torrents (icl.: jökulhlaup), devastating large areas in the neighbourhood of the affected glacier. Conventional theory explains jökulhlaups by floodwater travelling from a water reservoir within a single pre-existing conduit of fixed geometry and diameter eroded into the bottom of a glacier (Nye 1976). The frictional heat of meltwater flow enlarges the tunnel along the flood path leading to an almost exponential increase of discharge (RÖTHLISBERGER 1972, NYE 1976, BJÖRNSSON 1975, NG 1998). This theory established by NYE (1976) was adapted several times, but its main principles endure. However, new studies on some catastrophic flood events in Iceland have revealed that besides the exponentially rising jökulhlaups, a second type of glacier torrents exists (ROBERTS 2005).

For example the enormous jökulhaup from Grímsvötn in 1996 (~3.2 km³) is characterized by a steep short-time linear rise to maximum water discharge. This hydrograph curve cannot be explained solely by tunnel enlargement due to mechanical and thermal energy (BJÖRNSSON et al. 2001, BJÖRNSSON 2002, FLOWERS et al. 2004). Sheet-like flow across large portions of a glacier bed is necessary to explain this type of rapidly rising jökulhlaup (JÓHANNESSON 2002, FLOWERS et al. 2004).

Results of MAGNÚSSON et al. 2005, deriving a widespread increase of the ice flow velocities at Skeiðarárjökull due to basal spreading of the water reducing friction between the bedrock and the glacier during the jökulhlaup in 1996 by the use of Interferometric Synthetic Aperture Radar (InSAR), support this theory.

In autumn 2004 another jökulhlaup occurred at the Skeiðarárjökull outlet associated with a subglacial eruption at the Grímsvötn volcanic system. For this event, a pre (27/09/2004) and a post (30/11/2004) jökulhlaup ASTER image of Skeiðarárjökull is at our disposal. We investigated the impact of this jökulhlaup on the ice dynamics of the glacier, compared to the mean annual flow velocities derived for the period 2001-2005 by ASTER cross-correlation likewise.

2 Test site

Skeiðarárjökull is the largest southward trending outlet of Vatnajökull (Fig. 1). The catchment area of Skeiðarárjökull comprises approx. 1,428 km² (AÐALSGEIRSDÓTTIR 2003). Its elevation ranges from 1,740 m down to 100 m a.s.l. at the terminus. Three medial moraines divide the glacier into four different flow bands. Situated in a maritime climate, with relatively low summer temperatures and heavy winter precipitation, the glacier is characterized by high rates of surface mass exchange, resulting in high balance velocities (AÐALSGEIRSDÓTTIR 2003). Its dynamic character is intensified by the convergent flow of the ice mass from a wide accumulation area into a narrow channel (~7.4 km) between the ice free mountains of Skaftafellsfjöll and Eystrafjall, east and west of the glacial tongue.

Additionally the glacier is affected by subglacial drainage of episodic jökulhlaups. Skeiðarárjökull encompasses the floodpath of the Grímsvötn caldera, one of the most famous jökulhlaup systems throughout the world. The approx. 60 km² large subglacial caldera is situated in the central part of western Vatnajökull. The caldera is filled by the geothermally fed subglacial lake Grímsvötn, which itself is overlain by glacier ice, up to 250 m thick, forming the inner surface at approx. 1,450 m a.s.l. (BJÖRNSSON & EINARSSON 1990). For several hundred years, Grímsvötn has been the most active volcano beneath Vatnajökull (GUÐMUNDSSON & BJÖRNSSON 1991). Due to the ice cover, eruptions of Grímsvötn are phreato-magmatic and produce huge amounts of meltwater. The most recent eruption occurred on 1–6 November 2004, after a dormant phase of only six years since a last outbreak in December 1998 (SIGMUNDSSON & GUÐMUNDSSON 2004). In spite of the usual eruption characteristics, the jökulhlaup preceded the eruption, starting on 29 October 2004.

The jökulhlaup peaked on 2 November with maximum flood discharge of 3,300 m³ s^{-1}. Over a five day period 0.5 km³ of melt water were released. The phreato-magmatic eruption, triggered by the release of overburden water pressure, increased the total amount of outflowing water to 0.8 km³ and prolongated the flood until early December (HARDARDÓTTIR et al. 2005, MÜNZER et al. 2007). The floodwater ran approx. 50 km beneath Skeiðarárjökull and reached the Skeiðarársandur outwash plain with its braided river systems Skeidará, Súla and Gígjukvísl. During the subglacial outflow Roberts et al. (2005) detected several speedup events of the glacier's surface by the use of

high-precision GPS. The measurements yield a tenfold increase in horizontal velocity from 0.03 m h^{-1} to 0.3 m h^{-1} that was sustained for up to 10 hours.

3 Data and methodology

Six ASTER images were used to determine the surface velocity fields of Skeiðarárjökull by cross correlation (Tab. 1). The measurements were based on the nadir looking spectral band 3N (0.76 – 0.86 µm, spatial resolution 15 m). Compared to the other high-resolution VNIR bands 1 and 2, the spectral band 3N is less affected by atmospheric influences due to its longer wavelength.

Cross correlation of optical satellite imagery is an established method to derive glacier flow velocities (e.g. SCAMBOS et al. 1992, KÄÄB et al. 2005, BERTHIER et al. 2003), especially in cases when in situ measurements or terrestrial photogrammetry (e.g. MAAS et al. 2006, RENTSCH et al. 1997) are not possible.

In total, five image pairs were generated: Four image pairs with a time interval of nearly one year covering the period 2001 – 2005 (05/10/2001 – 13/09/2002, 13/09/2002 – 09/09/2003, 09/09/2003 – 27/09/2004, 27/09/2004 – 28/07/2005). They were used to calculate the mean annual velocity field of the Skeiðarárjökull glacier tongue. One image pair spans a period of 64 days in autumn 2004 (27/09/2004 – 30/11/2004) comprising the above mentioned jökulhlaup event from the Grímsvötn caldera. This image pair was used to study the impact of increased subglacial drainage on the surface velocity of the glacier, in comparison to the annual mean velocity. Glacier motion is strongly linked to precipitation and the amount of melt water available at the glacier base. Therefore, glacier velocity follows an annual cycle, reaching maximum velocities during the summer month. It can be assumed that without influences of a jökulhlaup the velocity of the 64 day period in autumn should give more or less the same values than the annual average velocity. This time interval covers a transitional period between high summer velocities and strongly reduced basal water and therefore flow velocity due to the beginning of the winter half.

Before applying the cross correlation algorithm on the data pairs, the individual images had to be pre-processed. First stripe noise was removed using the destriping algorithm implemented in ERDAS Imagine as a routine function. Thereafter the images were geocoded. This is the most important step in pre-processing because it influences the accuracy of the derived velocities, especially in case of short time separation.

Therefore, about 20-25 ground control points were measured at nunataks and in the ice free areas around the glacier in the individual images. Digital topographic maps (1:50,000) and already geocoded satellite images were used as references to transform the scenes into a common map projection by a second order polynomial (UTM, WGS 84 Zone 27). Additionally, in order to avoid also minor displacements, the two images of every data pair were co-registered, whereas the prior image always served as the master scene.

Subsequently the ice free areas surrounding the outlet were removed, by clipping the images with the glacier outline. This avoids correlation of surface features close to the glacier margin with the neighbouring ice free areas. Finally, the images were converted into TIF format with reduced image depth of 8 bit and imported into the IMCORR cross correlation software. The IMCORR software package is provided as freeware by the National Snow and Ice Data Center (SCAMBOS et al. 1992). The software computes the maximum correlation between the two images to subpixel precision using a fast Fourier-transform version of the normalized cross-covariance method (SCAMBOS et al. 1992, BERENSTEIN 1983). This technique tracks the motion of small-scale features like crevasses, debris, ash cones or other objects at the glacier surface. One of the critical factors of this method is the time separation between the acquired data: On the one hand a long interval reduces the efficiency of cross correlation technique due to the changing of surface features by physical effects like melting processes or snow accumulation. On the other hand the time interval must be long enough to determine glacier displacements significantly above the co-registration and the software induced errors (BERTHIER et al. 2003).

For runtime purposes IMCORR compares subscenes (image chips) from each of the two full images to restrict the area over which it attempts to find displacements. The smaller reference chip is taken from the respective former scene of each image pair, the larger search chip from the data set recorded afterwards. The size of the search chip is manually adapted to the expected maximum displacement. In this study a consistent reference chip size of 32 x 32 pixel (480 x 480 m) and a search chip size of 80 x 80 pixel (1200 x 1200 m) for the image pairs with an annual interval and 64 x 64 pixel (960 x 960 m) for the shorter interval were chosen. The used grid size was 4 pixel (60 m), i.e. a search window was centred around every fourth pixel. At each of these gridpoints IMCORR matches the search chip to the

reference chip by calculating the correlation values, leading to dense but overly smooth estimates, the latter due to the strong correlation between the highly overlapping chips.

The offset between the two chips at the peak correlation therefore corresponds to the displacement of the glacier. Considering the time separation between the data records and the spatial resolution of the images the offset values are converted into velocities per day and visualized as vector arrows in a GIS environment.

Furthermore, quality control parameters listed in the IMCORR output file were used to validate the correlation results, e.g. error estimations in x- and y-directions exceeding one pixel were rejected. A reliable threshold for the maximum velocity was defined by trial and error. By comparing the azimuth direction of the velocity vectors with the steepest downward slope of the Skeiðarárjökull using a digital elevation model (DEM) it has been found that values exceeding a velocity of 1.1 m d^{-1} return wrong flow vectors in the majority of cases. Additionally vectors deviating +/-20° from the direction of the steepest topographic gradient were eliminated.

4 Error estimation

The individual processing steps introduce some uncertainties in the flow velocity field derived from every image pair. The total error σ_v, computed in the standard deviation of the offset values, consists of the systematic σ_{syst} and the random error σ_{rand} (BERTHIER et al. 2003):

$$\sigma_v = \sqrt{\sigma^2{}_{syst} + \sigma^2{}_{rand}}$$

The systematic error depends on the accuracy of the co-registration of the ASTER data. It was calculated indirectly by applying cross-correlation to stable, ice-free areas of the respective image pairs. The offset of such areas would correspond to the co-registration error. This led to an error value of about one pixel (15m).

The cross-correlation inherent random error (σ_{rand}) can be determined by the error estimations for the x- and y-offsets returned by the IMCORR software. These values are derived from a correlation-peak-height-to-peak-width comparison (http://nsidc.org/data/velmap/imcorr.html. The σ_{rand} varies between 0.19–0.24 pixel in the ASTER correlation results. Now, calculating σ_v with the above equation a total error between 1.01–1.03 pixel is derived for all correlation pairs. The uncertainty of the velocity values (m d^{-1}) depends on the spatial resolution of the used data, the time separation between the correlated images, and on the flow velocity of the glacier. Thus, correlation outputs for the image pairs spanning an annual interval show possible error values of 0.04-0.05 m d^{-1} (cf. Tab. 1). This minor uncertainty is sufficient for a velocity analysis over the whole glacier. In contrast, the total error/day e.g. of the image pair 27/09/2004 – 30/11/04 is increased to 0.24 m d^{-1} due to its short time separation. The relative error would be 100% in a region moving 0.24 m d^{-1}, so velocity measurements are more confident in the fast moving central part of the glacier where the flow reaches higher values than the potential error.

5 Results

The following section describes the cross-correlation results of the five image pairs with a special focus on the Grímsvötn jökulhlaup of 2004. The inferred flow fields of the Skeiðarárjökull glacier tongue are described in terms of their correlation density, flow pattern and flow velocity.

5.1 Correlation density

The number of velocity points derived by the cross-correlation algorithm (four pixel grid size) varies between 14,201 and 30,482 (cf. Tab. 1) for the individual image pairs. In relation to the image overlap, the density of velocity points per km² ranges between 31.1 (27/09/2004 – 30/11/04) and 78.4 (27/09/2004 – 28/07/2005). Generally the annual ASTER pairs show a higher density of correlated points, due to the similar surface conditions during the summer period where the bare ice is exposed on the whole glacier tongue. Therefore surface features like crevasses or ash cones can easily be correlated. In contrast to that, snow coverage complicates cross correlation in the ASTER scene acquired on 30/11/2004 especially at higher elevations of Skeiðarárjökull. In the lower parts of the glacier tongue correlation point density is reduced only marginally, because surface features are not completely masked by the thin snow cover. It was found, that some areas of the glacier generally show sparse coverage with correctly matched pixels: the ash-laden lateral glacier margins as well as the glacier terminus, the medial moraines and the higher elevations close to the equilibrium line. The nearly analogue grey values in these areas often result in a multi-modal correlation surface without a distinctive peak, preventing a clear point-to-point correlation.

5.2 Flow pattern

The flow pattern of Skeiðarárjökull is shown Fig. 2b-f, represented by vector arrows. To eliminate small-

scale directional variations, the azimuth angles of the flow vectors have been averaged using a grid with a cell size of 800 x 800 meters. Therefore, the vectors originate at the centre pixel of each grid cell. It has been found, that the flow pattern derived from the annual ASTER pairs is constant throughout the period of investigation. Even the 64 days image pair, covering the 2004 Grímsvötn jökulhaup, provides the same pattern. This indicates a good reliability of the results of the individual correlation pairs. Especially the annual correlation results yield an almost complete picture of the flow pattern of Skeiðarárjökull. The southward trending ice influx from the wide accumulation area is funnelled into a narrow channel (~740 m a.s.l.) confined by the mountain ridges of Eystrafjall and Skaftafellsfjöll. Here, the ice discharge turns to a SSW direction. In the lower part of the glacier tongue, after passing this bottleneck, the ice disperses in an southeast- (~560 m a.s.l.) and southwest-ward direction (~400 m a.s.l.) and develops a lobe with a 23 km wide ice front.

5.3 Surface velocity

The glacier surface velocities of the annual correlation periods depicted in Fig. 2b-e, show good agreement with other studies (e.g. MAGNÚSSON 2005). A well-defined central flow line of maximum speed is clearly detectable, whereas the lateral parts of the outlet glacier reveal considerably slower velocities.

For better comparison of the results derived from the individual correlation pairs, longitudinal (A-B, Fig. 3) and transversal velocity profiles (C-D, Fig. 4) were extracted along predefined lines as shown in Fig. 2a. In order to obtain reliable measurements, velocity values within a distance of 300 m around the profile lines were used. Depending on the point density a running mean was calculated to visualize the data.

The longitudinal velocity profile has a length of 34 km. It starts about 1.5 km beneath the equilibrium line of the year 2004 at an altitude of 1,220 m a.s.l., proceeds along the main flow path and ends at the eastern part of the glacier terminus (~100 m a.s.l.)

The annual measurements indicate maximum displacements of up to 1.05 m d^{-1} at a distance of 3-4 km from point A. From there the velocity decreases downglacier to a value of 0.6 m d^{-1} at a distance of 8.5 km from A. The section between 8.5 and 22.5 km along the longitudinal profile line shows almost constant velocity values, followed by another zone of strong deceleration to a flow velocity of about 0.05 m d^{-1} at the glacier terminus (B). This deceleration from the equilibrium line towards the glacier snout

results from decreasing accumulation and therefore minor mass input at lower altitude and the reduced driving stress likewise. Furthermore, the high velocities in the upper part of Skeiðarárjökull (~section 0–11 km) coincide with the steepest surface slope of about 2 degrees. The slower section between 11 and 24 km shows a smoother gradient of about 1.1 degrees. In this section (11-24 km) the decrease of the velocity, caused by the reduced driving stress, is equalized by the lateral constriction of the ice mass, leading to more or less constant velocity values. After passing the bottleneck the glacier tongue slows down due to divergent flow.

The transversal velocity profile extends from west to east across the narrowest part (~7.4 km) of Skeiðarárjökull. Graphs of the annual correlation pairs show a similar distribution. Values increase continuously from <0.1 m d^{-1} at the western margin. Maximum velocity values of 0.55 m d^{-1} (27/09/2004 – 28/07/2005) and 0.65 m d^{-1} (09/09/2003 – 27/09/2004) respectively, are reached in the central part of the flow path at a distance of 4.5 to 5.0 km from point C. In the section between 6.0 km and the endpoint of the transversal profile at D, motion decelerates rapidly to about 0.1 m d^{-1}. The reduced speed at the lateral glacier margins is caused by increased friction at the valley sides. Consequently, highest velocities occur near the centre-line.

Looking at Fig. 3 and 4 the longitudinal as well as the transversal profile of the image pair 27/09/2004 – 30/11/2004 shows a similar trend but with significantly increased flow velocities compared to the annual correlations. Velocity values are up to 0.4 m d^{-1} higher. This is equivalent to a velocity increase of about 65 %. This speed-up in flow velocity is influenced by the jökulhlaup from Grímsvötn caldera during the period 29/10/2004 – 02/12/2004. The subglacial floodwave propagated beneath Skeiðarárjökull causing an enhanced basal sliding at the glacier bed for several days. As shown in Fig. 4 the speedup nearly affects the whole width of the glacier tongue, whereas the most prominent increase of flow velocity occurs from about 3.4 km towards point D in the cross-profile. Most likely the main part of the melt water was discharged within that region and thus generated the most effective lubrication. MAGNÚSSON et al. (2005) detected a similar variation in flow velocity and flow pattern of Skeiðarárjökull during a jökulhlaup in 1996. They argue that the water disperses laterally at the glacier bed and, contrary to the classical jökulhlaup theory, does not solely drain via a single subglacial conduit. This theory of basal meltwater spreading explains the extensive speedup of Skeiðarárjökull shown in our

data set. Therefore, our results concerning the jökulhlaup from Grímsvötn caldera in autumn 2004 contribute to the new intensely discussed theory of meltwater discharge during glacial torrents.

6 Conclusions

Ice dynamics of Skeiðarárjökull were investigated with special focus on autumn 2004, when a jökulhlaup drained subglacially under this outlet. Skeiðarárjökull is the largest southward trending outlet of Vatnajökull ice cap. Its elevation ranges from 1,740 m down to 100 m a.s.l. at the terminus. Three medial moraines divide the glacier into four different flow bands. The jökulhlaup draining under Skeiðarárjökull in autumn 2004 accompanied a volcanic eruption at the subglacial Grímsvötn caldera (01–06 November 2004). Meltwater discharge of this outburst flood peaked on 2 November and finally ended in early December, having released a total volume of ~0.8 km³ from Grímsvötn.

We used six optical ASTER scenes (spectral band 1: 0.52 – 0.60 μm) covering the time period 2001-2005 to compare the short-term variation in surface velocity related to the jökulhlaup with the mean annual velocities. Surface velocity values and the flow pattern of the glacier were derived by image-to-image cross-correlation applying the IMCORR software on five ASTER image pairs. Generally the four annual ASTER pairs (2001–2002, 2002–2003, 2003–2004, 2004–2005) show a higher density of correlated points, due to the similar surface conditions during the summer period where the bare ice is exposed on the whole glacier tongue. Therefore surface features like crevasses or ash cones can easily be correlated. Cross- correlation of the annual pairs yield very similar flow patterns with a pronounced NE-SW trending central flow line of maximum speed (up to 1.05 m d^{-1}) in contrast to the lateral parts of slower movement (< 0.1 m d^{-1}). Cross correlation of the data pair 27/09/04 – 30/11/2004 covering the jökulhlaup, was complicated by snow coverage in the ASTER scene acquired on 30/11/2004 especially at higher elevations of Skeiðarárjökull. Nevertheless, correlation point density is reduced only marginally in the lower parts of the glacier at this date, because surface features are not completely masked by the thin snow cover. A considerable increase in flow velocity of up to 0.4 m d^{-1} compared to the annual values was observed probably due to enhanced glacier sliding triggered by the higher amount of subglacial meltwater during the jökulhlaup. The extensive acceleration over nearly the whole width of the glacier suggests a widespread lubrification at the glacier bed. This is only hardly explainable by the classical jökulhlaup theory of floodwater drainage in a single subglacial conduit, a sheet flow or coupled sheet and tunnel seems more likely. This corresponds to the new theory of meltwater discharge during glacial torrents already confirmed for a major jökulhlaup at Skeiðarárjökull in 1996. Considering our results, an at least partial spreading of meltwater at the glacier base occurs at Skeiðarárjökull even during moderate jökulhlaups.

References

AÐALSGEIRSDÓTTIR, G., 2003: Flow dynamics of Vatnajökull ice cap, Iceland. - PhD Thesis, 178 pp., ETH Zürich.

BERENSTEIN, R., 1983: Image geometry and rectification. Manual of Remote Sensing (R.N. Colwell, ed.). - American Society of Photogrammetry, Falls Church, VA.

BERTHIER, E., RAUP, B. & SCAMBOS, T., 2003: New velocity map and mass-balance estimate of Mertz Glacier, East Antarctica, derived from Landsat sequential imagery. - Journal of Glaciology, **49**: 503-511.

BERTHIER, E., VADON, H., BARATOUX, D., ARNAUD, Y., VINCENT, C., FEIGL, K.L., RÉMY, F. & LEGRÉSY, B., 2005: Surface motion of mountain glacier derived from satellite optical imagery. - Remote Sensing of Environment, **95**: 14-28.

BJÖRNSSON, H., 1975: Subglacial water reservoirs, jökulhlaups and volcanic eruptions. - Jökull, **25**: 1-11.

BJÖRNSSON, H. & EINARSSON, P., 1990: Volcanoes beneath Vatnajökull, Iceland: Evidence from radio echo-sounding, earthquakes and jökulhlaups. – Jökull, **40**: 147-168.

BJÖRNSSON, H., PÁLSSON, F., FLOWERS, G. E. & MAGNÚSSON, M. T., 2001: The extraordinary 1996 Jökulhlaup from Grímsvötn, Vatnajökull, Iceland. - Eos Trans. AGU **82** (47), Fall Meet. Suppl., Abstract IP21A-0667.

BJÖRNSSON, H., 2002: Subglacial lakes and jökulhlaups in Iceland. - Global Planetary Change, **35**: 255-271.

BJÖRNSSON, H., PÁLSSON, F. & MAHLMANN, A., 2004: Inventory and database of Icelandic jökulhlaups. In Glaciorisk - Survey and prevention of extreme glaciological hazards in European mountainous regions (D. RICHARD & M. GAY, ed.). - EVGI 2000 00512, Final Report, Grenoble.

FLOWERS, G., BJÖRNSSON, H., PÁLSSON, F. & CLARKE, G., 2004: A coupled sheet-conduit mechanism for jökulhlaup propagation. - Geophysical Research Letters, **31** (5): doi: 10.1029/2003GL019088. issn: 0094-8276.

GUÐMUNDSSON, M.T., & BJÖRNSSON, B., 1991: Eruptions in Grímsvötn, Vatnajökull, Iceland, 1934-1991. - Jökull, **41**, 21-45.

HARDARDÓTTIR, J., JÓNSSON, P., SIGURÐSSON, G., ELEFSEN, S.O., SIGFÚSSON, B. & GÍSLASON, S.R., 2005: Discharge and Sediment Monitoring of the 2004 glacial Outburst Flood Event (Jökulhlaup) on Skeiðará Sandur Plain, South Iceland. - International symposium on earth and planetary ice-volcano interactions, Reykjavík June 2006, Abstract 45A072.

JÓHANNESSON, T., 2002: Propagation of a subglacial flood wave during the initiation of a jökulhlaup. - Hydrological Sciences Journal, **47** (3): 417-434.

KÄÄB, A., LEFAUCONNIER, B. & MELVOLD, K., 2005: Flow field of Kronebreen, Svalbard, using repeated Landsat 7 and ASTER data. - Annals of Glaciology, **42**: 7-13.

MAAS, H.-G., DIETRICH, R., SCHWALBE, E., BÄßLER, M. & WESTFELD, P., 2006: Analyse des Bewegungsverhaltens des Jakobshavn Isbrae Gletschers in Grönland durch monokulare Bildsequenzanalyse. - Photogrammetrie Fernerkundung Geoinformation, **2**: 93-102.

MAGNÚSSON, E., ROTT, H., BJÖRNSSON, H., ROBERTS, M.J., BERTHIER, E. & PÁLSSON, F., 2005: The effects of basal water beneath Vatnajökull, Iceland, observed by SAR interferometry. - Proceedings of: The FRINGE`05 Workshop, Frascati November 2005.

MÜNZER, U., SCHARRER, K., GUDMUNDSSON, Á. & MARTINIS, S., 2007: NRT monitoring of the 2004 subglacial Grímsvötn eruption (Iceland) with ENVISAT-ASAR data. - ENVISAT Symposium, April 2007, Montreux, ESA **SP**-634, Noordwijk (in press).

NG, F.S.L., 1998: Mathematical modelling of subglacial drainage and erosion. - PhD/DPhil Thesis, 178 pp., University of Oxford.

NYE, J.F., 1976: Water flow in glaciers: jökulhlaups, tunnels and veins. - Journal of Glaciology, **17** (76): 181-207.

RENTSCH, H., WELSCH, W.M., HEIPKE, C. & MILLER, M.M., 1997: Digital terrain models as a tool for glacier studies. - Schriftenreihe Studiengang Vermessungs-wesen, (Eds. Welsch, W.M., Lang, M. and Miller, M.M), Universität der Bundeswehr München, **50**: 171-184.

ROBERTS, M.J., 2005: Jökulhlaups: A reassessment of floodwater flow through glaciers. - Reviews of Geophysics, **43**: 1-21.

ROBERTS, M.J., STURKELL, E., GEIRSSON, H., GUÐMUNDSSON, M.T., PÁLSSON, F., BJÖRNSSON, H., GUÐMUNDSSON, G.B., ELEFSEN, S.O., GÍSLASSON, S., SÍGFUSSON, B. & JÓNSSON, P., 2005: Large increase in glacier sliding during subglacial flooding. - Geophysical Research Abstracts, Vol. **7**, 09946.

RÖTHLISBERGER, H., 1972: Water pressure in intra- and subglacial channels. - Journal of Glaciology, **11**: 177-203.

SCAMBOS, T.A, DUTKIEWICZ, M.J., WILSON, J.C. & BINDSCHADLER, R.A., 1992: Application of image cross-correlation to the measurements of glacier velocity using satellite image data. - Remote Sensing of Environment, **42** (3): 177-186.

SIGMUNDSSON, F. & GUÐMUNDSSON, M.T., 2004: Gos í Grímsvötnum 1. - 6. nóvember 2004. - Jökull, **54**: 139-142.

Anschriften der Autoren:

Luisenstr. 37, 80333 München

Dipl.-Geogr. Sandro Martinis
Tel.: 0049-89-21806584
e-mail: s.martinis@iaag.geo.uni-muenchen.de
Dipl.-Geogr. Kilian Scharrer
Tel.: 0049-89-21806584
e-mail: K.Scharrer@iaag.geo.uni-muenchen.de
Dr. Ulrich Münzer
Tel.: 0049-89-21806589
Fax: 0049-8921806587
e-mail: ulrich.muenzer@iaag.geo.uni-muenchen.de
Department für Geo- und Umweltwissenschaften,
Sektion Geologie
Ludwig-Maximilians-Universität München

Dr. Christoph Mayer
Tel.: 0049-89-230311260
e-mail: Christoph.Mayer@lrz.badw-muenchen.de
Bayerische Akademie der Wissenschaften
Kommission für Glaziologie
Alfons-Goppel Str. 11, 80539 München

Ágúst Gudmundsson
Tel.: 00354-869-1849
e-mail: fjarkonn@simnet.is
Fjarkönnun ehf
Furugrund 46, Kópavogur, Iceland

Tab. 1: Characteristics of the correlation pairs.

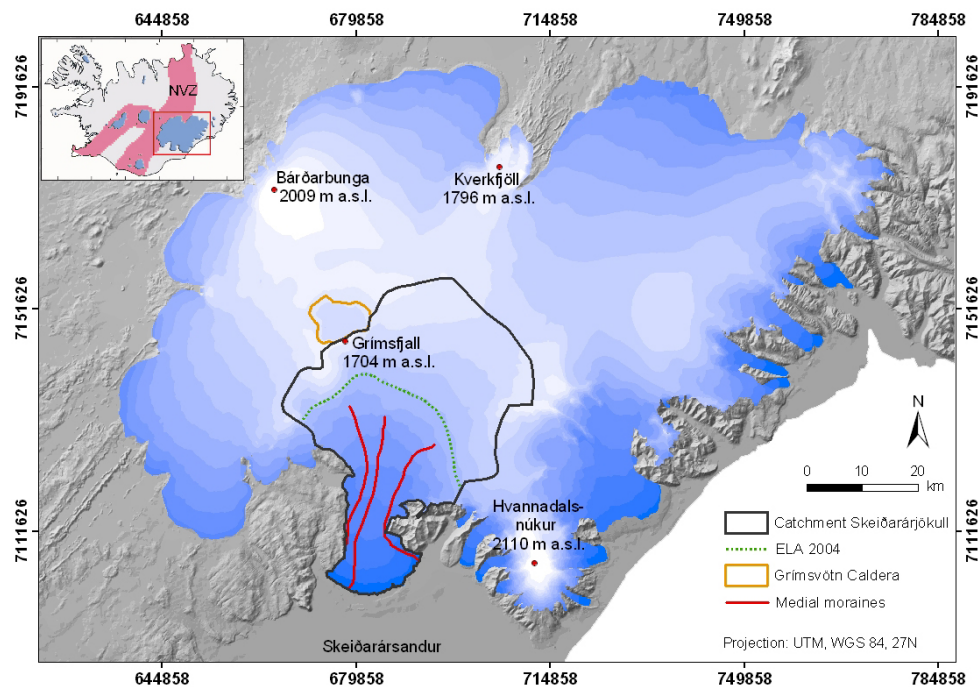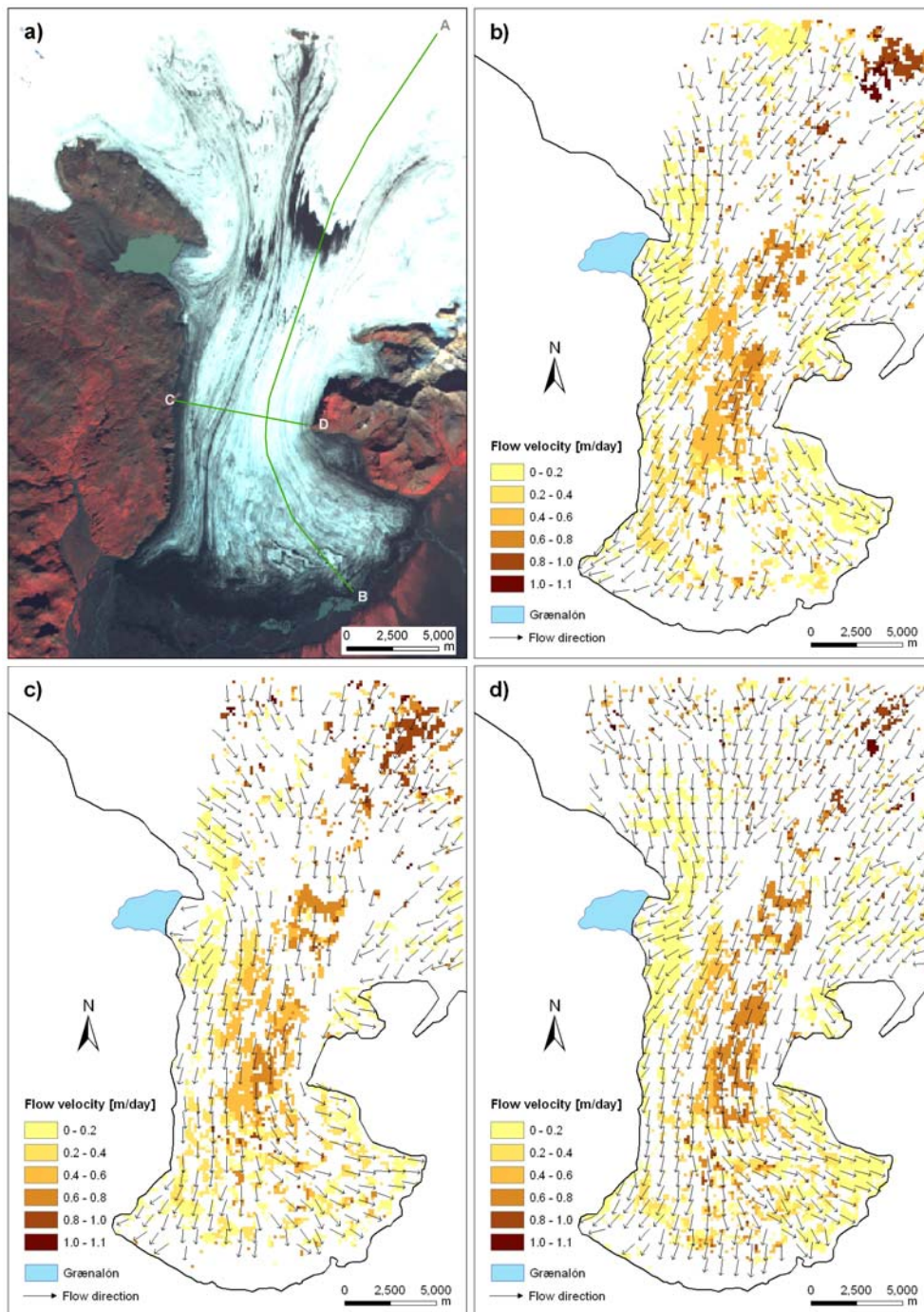| Correlation pair	Accuracy (m d^{-1})	Correlation area overlap (km²)	Correlated pixel	Correlated pixel / km²
05/10/2001 – 13/09/2002	± 0.05	412.9	27,583	66.8
13/09/2002 – 09/09/2003	± 0.04	413.4	23,192	56.1
09/09/2003 – 27/09/2004	± 0.04	455.9	25,170	55.2
27/09/2004 – 28/07/2005	± 0.05	388.8	30,482	78.4
27/09/2004 –30/11/2004	± 0.24	456.6	14,201	31.1

Fig. 1: Vatnajökull and its outlet glacier Skeiðarárjökull
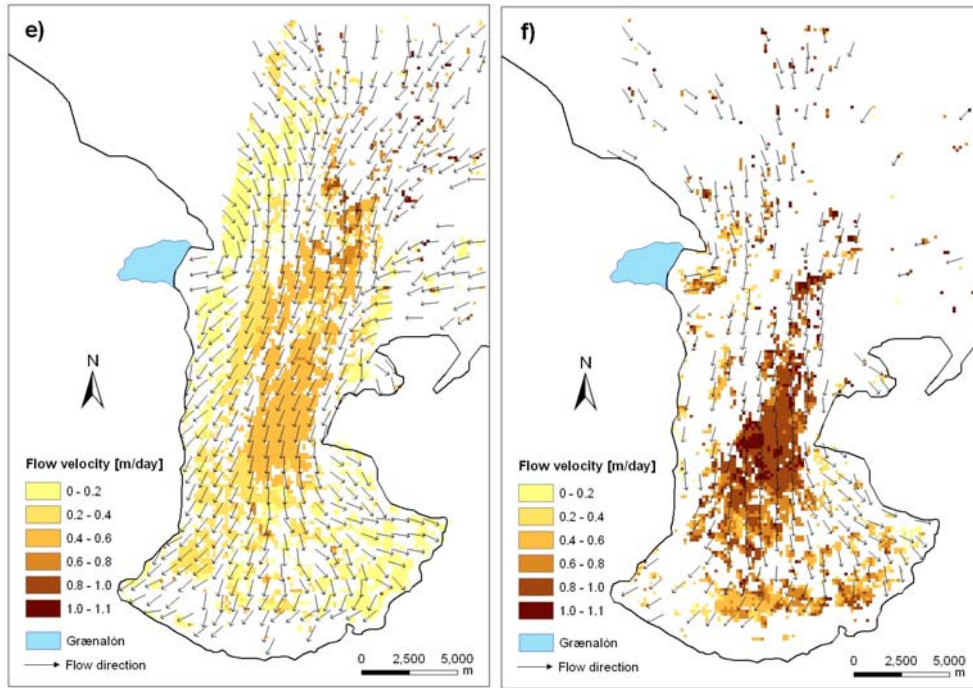
Fig. 2: a) Terra ASTER subscene from 27/09/2004 (RGB), © NASA. Surface velocity field of Skeiðarárjökull outlet, derived from ASTER imagery for the periods b) 05/10/01 - 13/09/02, c) 13/09/02 - 09/09/03, d) 09/09/03 - 27/09/04, e) 27/09/04 - 28/07/05, f) 27/09/04 - 30/11/04.
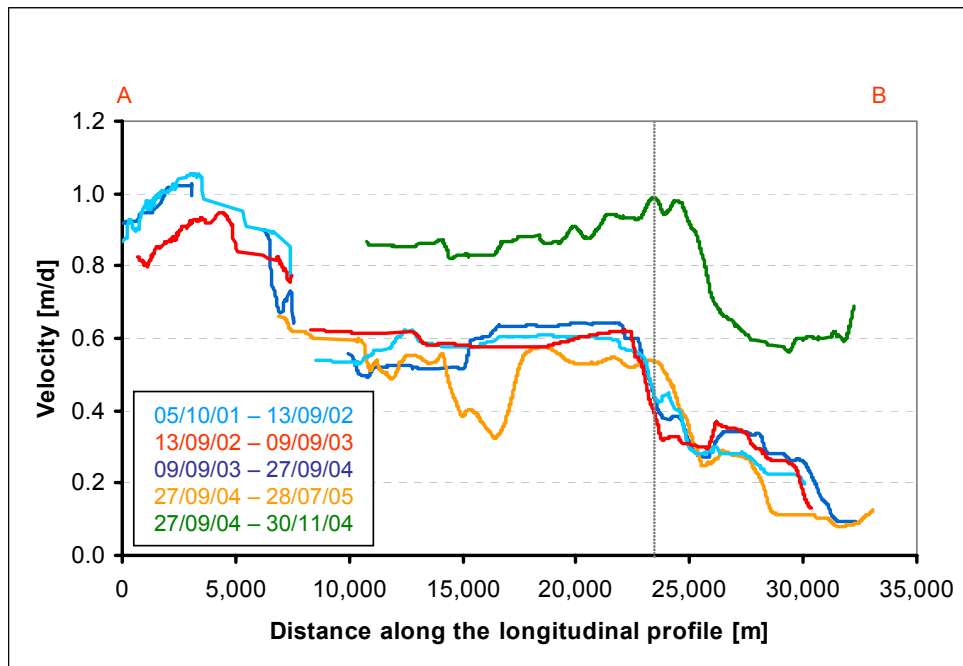

Fig. 3: Longitudinal profiles of ice velocity (A-B, see Fig. 2a). The vertical grey line marks the intersection with the transversal profile (C-D).
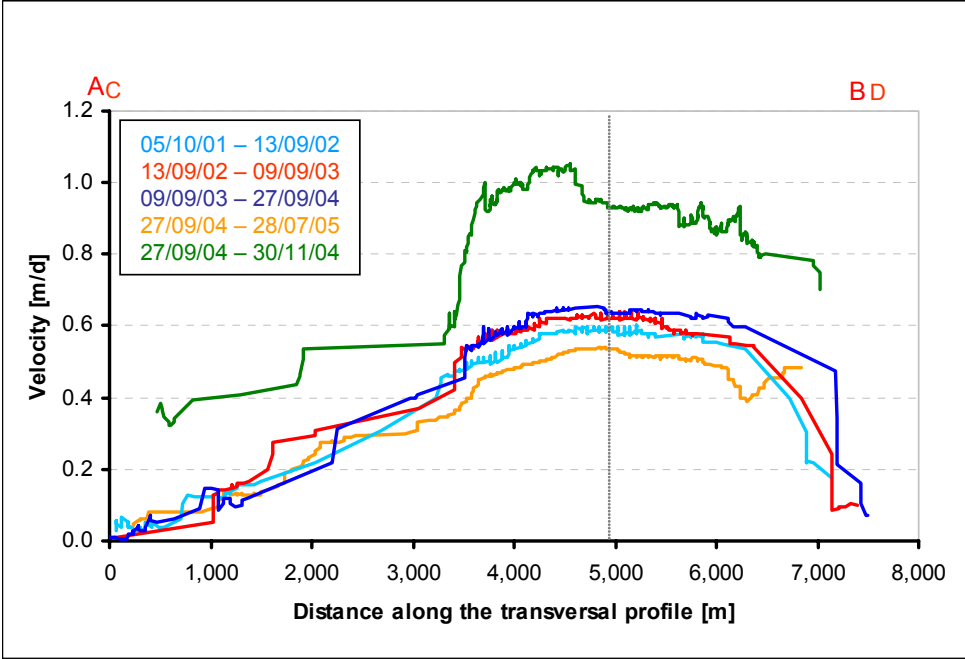
Fig. 4: Transversal profiles of ice velocity (C-D, see Fig. 2a). The vertical grey line marks the intersection with the longitudinal profile (A-B).

Paper 4

Scharrer K, Spieler O, Mayer Ch Münzer U (2007, available online) Imprints of subglacial volcanic activity on a glacier surface – SAR study of Katla volcano (Iceland). Bull. Volcanol., DOI 10.1007/s00445-007-0164-z

RESEARCH ARTICLE

Imprints of sub-glacial volcanic activity on a glacier surface—SAR study of Katla volcano, Iceland

K. Scharrer · O. Spieler · Ch. Mayer · U. Münzer

Abstract The Katla central volcano, covered by the fourth largest Icelandic glacier Mýrdalsjökull, is among the most dangerous and active volcanoes in Iceland. Due to the ice cover, several indicators of its volcanic activity can only be identified indirectly. We analysed a total of 30 synthetic aperture radar (SAR) images with special focus on identifying circular and linear depressions in the glacier surface. Such features are indicative of sub-glacial geothermal heat sources and the adjacent sub-glacial tunnel (melt water drainage) system. The time series comprises images from five different SAR sensors (ERS-1, ERS-2, JERS-1/SAR, RADARSAT and ENVISAT-ASAR) covering a time period of 12 years, starting in 1994. Individual SAR scenes only partly map the glacier surface morphology due to the environmental influences on the SAR backscatter intensity. Thus, only surface features detectable in several SAR scenes at the same location were considered and merged to form an overall picture of the surface morphology of Mýrdalsjökull and its modification by sub-glacial volcanic activity between 1994 and 2006. Twenty permanent and 4 semi-permanent ice cauldrons could be identified on the surface of Mýrdalsjökull indicating geothermally active areas in the underlying caldera. An analysis of their size was not possible due to the indistinct outline in the SAR images. The spatial distribution of the geothermally active areas led to a new, piecemeal caldera model of Katla volcano. All cauldrons are connected to tunnel systems for melt water drainage. More than 100 km of the sub-glacial drainage system could be identified under the Mýrdalsjökull in the SAR time series. It has been found that the tunnel systems are not in agreement with estimated water divides. Our results allow improved assessment of areas of potential Jökulhlaup hazard accompanying a sub-glacial eruption.

K. Scharrer (✉) · U. Münzer
Section Geology, Department of Earth and Environmental Sciences, Ludwig-Maximilians-University,
Luisenstr. 37,
80333 Munich, Germany
e-mail: k.scharrer@iaag.geo.uni-muenchen.de

O. Spieler
Section Mineralogy, Petrology and Geochemistry,
Department of Earth and Environmental Sciences,
Ludwig-Maximilians-University,
Theresienstr. 41/III,
80333 Munich, Germany

Ch. Mayer
Bavarian Academy of Sciences and Humanities,
Commission for Glaciology,
Alfons-Goppel Str. 11,
80539 Munich, Germany

Introduction

The purpose of this study is to investigate the imprints of sub-glacial volcanic processes on the glacier surface by synthetic aperture radar (SAR) time series analyses to draw conclusions regarding the associated volcanic activity and potential hazard. Monitoring of volcanoes covered by glaciers is a challenging task. Due to the ice cover, several indicators of volcanic activity can only be identified indirectly. Small scale crustal deformations caused by magma movements interfere with ice flow of the overlying glacier, preventing a distinct classification of the signal.

This complicates the application of interferometric SAR or GPS measurements for ground motion detection preceding a sub-glacial volcanic eruption (Sturkell et al. 2003). Seismicity also appears to be influenced by glacier loading and deloading throughout the year (Einarsson and Brandsdóttir 2000; Gudmundsson and Stefansson 2007). An estimation of the degassing rate may be obtained by conductivity measurements and chemical analyses of the glacial rivers (Kristmannsdóttir et al. 2002).

Furthermore, monitoring surface temperatures of volcanoes is one of the essential elements in understanding their state of activity (e.g. Dehn et al. 2000). Remotely sensed thermal infrared imagery (TIR) have been successfully applied on numerous parameters at ice-free systems, such as lava flow cooling and lava effusion rates (e.g. Oppenheimer 1991; Harris et al. 1998; Lombardo et al. 2004). However, although the surface temperature distribution of an ice-free volcano can be observed by using TIR imagery, the energy produced by sub-glacial geothermal activity is absorbed by ice melting at the base of the glacier. However, if the melt water finds a way to leak from the basal reservoir, the volume loss at the glacier bottom will create a depression in the glacier surface. Such a depression has a circular shape and is surrounded by several rings of concentric crevasses, indicating ice deformation (Fig. 1). An analogue feature forms on the glacier surface when the local pressure gradients of the overburden ice prevent melt water drainage, resulting in a cupola-shaped lake at the glacier bed (Björnsson 1975, 1988; Benn and Evans 1998). In such a case, melt water accumulates in the reservoir until the water pressure exceeds the ice overburden pressure and the water escapes in a glacial torrent (Jökulhlaup). In the majority of cases, basal melt water travels within a distinct conduit eroded into the underside of the glacier or in the underlying sediment (Röthlisberger 1972; Nye 1976; Björnsson 1988, 2002; Benn and Evans 1998; Roberts 2005). Due to the plasticity of ice, the course of sub-glacial melt water tunnels is indicated by half-pipe-shaped sinks (Sturm and Benson 1985; Björnsson 2002; Roberts 2005).

Hence, geothermal activity under a glacier is manifested by depressions in the glacier surface and the accompanying tunnel system for melt water drainage, which can be detected with remote sensing techniques. SAR remote sensing is an appropriate method for monitoring glacier deformation and thus sub-glacial volcanoes. One of the main advantages, especially in the light of the Icelandic weather conditions, is the independence from cloud cover and daylight, allowing a sufficient number of SAR images for analysis. Early SAR studies of Iceland using SEASAT data proved the applicability of SAR to Icelandic geological issues such as discrimination of surface types or identification of faults and lineaments (Malin et al. 1978; McDonough and Martin-Kaye 1984). The tandem mission of the satellites ERS-1 and ERS-2 enabled the investigation of glacier–volcano interaction by SAR interferometry particularly during an eruption of Grímsvötn under Vatnajökull in 1996 (Björnsson et al. 2001). Furthermore, several studies showed that SAR amplitude data are useful to study the imprints of sub-glacial morphology (Molnia and Jones 1989, 1990). The ability to penetrate the upper layers of snow and firn enables the detection of buried topographic features of a glacier that

Fig. 1 Painted relief of the Mýrdalsjökull test site. The glacier covers the caldera of the Katla central volcano. The glacial outlets of Mýrdalsjökull, the Eldgjá fissure and the neighbouring ice cap Eyjafjallajökull are labelled. The coverage is shown on the *inset* map on which the Neovolcanic Zone is also highlighted (*top left*). The oblique photograph (*bottom right*) shows an ice cauldron on Mýrdalsjökull. Their circular shape and the surrounding crevasses are clearly visible and are indicative of sub-glacial geothermal activity
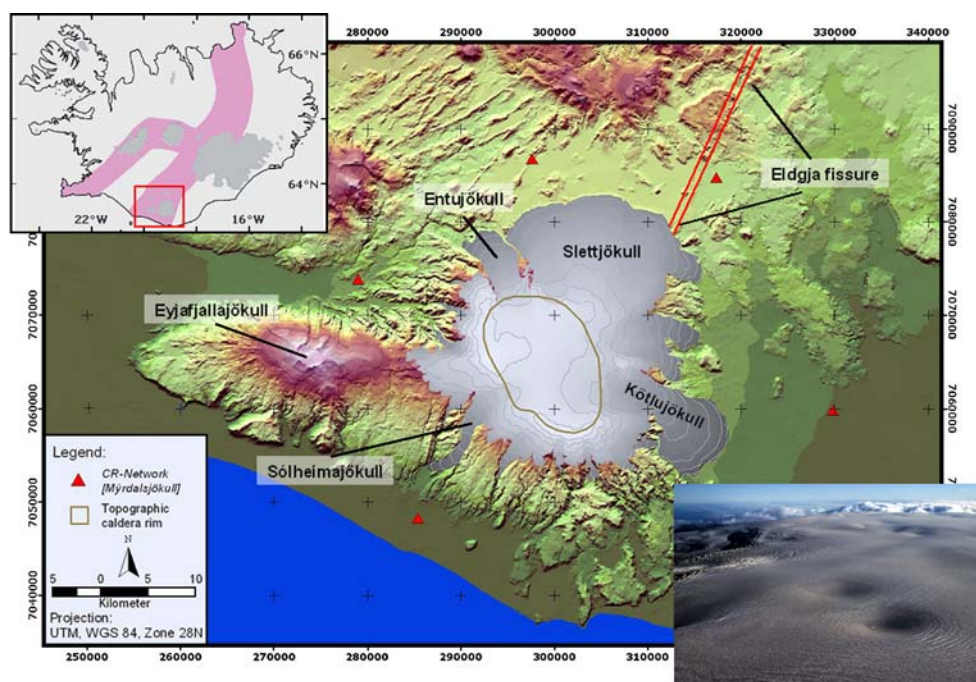
are related to the underlying glacially and fluvially eroded bedrock or to sub-glacial volcanic activity.

If deformation at a depression in the glacier surface is high enough to cause fracture, then the sink is surrounded by crevasses. Due to surface roughness the crevasses result in high backscatter values that can easily be used to outline an ice cauldron or elongate depressions associated with melt water tunnels. Furthermore, the slopes and floor of a depression often appear darker in SAR images (lower backscatter) than the undisturbed surrounding area. This is caused by the accumulation of fine-grained snow due to wind drift or a higher moisture content at the slopes receiving a higher amount of solar radiation (Henderson and Lewis 1998).

In this study, we analyse 30 SAR images spanning a 12-year period with special focus on identifying the circular and linear depressions indicative of sub-glacial geothermal heat sources and the sub-glacial channel systems for melt water drainage.

Test site

The Katla central volcano is among the most dangerous and active volcanoes in Iceland. It is located at the south coast of Iceland and at the southern tip of the Neovolcanic Zone (NVZ) (Fig. 1). The NVZ is an active section of the Mid-Atlantic ridge and therefore responsible for the high rates of seismic and volcanic activity across this zone. The Katla volcanic rock series is characterised by a well-defined bi-modal composition. The two end-members are Fe–Ti transitional-alkali basalts and mildly alkalic rhyolithes (Lacasse et al. 2006). On average, two eruptions have occurred within the Katla system every century during the last 1,100 years with the last major eruption in 1918 (Larsen 2000) with minor sub-glacial events occurring in 1955 and 1999 (Sigurdsson et al. 2000; Soosalu et al. 2006). The Katla volcanic system comprises an approximately 100 km^2 caldera connected to an 80-km SW–NE trending fissure swarm (Jakobsson 1979) (Fig. 1).

The caldera is covered by Mýrdalsjökull, which is the fourth largest Icelandic glacier (Fig. 1). Morphologically the ice cap can be divided into a plateau where the ice forms a contiguous cover down to about 1,300–1,000 m a.s.l., and a lower peripheral zone below this altitude where the ice cap splits into separate outlet glaciers (Fig. 1). Ice lobes exist in the east and the north, like Sléttjökull with a slope of less than 5°. Outlet glaciers on the western and southern sides are much steeper. Sólheimajökull in the south–west terminates at an altitude of 120 m a.s.l., the lowest point of Mýrdalsjökull, whilst the highest point is at about 1,500 m a.s.l. (Goðabunga). A total area of approx. 586 km^2 was determined for Mýrdalsjökull in 2004 (Jaenicke et al. 2006).

Ice thickness and sub-glacial morphology of Mýrdalsjökull were investigated by radio echo sounding (Björnsson et al. 2000). The caldera is 600 to 750 m deep and its highest rims reach 1,380 m a.s.l. Ice thickness reaches 600 to 740 m across a 12-km^2 area in the northern section of the Katla caldera. According to Björnsson et al. (2000), Mýrdalsjökull contains a total ice volume of 140 km^3 with 45 km^3 of ice being located inside the rims of the caldera. The ice–volcano interaction during sub-glacial eruptions leads to enormous melt water torrents (jökulhlaups), which devastate large areas surrounding the glacier. For example, at the peak of the last major Katla eruption in 1918, the maximum melt water discharge was estimated as 300,000 m^3/s (Tómasson 1996). Breaches in the caldera rim coincide with the outlet glaciers, which will therefore determine the jökulhlaup pathways during future Katla eruptions.

Data and methods

A time series of 30 multi-sensor SAR images covering the period 1994 to 2006 was analysed in this study (Table 1). The images were acquired as part of several remote sensing projects carried out under the auspices of European Space Agency (ESA), National Space Development Agency of Japan (NASDA) and Canadian Space Agency (CSA) with the aim of monitoring geodynamic processes related to geothermal, seismic and volcanic activity and examining climate change in the Neovolcanic Zone of southern Iceland.

Due to different focuses and data policies within the aforementioned projects, the time series can be divided into two parts. The data spanning 1994–2000 covers the lifetime of the satellites ERS-1/2, JERS-1 and RADARSAT, and images over Mýrdalsjökull were not ordered at regular intervals. For this period, 15 scenes from these sensors were at our disposal. Due to the limited number of images, all available images were used to achieve the best possible temporal coverage. This first part of the time series comprises four JERS-1 images, plus two from ERS-1, seven from ERS-2 and one from RADARSAT. An overview of the main sensor characteristics of these SAR instruments is shown in Table 2. In the period spanning 2000–2002, no SAR scenes were available for this area.

The second part of the time series starts in 2002, coinciding with the start of ENVISAT-ASAR acquisitions over Mýrdalsjökull (Table 1). Due to its beam steering capability, the ASAR instrument can acquire images in seven different swathes (IS1–IS7), covering an incidence angle range from 15° to 45° (Table 2). Images of the swathes IS2 and IS5 have been recorded continuously over Mýrdalsjökull since autumn 2002, leading to a substantial collection of ASAR images over the site. Considering the

Table 1 Overview and specifications of all SAR images analysed in this study

Date	Satellite	Look direction/orbit	Swath
16.09.1994	JERS-1	West/descending	–
14.12.1995	ERS-1	West/descending	–
22.02.1996	ERS-1	West/descending	–
07.08.1997	JERS-1	West/descending	–
20.09.1997	JERS-1	West/descending	–
30.01.1998	JERS-1	West/descending	–
21.08.1998	ERS-2	West/descending	–
18.06.1999	ERS-2	East/ascending	–
21.07.1999	ERS-2	West/descending	–
23.07.1999	ERS-2	East/ascending	–
06.08.1999	ERS-2	West/descending	–
22.08.1999	ERS-2	West/descending	–
25.08.1999	ERS-2	West/descending	–
23.11.1999	RADARSAT	East/ascending	–
02.03.2000	ERS-1	West/descending	–
15.11.2002	ENVISAT-ASAR	West/descending	IS5
27.07.2003	ENVISAT-ASAR	West/descending	IS2
31.10.2003	ENVISAT-ASAR	West/descending	IS5
09.01.2004	ENVISAT-ASAR	West/descending	IS5
23.04.2004	ENVISAT-ASAR	West/descending	IS5
24.10.2004	ENVISAT-ASAR	West/descending	IS2
19.11.2004	ENVISAT-ASAR	West/descending	IS5
23.01.2005	ENVISAT-ASAR	East/ascending	IS2
27.02.2005	ENVISAT-ASAR	East/ascending	IS2
12.06.2005	ENVISAT-ASAR	East/ascending	IS2
09.10.2005	ENVISAT-ASAR	West/descending	IS2
08.01.2006	ENVISAT-ASAR	East/ascending	IS2
19.03.2006	ENVISAT-ASAR	East/ascending	IS2
11.07.2006	ENVISAT-ASAR	West/descending	IS2
29.09.2006	ENVISAT-ASAR	East/ascending	IS2

35-day repeat pass of the ENVISAT satellite, and acquisition of the two swathes on ascending and descending orbits, respectively, an image of Mýrdalsjökull is obtained, theoretically, every 9 days.

Table 2 Characteristics of SAR sensors used in this study

| Satellite	Wavelengths (cm)	Polarisation	Incidence angle (°)	Spatial resolution (m)
ERS-1	5.6 [c-band]	VV	23.5	25
ERS-2	5.6 [c-band]	VV	23.5	25
JERS-1	23.5 [l-band]	HH	35	18
RADARSAT	5.6 [c-band]	HH	37	10
ENVISAT	5.6 [c-band]	VV	21 [IS2] and 38 [IS5]	25

The high number of available ASAR images allowed the pre-selection of eligible scenes. Only images where the glacier surface morphology was clearly detectable were thus selected for analysis. Many summer images had to be rejected because surface scattering (due to wet snow) is the dominant scattering mechanism during this season (Scharrer et al. 2007). This leads to low backscatter intensity, preventing the discrimination of glacier surface features especially if they are buried by the upper layers of the snow and firn. In total, 15 ENVISAT-ASAR images from autumn 2002 to autumn 2006 were selected and added to the time series.

Regardless of the sensor, the ability of SAR to detect glacier surface structures is determined by a number of environmental conditions (Fig. 2). SAR backscatter is strongly affected by topography, surface roughness and moisture of the illuminated ground target. Backscatter intensity, in particular, varies strongly with the annual and short-term weather conditions on a glacier. For additional and more technical information about SAR electromagnetic interactions see, for example, Henderson and Lewis (1998), Ulaby et al. (1986), Gao and Yansui (2001) and König et al. (2001).

To allow comparison of glacier surface features across the time series, a common reference system is required. This was achieved by applying and fitting all SAR images to a common DEM, allowing for the correction of inherent SAR recording characteristics (i.e. side looking geometry) and the influence of topography (layover, foreshortening, shadow). A digital elevation model (DEM, contour intervals 20 m) of the Mýrdalsjökull area based on 1:50,000 topographic maps produced in the 1990s was used for the terrain correction. The quality of terrain geocoding depends on the quality of the reference DEM and the accuracy of the SAR imaging parameters. To fit each SAR image to the DEM, ground control points (GCP) need to be identified in the SAR images. Due to the lack of structure in the area surrounding Mýrdalsjökull, identifying features suitable for use as GCPs is a difficult task. Hence, ten corner reflectors (CR) were installed in 1995 at five locations around the glacier (Fig. 1). At each location, one CR was oriented towards the ascending orbit and a second towards the descending orbit of the ERS-1/2 satellites. Because the ENVISAT satellite has the same orbit characteristics as ERS, the corner reflectors could be used as ground reference for images acquired during both missions. The distinct backscatter maximum of the CR is easily identifiable on the ERS-1/2 and ENVISAT-ASAR images and thus serve as high quality GCP, resulting in position accuracy of less than 1 pixel (i.e. 20 m).

Due to differing orbit parameters and wavelengths, the corner reflectors could not be used for geocoding of the JERS-1 and RADARSAT images. The retrieval of the GCPs for these scenes required the use of topographic 1:50,000 maps, making this processing step time-consuming and less

Fig. 2 Examples of the SAR time series showing Mýrdalsjökull under different conditions. The corresponding backscatter profiles cover cauldrons 9 and 10 (*profile A–B*) and the north-western part of Sléttjökull (*profile C–D*) with several elongate depressions also apparent due to melt water tunnels (*red arrows*). The *upper image* was recorded by ERS-2 on an ascending orbit at the end of July 1999 (23/07/1999). A layer of wet snow on the glacier leads to low backscatter intensity precluding discrimination of glacier surface features especially if they are buried by layers of snow and firn. Therefore, only one melt water tunnel can be detected in this image. The *lower image* was recorded by ENVISAT-ASAR on a descending orbit in October 2005 (09/10/2005). The lower content of liquid water in the snow layer on the glacier enables a deeper penetration depth of the radar signal and therefore provides more information on buried structures. Hence, four melt water tunnels can be detected
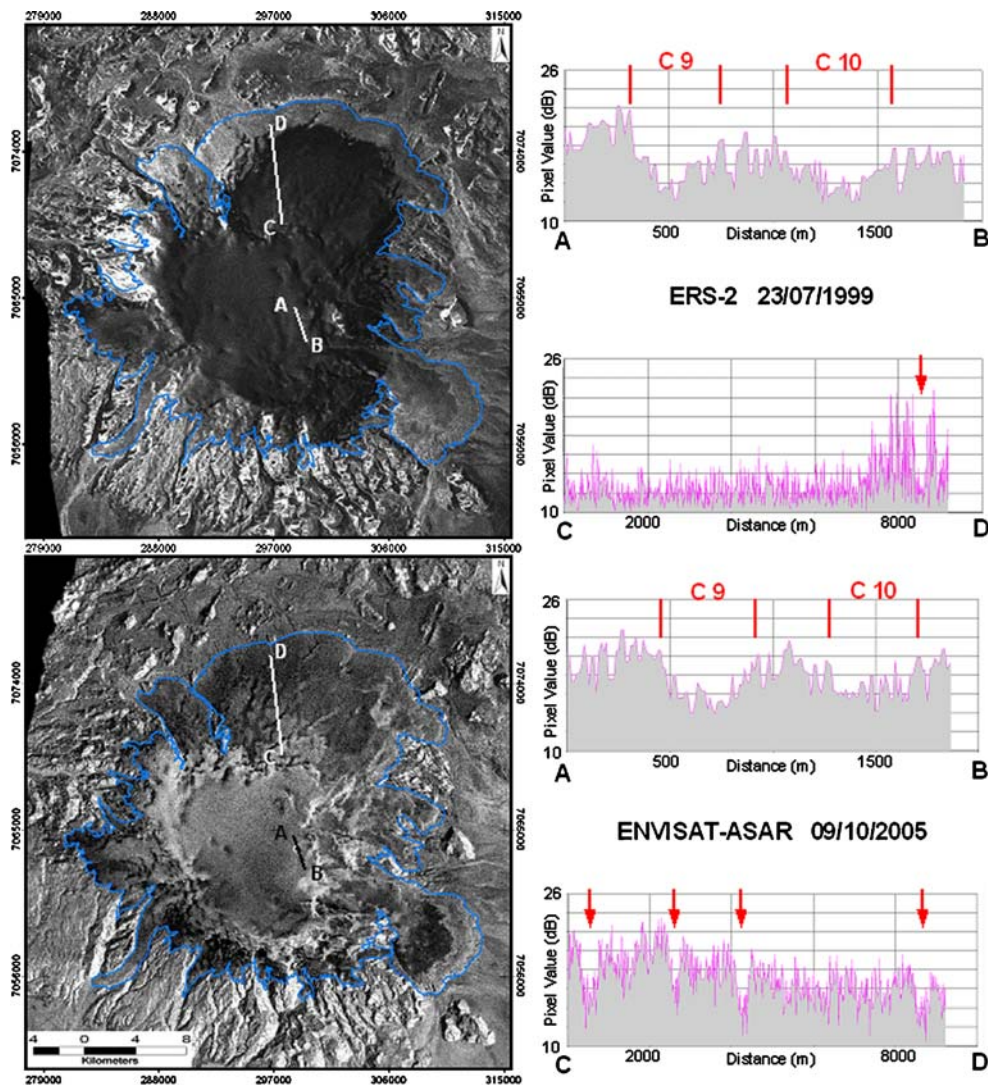
precise. After geocoding, the JERS-1 and RADARSAT images still showed slight displacements compared to the very accurately geocoded ERS-1/2 and ENVISAT-ASAR scenes. Therefore image-to-image co-registration was applied to avoid mismatching among the SAR images of the different sensors.

Finally, depending on the quality of individual images, additional filtering and contrast enhancement was performed to enhance the information content for glacier surface morphology. If necessary, a Lee-Sigma filter was applied for speckle suppression, using a 3×3-pixel window. Therefore, an error value of 1.5 pixels was included into the dimensional analysis. After image processing, ice structures were manually digitised on the satellite images. The shared reference system (UTM, WGS 84, Zone 28 North) enabled stacking of the individual results so that an overall picture of the surface morphology of Mýrdalsjökull, induced by sub-glacial volcanic activity between 1994 and 2006, could be derived.

Results

Environmental parameters are found to be the dominant factor in influencing the quality of the SAR scenes when studying glacier surface features. Variations in sensor specific incidence angle, spatial resolution, polarisation and wavelength are only of minor importance for the analysis of surface features at Mýrdalsjökull. The longer wavelength of JERS-1 and the better spatial resolution of RADARSAT showed no advantage when compared with ERS or ENVISAT data (Table 1). However, the use of ascending and descending orbits was essential for the detection of surface features on varying slope expositions. Due to the look direction, descending scenes provide a higher information content on the eastern slopes of Mýrdalsjökull, whereas ascending scenes show more details on western slopes.

Generally, the sensitivity of the SAR signal to variations in environmental factors required use of a high number of scenes

to draw a reliable and complete picture of the glacier surface structures. As previously mentioned, the time-variant surface roughness and moisture content strongly influences the SAR backscatter intensity. Individual SAR scenes only partly map the glacier surface morphology due to environmental perturbations or to orbit-induced effects (Fig. 2). In this study, only surface features detectable in several SAR scenes at the same location were considered. Surface features only apparent on a single date were neglected.
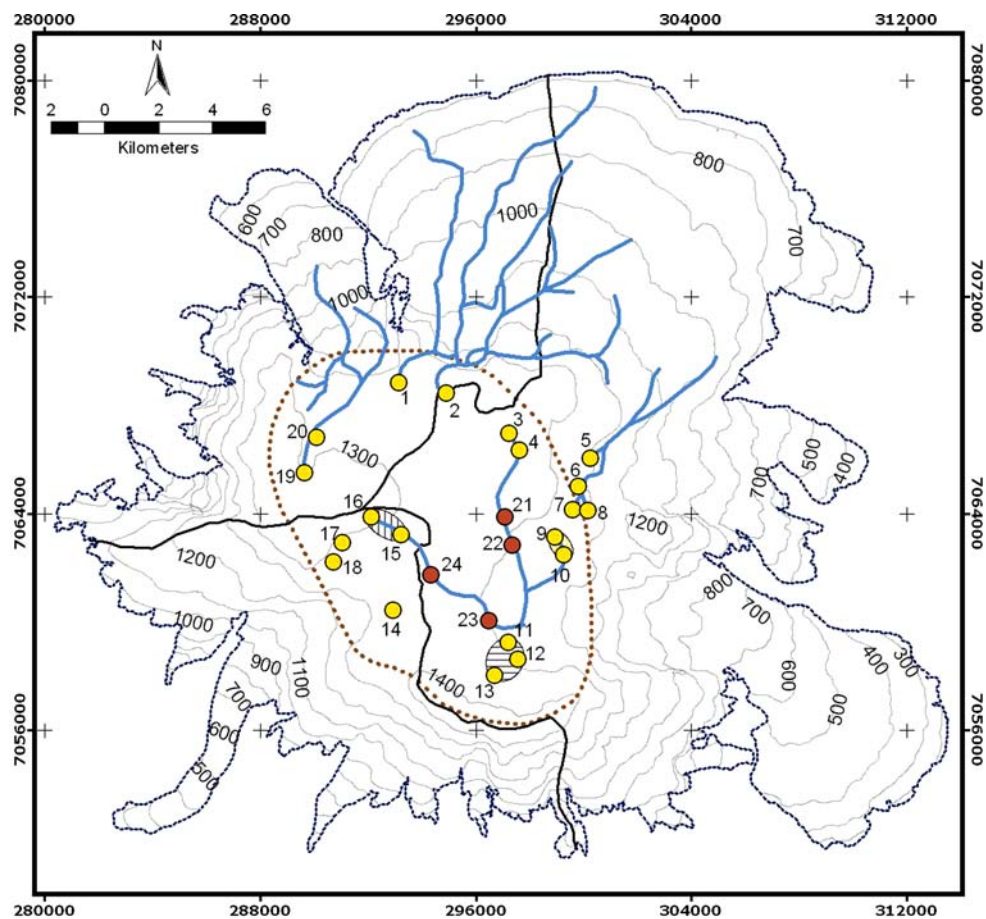
Ice cauldrons

Altogether, 24 active geothermal areas, represented by ice cauldrons, were found at Katla volcano: 20 within the caldera and 4 on and/or marginally outside, the eastern rim (Fig. 3). The cauldrons were classified into permanent and semi-permanent because depressions 21–24 were only detectable intermittently in the SAR images of the time

sequence. Hence, such intermittently detectable features were termed semi-permanent. Considering the bedrock topography mapped by Björnsson et al. (2000), the active geothermal areas were located across an altitude range spanning approximately 720 m a.s.l. (cauldron 10) and approximately 1,160 m a.s.l. (cauldron 8). At the majority of the active geothermal areas the thickness of the overlying ice cover was at least approximately 230 m (cauldron 18) with a maximum of approximately 530 m (cauldron 20). Cauldron 8, located outside of the caldera rim, was covered by only approximately 60 m of glacier ice.

The location of the depressions and therefore of the active geothermal areas was constant over the whole period of investigation. In the northern part of the Katla caldera, the active areas form a string running along the inner slopes of the rim (cauldrons 1–4, 9, 10, 17, 19 and 20) (Fig. 3). Permanent cauldrons 11–16 and semi-permanent cauldrons 21–24 indicate geothermal activity at the centre and

Fig. 3 Surface morphologies of Mýrdalsjökull associated with sub-glacial volcanic activity mapped using the full SAR time series. Ice cauldrons indicate geothermal activity in the sub-glacial Katla caldera. More than 100 km of the sub-glacial tunnel systems, draining the melt water from the active geothermal areas, can be mapped

southern sector of the caldera. A comparison with the sub-glacial topography (Björnsson et al. 2000) shows that these geothermal areas (11–16 and 21–24) coincide with sub-glacial ridges and isolated mounts. No activity is apparent across the southern caldera flanks, but a cluster of four cauldrons (5–8) are apparent on and/or marginally outside the north-eastern rim. This cluster is located exactly on the linear extension of the sub-aerial part of the Eldgjá fissure associated with the Katla volcanic system (Figs. 3 and 5). Furthermore, several active geothermal active areas correspond with the known eruption sites of 1,755 (cauldrons 15 and 16) and 1,823/1,918 (cauldrons 11–13) (Fig. 3) (Björnsson et al. 2000). Furthermore, cauldrons 9 and 10 are associated with the minor sub-glacial event of 1955 and cauldron 14 was the source of the 1999 jökulhlaup at Sólheimajökull.

The size of the cauldrons was not extracted. This measurement was problematic due to seasonal variations in snow coverage and surface properties, which will influence the measured cauldron dimensions in individual SAR images. In addition, no distinct outline was identifiable in the SAR images. Cauldrons 3, 4, 9, 10, 11, 12, 15 and 16 were the most prominent or best detectable depressions in the SAR time series. To provide a rough estimation of their proportions in the SAR scenes, the average diameter of the cauldrons was measured for the years 2005–2006, as shown in Fig. 4. To delineate the subsided area, we only used the innermost backscatter peaks, if crevasses existed, or the changeover to the lower backscatter values induced by the subsided slopes. An error value of 4 pixels, corresponding to 80 m, takes into account the indistinct outline and filtering during image processing. The SAR-derived diameter of the cauldrons when compared with radar altimeter measurements carried out since

1999 (Gudmundsson et al. 2007; University of Iceland 2006) show a good agreement except for five outliers corresponding to cauldrons 2, 3, 9, 17 and 19 (Fig. 4). The differing diameters for these cases can be explained by the direction of the measured profile. The direction of the measured profile in the SAR images matches the direction of the altimetry flight lines for the cauldrons at which the diameters are found to agree with those obtained from the altimeter data. At the five cauldrons were the SAR-derived diameter appears to provide an underestimate in comparison with the altimeter data, the measurement was made on a profile transverse to the altimeter flight lines. The varying directions of the measured profiles in the SAR images are caused by the often indistinct outlines of the cauldrons.

Subglacial drainage system

More than 100 km of melt water tunnels could be identified running beneath Mýrdalsjökull in the SAR time series (Fig. 3). Every detectable tunnel originates at an ice cauldron, and therefore at an active geothermal area, or connects geothermal areas. The location and extent of the drainage system is persistent over the entire period of investigation. The width of the linear surface features, corresponding to subglacial tunnels, typically ranges between 150 and 250 m in the SAR images.

Some tunnels are connected and form four discrete drainage systems; the Entujökull, Sléttjökull, Eldgjá and inner caldera systems (Fig. 3). The Entujökull system consists of two main tunnels originating in the NW part of the caldera. Over their proximal sections they run parallel to the caldera rim and take the first exit down the Entujökull valley. The tunnels are connected to, and thereby drain, the

Fig. 4 Average diameter of the ice cauldrons measured in SAR images from 2005 to 2006 compared with radar altimetry measurements carried out since 1999 by Gudmundsson et al. (2007); University of Iceland 2006)
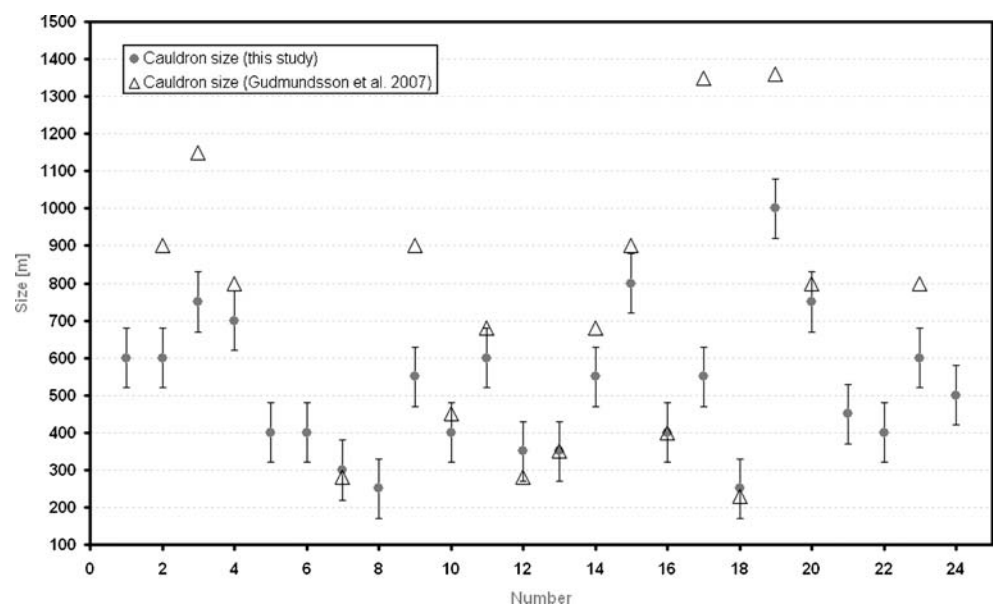
melt water of cauldrons 19 and 20. The drainage system could not be tracked down to the terminus of Entujökull.

The Sléttjökull system shows the best developed tunnel system (Fig. 3). Several major tunnels are apparent especially the NW part of the ice lobe where they are predominantly slope-parallel. Transverse passages establish a connection between all detectable tunnels. Considering the flow direction of the eastern tunnels, a widespread dendritic drainage system seems to be developed under the entire Sléttjökull. The whole system originates inside the caldera rim, draining the melt water from under cauldrons 1 and 2.

The Eldgjá system drains the melt water of cauldrons 5 to 8, which are all located outside of the caldera. The direction of the tunnels follows the sub-glacial extension of the Eldgjá fissure emerging at the north-eastern part of Sléttjökull.

Inside the caldera, a system of three linked tunnels is detectable (Fig. 3). This tunnel system collects melt water from ten cauldrons to channel water towards the Kötlujökull outlet where the lowest breach in the caldera rim is located. The left branch drains cauldrons 15, 16, 23 and 24, the central drains 3, 4, 21 and 22, and the right branch drains 9 and 10. At the steep outlets (Sólheimajökull, Kötlujökull) in the south, no tunnel system is detectable.

Discussion

A comparison of the ice cauldrons associated drainage systems with the sub-glacial topography is very informative (Fig. 5) (Björnsson et al. 2000). Despite the rather poor resolution of the sub-glacial topography, it becomes obvious that no major ridges or valleys are developed in the bedrock below the impressions of the sub-glacial tunnels, which could be responsible for the surface features in the SAR images.

The northern outlet, Sléttjökull, experienced a glacial surge in 1992, raising the question as to whether the surface features are related to this event (Björnsson et al. 2003). The occurrence of half-pipe-shaped depressions in many other areas of Mýrdalsjökull not affected by the surge indicates that the features on Sléttjökull are not related to the event. The dendritic shape of the tunnel system under Sléttjökull, showing no relation to the flow direction of the surge, likewise confirms this interpretation. Furthermore, the persistent location and the almost constant dimensions of this system during the period of investigation suggest a relation to sub-glacial melt water flow.

All tunnel systems originate at one or several ice cauldrons, beneath which geothermal heat will melt the base of the glacier. Therefore, it can be assumed that the tunnels develop at the ice–bedrock interface, at least close to the source-cauldron. The steady heat output at the geothermal

areas supplies a constant amount of melt water to the drainage system, resulting in equilibrium between a tendency for tunnel closure by ice deformation and enlargement by frictional heat of melt water flow. Frequent observations of sulphurous smells at the glacial rivers Múlakvísl (collecting water from Kötlujökull) and Jökulsá á Sólheimasandi (collecting water from Sólheimajökull) confirm a continual supply from at least several active geothermal areas (possibly cauldrons 3–4, 9–18 and 21–24) (Björnsson et al. 2000). Due to the ice overburden pressure, water in the conduits is pressurised, allowing water to travel uphill along certain sections, which is especially apparent in tunnel sections at the caldera rim (Figs. 3 and 5).

The SAR-derived width (150–250 m) of the linear surface impressions associated with the tunnels appears large. At the Kötlujökull outlet, Näslund and Hassinen (1996) describe englacial melt water conduits having a diameter of 12–15 m not being destroyed by ice deformation. The much slower ice flow velocities inside the Katla caldera and at the Sléttjökull compared to Kötlujökull, may allow the formation of larger conduits. We can also make inferences as to the type of tunnels involved. So-called Röthlisberger (R)-channels are incised into the ice, whereas Nye (N)-channels are incised into the bed and tend to form braided canals (Röthlisberger 1972; Nye 1976). Considering the cross-section of their surface imprints, a braided network of N-channels seems more likely than a single R-channel. The presence of glacial sediments under Sléttjökull would allow the formation of N-channels with the stable position of their surface impressions reinforcing this assumption (Kjaer et al. 2003). Modelling of ice surface deformation over conduits with various dimensions could help to relate the affected area on the glacier surface measured in the SAR images to the actual diameter and shape of the underlying conduit.

Derived from a potential map describing the sum of the gravitational and pressure potential at the glacier bed, Björnsson et al. (2000) divide Mýrdalsjökull ice cap into three main drainage basins (Fig. 3). Both inside the caldera and at Sléttjökull in the north, the sub-glacial tunnels transcend the estimated water divides between these basins. This indicates that the potential map, based on the interpolated sub-glacial topography, is not accurate enough to describe the sub-glacial drainage system correctly. For example, cauldrons 15 and 16 are located within the catchments basin of Sólheimajökull whereas the sub-glacial tunnel system drains their melt water towards Kötlujökull. Melt water from the 1755 eruption site below cauldrons 15 and 16 also follows this drainage system, indicating the relevance of our findings for hazard zonation. The pre-existing sub-glacial tunnels would at least serve as the initial transport network for the basal passage of melt water during a catastrophic jökulhlaup (Björnsson et al. 2001;

Fig. 5 Location of ice cauldrons on the bedrock topography of Mýrdalsjökull. The structural elements and the locations of the ice cauldrons are shown in the *block diagram* across Mýrdalsjökull based on bedrock topography by Björnsson et al. (2000)
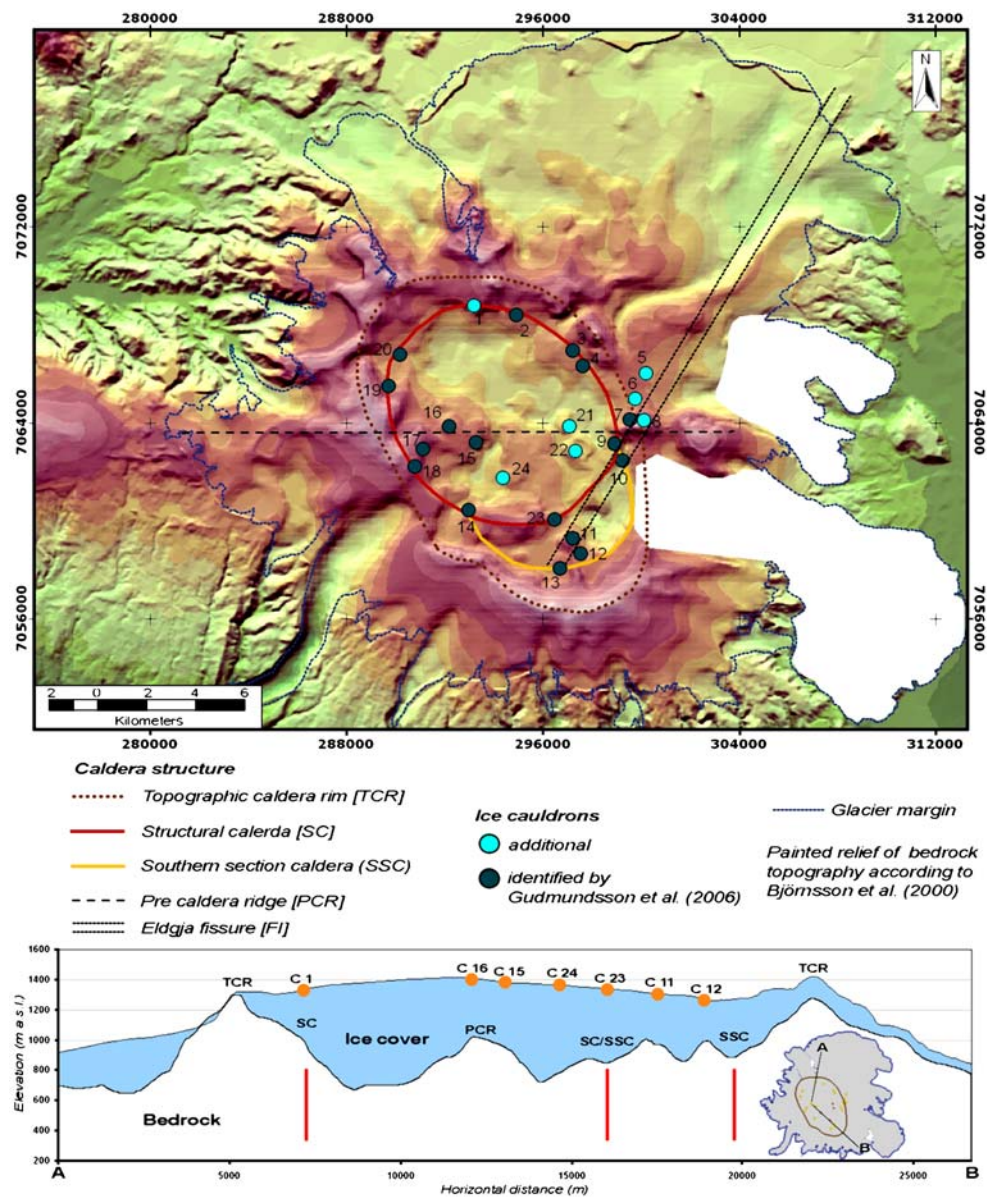
Björnsson 2002; Roberts 2005). Knowledge of the subglacial drainage system allows areas surrounding the glacier, potentially endangered by a jökulhaup during a sub-glacial eruption, to be predicted more precisely. For example, in case of a jökulhlaup draining Sléttjökull, the adjacent western and eastern river catchments would be affected. These new findings thus contribute to hazard assessment around Mýrdalsjökull.

The ice cauldrons associated with active geothermal areas at Mýrdalsjökull have been monitored on a regular basis since 1999 by radar altimetry (Gudmundsson et al. 2007; University of Iceland 2006). However, only 17 cauldrons have been identified so far in these data compared with 24 identified in our study (Fig. 5). The locations of the 17 altimeter-located cauldrons correspond well with those identified by us. One additional ice cauldron (cauldron 1) was found at the north-western margin of the caldera. It is connected to the Sléttjökull drainage system. Another three (cauldrons 5, 6 and 8) are located marginally outside the caldera on the eastern slopes. They are part of the Eldgjá drainage system. A further three semi-permanent cauldrons (21, 22 and 24) are situated in the centre of the Katla caldera. All semi-permanent depressions are located in the middle or lower section of a melt water tunnel. Only minor or sporadic activity can be assumed to be associated with these cauldrons or the melt water flow from the upstream cauldrons reduces the thermal effect on the glacier bottom at the locations. The circular shape of the seven additional cauldrons identified in our SAR time series, and their connection to the sub-glacial drainage systems, is a strong indicator that they are linked to underlying geothermal heat sources.

The location of the active geothermal areas in association with the sub-glacial topography (Björnsson et al. 2000) enables new insights on the structure of Katla caldera (Fig. 5). The caldera is delimited by a steep rim with a 14-km long major axis and a 9-km long minor axis (Björnsson et al. 2000). We assume that those active geothermal areas arranged in a circular pattern around the caldera perimeter (Fig. 5) are located above a ring fault, therefore indicating a structural feature with the dimensions 9.5 km (SE–NW) and 8 km (SW–NE), respectively. The spatial distribution of the heat sources thus provides further information on the structure of the caldera. The cauldrons can be associated with one or more of the structural elements as shown in Table 3. Specifically, heat sources can be found at the ring fault (SC), an E–W striking pre-caldera ridge (PCR) connecting Eyjafjallajökull and its extension E of Katla, the NE–SW trending Eldgjá fissure (FI) and the southern section of the caldera (SSC). Therefore, the structural caldera floor can be divided into two sections suggesting a piecemeal caldera (Lipman 1997) (Fig. 5). The accumulation of cauldrons east of the caldera focuses on the intersection of the four structural elements SC, SSC, FI and PCR. Four depressions in the centre of the caldera follow the PCR position where the western cauldrons 15 and 16 mark the eruptive centre of 1755.

Conclusion

Results presented in this paper demonstrate that SAR remote sensing is an appropriate method for mapping sub-glacial volcanoes. Due to its special characteristics, the detection of topographic features on the glacier surface related to sub-glacial volcanic activity is possible. Ice deformation over active geothermal zones result in circular depressions on the glacier surface surrounded by several rings of concentric crevasses. Likewise, the adjacent basal system for melt water drainage tunnels is manifested by elongate surface depressions.

A high number of SAR scenes are required to draw reliable and complete conclusions regarding the glacier surface structures. We used a total of 30 SAR images covering a period of 12 years and using data from five different SAR sensors. These allow the identification of 20 permanent and 4 semi-permanent ice cauldrons across the

Table 3 Association of ice cauldrons to different structures of the Katla caldera (see Fig. 5 for location)

Cauldron no.	SC	SSC	FI	PCR	YV	Location	
						X	Y
1	X					289,733.31227	7,065,494.60052
2	X					290,187.22690	7,066,769.88448
3	X					293,191.70945	7,068,780.07784
4	X					294,920.90804	7,068,391.00816
5			X			297,233.71115	7,066,942.80434
6			X			297,622.78083	7,066,315.96985
7			X			300,194.96373	7,066,013.36010
8			X			299,762.66408	7,064,975.84095
9	X	X	X	X	1955	299,546.51426	7,064,132.85663
10	X	X	X	X	1955	300,130.11878	7,064,089.62667
11		X	X		1823/1918	298,919.67977	7,063,138.56745
12		X	X		1823/1918	299,243.90450	7,062,468.50299
13		X	X		1823/1918	292,175.80528	7,063,851.86186
14	X	X			1999	293,278.16938	7,063,203.41239
15				X	1755	294,380.53348	7,061,755.20858
16				X	1755	296,693.33659	7,058,059.04660
17	X			X		297,212.09616	7,059,269.48561
18	X			X		297,557.93588	7,058,642.65112
19	X					292,975.55963	7,060,436.69465
20	X					296,479.52713	7,060,051.22864
21				X		297,086.73377	7,063,854.25966
22				X		297,342.39972	7,062,831.59585
23	X					291,120.12964	7,062,924.27476
24		Not clearly classifiable/young volcanism?				290,787.76390	7,062,208.41010

Projection of their centre coordinates/location is UTM, WGS 84, Zone 28 North.
SC: structural caldera, *SSC*: southern section or piecemeal caldera, *FI*: fissure, *PCR*: pre-caldera ridge, *YV*: young volcanism.

surface of Mýrdalsjökull, indicating geothermal active areas of the underlying Katla caldera and their associated melt water tunnels. Several cauldrons coincide with known historic eruption sites but are mostly associated with four structural elements in the caldera: the ring fault or structural caldera (SC), an E–W striking PCR, the NE–SW trending Eldgjá FI, and the SSC.

All cauldrons are connected to tunnel systems, which drain melt water from them, except cauldrons 14, 17 and 18 in the catchment of Sólheimajökull where no tunnels could be identified. The continuous heat flow at the geothermal spots supplies a constant source of melt water to each tunnel system, resulting in equilibrium of tunnel closure by ice deformation and enlargement by frictional heat of melt water flow. More than 100 km of melt water tunnels could be identified under the Mýrdalsjökull in the SAR time series.

It was found that the tunnel systems can transcend estimated water divides. This indicates that the theoretical model for deriving the drainage basins is not accurate enough to describe the sub-glacial drainage system correctly. Knowledge of the sub-glacial drainage system allows areas surrounding the glacier, potentially endangered by a jökulhaup during a sub-glacial eruption, to be predicted more precisely.

Future work will focus on the application of new SAR sensors, such as TerraSAR-X, on the Mýrdalsjökull test site. The considerably higher ground resolution of this instrument may allow a more accurate determination of cauldron size, therefore allowing their use as natural calorimeters. Furthermore, we consider the possibility of ordering SEASAT data, which would extend our analysis by more than 15 years back to 1978. The network of more than 100 km of known drainage tunnels draining each cauldron could be targeted for dye-tracing experiments, enabling new insights on sub-glacial flow processes over volcanic regions. Considering the recent findings of Wingham et al. (2006), we support a widespread application of SAR time series for analysis of glacier surface morphology in other glaciated regions worldwide.

References

Benn DJ, Evans DJA (1998) Glaciers and glaciation. Arnold, London

Björnsson H (1975) Subglacial water reservoirs, Jökulhlaups and volcanic eruptions. Jökull 25:1–15

Björnsson H (1988) Hydrology of ice caps in volcanic regions. Societas Scientiarium Islandica 45:1–139

Björnsson H (2002) Subglacial lakes and Jökulhlaups in Iceland. Global Planet Change 35:255–271

Björnsson H, Pálsson F, Gudmundsson MT (2000) Surface and bedrock topography of the Mýrdalsjökull ice cap, Iceland: the Katla caldera, eruption sites and routes of Jökulhlaups. Jökull 49:29–46

Björnsson H, Rott H, Gudmundsson S, Fischer A, Siegel A, Gudmundsson MT (2001) Glacier–volcano interaction deduced by SAR interferometry. J Glaciol 47:58–70

Björnsson H, Pálsson F, Sigurdsson O, Flowers GE (2003) Surges of glaciers in Iceland. Ann Glaciol 36:82–90

Dehn J, Dean K, Engle K (2000) Thermal monitoring of North Pacific volcanoes from space. Geology 28:755–758

Einarsson P, Brandsdóttir B (2000) Earthquakes in the Mýrdalsjökull area, Iceland, 1978–1985: seasonal correlation and connection with volcanoes. Jökull 49:59–74

Gao J, Yansui L (2001) Application of remote sensing, GIS and GPS in glaciology: a review. Prog Phys Geogr 25:520–540

Gudmundsson GB, Stefansson R (2007) Seismicity beneathMýrdalsjökull and Eyjafjallajökull ice caps, Iceland. Ann Glaciol 45 (in press)

Gudmundsson MT, Högnadóttir T, Kristinsson AB, Gudbjörnsson S (2007) Geothermal activity in the subglacial Katla caldera, Iceland, 1999–2005, studied with radar altimetry. Ann Glaciol 45:66–72

Harris AJL, Flynn LP, Keszthelyi L, Mouginis-Mark PJ, Rowland SK, Resing JA (1998) Calculation of lava effusion rates from Landsat TM data. Bull Volcanol 60:52–71

Henderson FM, Lewis AJ (eds) (1998) Principles and application of imaging radar: manual of remote sensing, 3rd edn., vol. 2. Wiley, New York

Jakobsson SP (1979) Petrology of recent basalts of the eastern volcanic zone, Iceland. Acta Nat Isl 26:1–103

Jaenicke J, Mayer Ch, Scharrer K, Münzer U, Gudmundsson Á (2006) The use of remote sensing data for mass balance studies at Mýrdalsjökull ice cap, Iceland. J Glaciol 52:565–573

Kjaer KH, Krüger J, van der Meer JJM (2003) What causes till thickness to change over distance? Answers from Mýrdalsjökull, Iceland. Quat Sci Rev 22:1687–1700

König M, Winther JG, Isaksson E (2001) Measuring snow and glacier ice properties from satellite. Rev Geophys 39:1–27

Kristmannsdóttir H, Snorrason A., Gislason SR, Haraldsson H, Gunnarsson A, Hauksdottir S, Elefsen SO (2002) Geochemical warning for subglacial eruptions—background and history. In: Snorrason Á, Finnsdóttir HP, Moss ME (eds) The extremes of the extremes: extraordinary floods. Proc. Reykjavík, Iceland Symp. July 2000. IAHS Publ 271:231–236

Lacasse C, Sigurdsson H, Carey SN, Jóhannesson H, Thomas LE, Rogers NW (2006) Bimodal volcanism at the Katla subglacial caldera, Iceland: insight into the geochemistry and petrogenesis of rhyolitic magmas. Bull Volcanol 69:373–399. DOI 10.1007/s00445-006-0082-5

Larsen G (2000) Holocene eruptions within the Katla volcanic system, south Iceland: characteristics and environmental impact. Jökull 49:1–28

Lipman PW (1997) Subsidence of ash-flow calderas: relation to caldera size and magma-chamber geometry. Bull Volcanol 59:198–218

Lombardo V, Buongiorno MF, Pieri D, Merucci L (2004) Differences in Landsat TM derived lava flow thermal structures during summit and flank eruption at Mount Etna. J Volcanol Geotherm Res 134:15–34

Malin MC, Evans DL, Elachi C (1978) Imaging radar observations of Askja Caldera, Iceland. Geophys Res Lett 5:931–934

McDonough M, Martin-Kaye PHA (1984) Radargeologic interpretation of Seasat imagery of Iceland. Int J Remote Sens 5:433–450

Molnia BF, Jones JE (1989) View through ice: are unusual air-borne radar backscatter features from the surface of the Malaspina Glacier, Alaska, expressions of subglacial morphology? EOS Trans AGU 70:701–710

Molnia BF, Jones JE (1990) Radar remote sensing of glacial features, Malaspina Glacier, Alaska. Am Assoc Pet Geol Bull 74:723

Näslund JO, Hassinen S (1996) Supraglacial sediment accumulations and large englacial water conduits at high elevations in Mýrdalsjökull, Iceland. J Glaciol 42:190–192

Nye JF (1976) Water flow in glaciers: Jökulhlaups, tunnels and veins. J Glaciol 76:181–207

Oppenheimer C (1991) Lava flow cooling estimated from Landsat Thematic Mapper infrared data: the Lonquimay eruption (Chile, 1989). J Geophys Res 96:21865–21878

Roberts MJ (2005) Jökulhlaups: a reassessment of floodwater flow through glaciers. Rev Geophys 43:RG1002. DOI 10.1029/2003RG000147

Röthlisberger H (1972) Water pressure in intra- and subglacial channels. J Glaciol 62:177–203

Scharrer K, Mayer Ch, Nagler T, Münzer U, Gudmundsson Á (2007) Effects of ash-layers of the 2004 Grímsvötn eruption on SAR backscatter in the accumulation area of Vatnajökull. Ann Glaciol 45:189–196

Sigurdsson O, Zóphoníasson S, Ísleifsson E (2000) The Jökulhlaup from Sólheimajökull, July 18th 1999. Jökull 49:60–75

Soosalu H, Jónsdóttir K, Einarsson P (2006) Seismicity crisis at the Katla volcano, Iceland—signs of a cryptodome? J Volcanol Geotherm Res 153:177–186

Sturkell E, Sigmundsson F, Einarsson P (2003) Recent unrest and magma movements at Eyjafjallajökull and Katla volcanoes, Iceland. J Geophys Res 108:2369. DOI 10.1029/2001JB000917

Sturm M, Benson CS (1985) A history of Jökulhlaups from Strandline Lake, Alaska, U.S.A. J Glaciol 31:272–280

Tómasson H (1996) The Jökulhlaup from Katla in 1918. Ann Glaciol 22:249–254

Ulaby FT, Moore RK, Fung AK (1986) Microwave remote sensing active and passive, vol. III. Addison-Wesley, Reading

University of Iceland (2006) Katla monitoring. http://www.earthice.hi.is/page/iesmysurv. Cited on 03 Dec 2006

Wingham DJ, Siegert MJ, Shepherd A, Muir AS (2006) Rapid discharge connects Antarctic subglacial lakes. Nature 440:1033–1036. DOI 10.1038/nature04660

Paper 5

Scharrer K, Malservisi R, Mayer Ch, Spieler O, Münzer U (in review) Combination of SAR remote sensing and GIS for monitoring subglacial volcanic activity - Recent results from Vatnajökull ice cap (Iceland). submitted to Natural Hazards and Earth System Sciences.

Combination of SAR remote sensing and GIS for monitoring subglacial volcanic activity - Recent results from Vatnajökull ice cap (Iceland)

K. Scharrer[1] ,R. Malservisi[2] , Ch. Mayer[3], O. Spieler[4], U. Münzer[1]

[1] {Ludwig-Maximilians-University, Department of Earth and Environmental Sciences, Section Geology, Luisenstr. 37, 80333 Munich, Germany,}

[2] {Ludwig-Maximilians-University, Department of Earth and Environmental Sciences, Section Geophysics, Theresienstrasse 41, 80333 Munich, Germany}

[3] {Bavarian Academy of Sciences and Humanities, Commission for Glaciology, Alfons-Goppel Str. 11, 80539 Munich, Germany}

[4] {Ludwig-Maximilians-University, Department of Earth and Environmental Sciences, Section Mineralogy, Petrology and Geochemistry, Theresienstrasse 41, 80333 Munich, Germany}

Correspondence to: K. Scharrer (k.scharrer@iaag.geo.uni-muenchen.de)

Abstract

This paper presents latest results from the combined use of SAR (Synthetic Aperture Radar) remote sensing and GIS providing detailed insights into recent volcanic activity under Vatnajökull ice cap (Iceland). Glaciers atop active volcanoes pose a constant potential danger to adjacent inhabited regions and infrastructure. Besides the usual volcanic hazards (lava flows, pyroclastic clouds, tephra falls, etc.), the volcano-ice interaction leads to enormous meltwater torrents [icelandic: jökulhlaup], devastating large areas in the surroundings of the affected glacier. The presented monitoring strategy addresses the three crucial questions: When will an eruption occur, where is the eruption site and which area is endangered by the accompanying jökulhlaup. Therefore, sufficient early-warning and hazard zonation for future subglacial volcanic eruptions becomes possible, as demonstrated for the Bardárbunga volcano under the northern parts of Vatnajökull. Seismic activity revealed unrest at the northern flanks of Bardárbunga caldera at the end of September 2006. The exact location of the corresponding active vent and therefore a potentially eruptive area could be detected by continuous ENVISAT-ASAR monitoring. With this knowledge a precise prediction of peri-glacial regions prone to a devastating outburst flood accompanying a possible future eruption is possible.

1 Ice-Volcano interactions in Iceland

As the recent formation of the IAVCEI (International Association of Volcanology and Chemistry of the Earth's Interior) working group of Volcano-Ice interactions demonstrates, the interactions and hazardous effects of subglacial volcanic eruptions are a growing and highly up to date study field. Glaciers atop active volcanoes pose a constant potential danger to adjacent inhabited regions and infrastructure. Besides the usual volcanic hazards (lava flows, pyroclastic clouds, tephra falls, etc.), the volcano-ice interaction leads to enormous meltwater torrents [icelandic: jökulhlaup], devastating large areas in the surroundings of the affected glacier. The subglacial eruption of Gjálp (Sept. 30 - Oct. 13, 1996) beneath Vatnajökull and the subsequent jökulhlaup (Nov. 5 – 7, 1996) are a good example of the hazardous nature of such an event. During this 48 hour cataclysm, a volume of 3.2 km³ of meltwater was discharged at peak rates of about 4×10^4 m³ s^{-1}, destroying the local infrastructure (roads, bridges, dams, power and telephone lines, etc.) in the adjacent Skeidarársandur [*Björnsson,* 2002].

Only a multidisciplinary approach seems capable of addressing the manifold questions arising with this phenomenon, where we present latest results from the combined utilisation of SAR (Synthetic Aperture Radar) remote sensing and GIS providing detailed insights into recent volcanic activity under Vatnajökull ice cap.

2 Subglacial volcanoes Grímsvötn and Bardárbunga

In Iceland, several active central volcanoes, crater chains and fissures are covered by glacier ice. Several of Iceland's most active and dangerous volcanic centres (Figure 1) are covered by the largest European glacier, Vatnajökull (approximately 8100 km^2) (Björnsson & Einarsson, 1990; Adalgeirsdóttir, 2003). The Neovolcanic zone, an active section of the Mid-Atlantic ridge responsible for the high seismic and volcanic activity, propagates under the western parts of Vatnajökull ice cap. Furthermore, this area is the centre of the Iceland mantle plume (Wolfe et al., 1997; Shen et al., 2002).

The Grímsvötn volcanic system shows the highest eruption frequency of all subglacial volcanoes beneath Vatnajökull with about 70 eruptions in historical time (Thordarson & Larsen, 2007). The about 62 km² large caldera of the central volcano is situated in the central part of western Vatnajökull (Fig. 1). The adjacent fissure swarm extends about 90 km in south-westerly direction. The southern rim of the caldera protrudes through the ice cover at an elevation of 1722 m a.s.l., whereas the rest of the crater rim is covered by the ice cap. The

caldera (approx. 1450 m a.s.l.) is filled by the geothermally heated subglacial lake Grímsvötn, which is overlain by glacier ice up to 250 m thick (Björnsson & Einarsson, 1990). Due to the constant heat flux in the caldera, jökulhlaups occur even without an eruption. Meltwater accumulates in the caldera, until the subglacial lake reaches a critical level. Then, water pressure breaks the glacial seal and a floodwave travels over a distance of 50 km subglacially under the Skeidarárjökull outlet and finally reaches the huge plain Skeidarársandur in the South (Björnsson, 1992). Meltwater production rates during eruptions at Grímsvötn can increase by several orders of magnitude, leading to devastating outburst floods as the previously mentioned 1996 jökulhlaup.

The second most active volcano beneath Vatnajökull is the Bárdarbunga-Veidivötn volcanic system (Thordarson & Larsen, 2007). At least 23 eruptions are attributed to this system in historical time. The volcanic system consists of the Bárdarbunga central volcano, where eruptive activity is highest, and an associated 190 km long south-westward trending fissure swarm. Bárdarbunga is a large volcanic edifice girding an about 80 km^2 large caldera. The topographic caldera rim reaches an elevation of 1500-1850 m, whereas its bottom is at 1100 m a.s.l. The central volcano and about 60 km of the fissure swarm are covered by up to 850 m thick glacier ice (Björnsson & Einarsson, 1990). Several eruptions from the ice covered central volcano were accompanied by jökulhlaups, draining via the river Jökulsá á Fjöllum to the North.

Both, eruptions of Bárdarbunga and Grímsvötn show the same character. A single vent or part of a fissure erupts highly fragmented basaltic tephra in hydromagmatic eruptions, producing extensive tephra layers (Thordarson & Larsen, 2007). Larsen et al. (1998) used such tephra layers, preserved in ice cores and soil records, to reconstruct the eruption frequency of the volcanic systems under Vatnajökull. They found, that the volcanic activity has a 130-140 year periodicity, where 40-80 year long intervals of high eruption frequency alternate with low frequency intervals of about equal length. The mainspring of the cycle seems to be the Grímsvötn volcanic system. Other systems join in when activity is high at Grímsvötn, especially the Bárdarbunga-Veidivötn system. Considering the recent eruptive activity at Grímsvötn with three eruptions in the past decade (1996, 1998 and 2004) and the predictions of the tephrochronological record it seems likely, that the next 60-80 years are characterised by an interval of high activity (Larsen et al., 1998; Larsen et al., 2005).

3   Monitoring strategy

Considering the impacts of subglacial volcanic eruptions three major questions have to be addressed for sufficient early-warning and hazard zonation: When will an eruption occur, where is the eruption site and which area is endangered by the accompanying jökulhlaup.

As earthquake activity beneath a volcano almost always increases before an eruption, the "when" question can be addressed by seismic monitoring. In Iceland a nationwide digital network of 44 seismic stations is operated, to monitor seismic and volcanic activity (Bödvarsson et al., 1999). The importance of seismicity as tool to indicate an imminent eruption in Iceland, was clearly shown during the 2004 Grímsvötn eruption under the Vatnajökull ice cap. The considerable increase of earthquake activity beneath Grímsvötn lead to a detailed warning about 24 hours prior to the beginning of the eruption and the network proved its applicability for eruption forecasting (Vogfjörd et al., 2005).

Potential subglacial eruption sites can only be identified indirectly due to the ice cover. Ascent of magma in a volcanic edifice leads to an increased heat flux at the active vent or fissure well before its arrival to the surface. Due to the plasticity of ice, a volume loss at the glacier bottom, triggered by ice melting from geothermal activity, leads to a depression in the glacier surface. A circular depression develops over a more or less punctiform geothermal active spot and can therefore be detected with remote sensing techniques. Due to its special characteristics, SAR (Synthetic Aperture Radar) remote sensing is an appropriate method for monitoring glacier deformation and thus potentially eruptive vents. One of the main advantages of SAR monitoring, especially in the light of the Icelandic weather conditions, is its independence from cloud cover and day light allowing a continuous monitoring. Further, the ability to penetrate the upper layers of snow and firn enables the detection of buried topographic features on the glacier surface which are related to subglacial volcanic activity. Since November 2002 the ASAR (Advanced Synthetic Aperture Radar) sensor carried by the ENVISAT satellite collects data over Vatnajökull within the ESA project "Hazard Assessment and Prediction – Long-term Observation of Icelandic Volcanoes and Glaciers Using ENVISAT-ASAR and Other Radar Data (ID 142)". The ASAR instrument is a side looking C-band SAR antenna operating at a wavelength of 5.6 cm. Due to its beam steering capability the ASAR instrument can acquire images in seven different swathes (IS1 – IS7), covering an incidence angle range from 15 to 45 degrees. Images of the swathes IS 2 (incidence angle 21.5°) and IS 5 (incidence angle 37.5°) are continuously acquired over the ice cap for monitoring the subglacial volcanic activities with a temporal repetition of up to

nine days including ascending (asc) and descending (desc) orbits. ASAR image analysis during the last Grímsvötn eruption showed that 8 days ahead of the eruptive phase on 24/10/2004 the exact position of the eruption site inside the caldera could be located through the glacial ice cover due to the increased geothermal activity preceding the eruption. 35 hours prior to the outbreak, on 31/10/2004, the extent could be detected in detail (Fig. 2a; 2b). Thus, continuous ASAR monitoring enables the identification of active vents or fissures under an ice cap, by mapping the related circular depressions in the glacier surface.

In case of the thick Icelandic glaciers, meltwater produced by a subglacial eruption propagates subglacially from the eruption site to the glacier terminus (Björnsson, 1988). The prediction of jökulhlaup paths is based on drainage basins of the glaciated areas derived from a potential map describing the sum of the gravitational and the pressure potential at the glacier bed (Björnsson, 2002). By comparison of the location of a potential eruption site with the drainage basins, the areas in the surroundings of the glacier endangered by a jökulhaup can be identified. Therefore exact knowledge about the location of a subglacial eruption site is again crucial for the prediction of the potentially affected river catchment.

Both, the ground data (epicentres and glacial drainage basins) and the remotely sensed ENVISAT-ASAR images have a spatial component and can therefore be organized in a GIS database. An automated processing chain has been developed for continuous and fast integration of newly acquired ENVISAT-ASAR scenes into the database (Gutjahr et al., 2006; Gutjahr & Scharrer, 2007). The unified reference system (UTM, WGS 84, Zone 27) allows a combination and correlation of the layers to enable near real time hazard monitoring and risk prediction at Vatnajökull ice cap. Risk assessment and prediction models can be made available whenever needed (Münzer et al., 2005).

4   Recent activities at Bárdabunga and Grímsvötn

Recent earthquake data of the central volcanoes under the western part of Vatnajökull gives a good indication of the activity level of the various volcanic systems (Fig. 1b). At Pálsfjall (1), Hamarinn (3) and Kverkfjöll (5) no significant changes in activity are developed since 2001, whereas the 2004 eruption at Grímsvötn (2) is clearly reflected in the data. Looking at the seismic activity at Bárdarbunga (4) central volcano, with its prominent increase since December 2004, it seems likely that the last Grímsvötn eruption triggered the re-awakening of Bárdarbunga. So far the increase culminated in an extensive earthquake swarm in September 2006. It started on 23/09/2006 and lasted until 30/09/2006, with the highest activity on

26/09/2006. The strongest event reached a local magnitude of 3.8 on 24/09/2006, whereas the vast majority of events had local magnitudes between 1 and 2.5. The epicentres scattered around two focal areas, one directly at the northern slopes of Bárdarbunga caldera, a second one about 10 km to the North close to the glacier margin (Fig. 3a). The uncertainty if the scattering is related to 2 spatially different areas of activity, highlights the difficulty of an exact location of a potential eruption site under a glacier by the analysis of seismic data alone. Looking at the distribution of earthquake epicentres preceding the 2004 Grímsvötn eruption, the same problem appears (Fig. 2b). In the eruption warnings released by the Icelandic Meteorological Office only statements like "an eruption site at or near Grímsvötn" were possible (Vogfjörd et al., 2005).

Recent ASAR monitoring showed, that a new surface depression formed after the 2004 eruption in their north-western vicinity (X: 673670.425 / Y: 7147193.930; UTM, WGS 84, Zone 27N), first detectable in ENVISAT-ASAR scenes acquired in August 2005 (Fig. 2c, 2d). Considering the locations of the eruption sites in 1998 and 2004 a westward migration of the activity along the ring fault of the caldera is evident (Fig. 2d). When seismic activity at Grimsvötn increases again, this location should be in the focus because from our investigations the eruption site can be expected there. A future eruption at this location would cause a jökulhlaup via the Skeidarárjökull to the south.

Due to the abrupt increase of seismic activity at Bardárbunga end of September 2006, ENVISAT-ASAR's beam steering capability was fully utilised (antenna swathes IS1-IS7) until December 2006, leading to a sequence with at least two ASAR scenes per week. Therefore activity at Bardárbunga could be monitored with very high temporal resolution. Simultaneous ASAR acquisition at the onset of the swarm activity on 23/09/06 revealed the formation of two new ice depressions on the glacier surface (western depression X: 674496.845 / Y: 7178725.540; eastern depression X: 674862.662 / Y: 7178499.952; UTM, WGS 84, Zone 27N) (Fig. 3b, 3c). Both sink holes have approximately the same diameter of about 200 m. They are associated to the earthquake cluster at the northern slopes of the Bárdarbunga caldera, indicating the area of increased geothermal activity. Matching of their locations with drainage basins predicts a jökulhlaup path to the north via the river system Jökulsá á Fjöllum. Accompanied by the decreased seismic activity in November and December 2006 no further variation of these surface features could be detected. The two new surface depressions were probably refilled by accumulating snow and are not visible anymore in current ASAR images. Without a continuous ASAR monitoring, the two depressions would not have been recognized.

5   Conclusions

By applying a combined observation of seismicity and SAR monitoring sufficient early-warning of a subglacial volcanic eruption at Vatnajökull is possible. Continuous ASAR monitoring enables the identification of active vents or fissures under the ice cap and therefore an improved hazard zonation of areas endangered by a jökulhlaup accompanying a subglacial eruption. Seismic monitoring gives a good indication of the point in time an eruption is imminent. Considering the predicted period of high volcanic activity, the increased seismic activity since 2004 at Bardárbunga and the detected increased heat flux at the northern slopes of the caldera, it seems likely that the next subglacial volcanic eruption under Vatnajökull will occur at the northern flank of Bardárbunga at the location of the newly detected surface depressions. As glaciovolcanism is a worldwide phenomenon responsible for several disasters in the past, we suggest a widespread application of SAR monitoring for early detection of potentially eruptive areas improving existing early warning capabilities and hazard zonation. Knowing the potentially dangerous areas before an eruption starts is critical for planning emergency procedures that can help ensure public safety if the unrest leads to eruptive volcanic activity.

References

Adalgeirsdóttir, G.: Flow dynamics of Vatnajökull ice cap, Iceland, Ph. D. thesis, ETH Zürich, 2003.

Björnsson, H.: Hydrology of ice caps in volcanic regions. Soc. Sci. Isl. 45, Reykjavík, 1988.

Björnsson, H.: Subglacial lakes and jökulhlaups in Iceland, Global and Planetary Change, 35, 255-271, 2002.

Björnsson, H., Einarsson, P.: Volcanoes beneath Vatnajökull, Iceland: Evidence from radio echo-sounding, earthquakes and jökulhlaups, Jökull, 40, 147-169, 1990.

Björnsson, H.: Jökulhlaups in Iceland: prediction, characteristics and simulation, Annals of Glaciology, 16, 95–106, 1992.

Bödvarsson, R., Rögnvaldsson, S. T., Slunga, R., Kjartansson, E.: The SIL data acquisition system at present and beyond year 2000, Phys. Earth Planet. Inter., 113, 89-101, 1999.

Wolfe, C. J., Bjarnason, I. Th., VanDecar, J. C., Solomon, S. C.: Seismic structure of the Iceland mantle plume, Nature 385, 245-247, 1997.

Gutjahr, K. H., Scharrer, K.: Benefits of robust parameter estimation techniques in an automated geocoding processing chain, ISPRS Workshop 2007, May 29 – June 1 2007, Hannover, Germany, in press.

Gutjahr, K. H., Scharrer, K., Münzer, U.: Utilizing the CR-Network in Iceland for an automated interferometric processing chain – case study with ERS-Tandem data, ESA SP-610, 2006.

Larsen, G., Gudmundsson, M. T., Björnsson, H.: Eight centuries of periodic volcanism at the center of the Icelandic hotspot revealed by glacier tephrostratigraphy, Geology, 26, 943-946, 1998.

Larsen, G., Gudmundsson, M. T., Björnsson, H.: Increased Eruption Frequency in Volcanoes below the Vatnajökull Ice Cap, Iceland, predicted by Tephrachronology, Geophysical Research Abstracts, 7, 10066, 2005.

Münzer, U., Scharrer, K., Weber-Diefenbach, K., Gudmundsson, Á.: Integration of ENVISAT-ASAR Data in a Hazard-Monitoring-GIS, ENVISAT-Project [ID 142], ESA SP-572, 2005.

Shen, Y., Solomon, S. C., Bjarnason, I. TH., Nolet, G., Morgan, W. J., Allen, R. M., Vogfjörd, K., Jakobsdóttir, S., Stefánsson, R., Julian, B. R., Foulger, G. R.: Seismic evidence for a tiled mantle plume and north-south mantle flow beneath Iceland, Earth and Planetary Science Letters, 197, 261-272, 2002.

Thordarson, T., Larsen, G.: (2007), Volcanism in Iceland in historical time: Volcano types, eruption styles and eruptive history, Journal of Geodynamics, 43, 118-152, 2007.

Vogfjörd, K., Jakobsdóttir, S., Guðmundsson, G. B., Roberts, M. J., Ágústsson, K., Arason, T., Geirsson, H., Karlsdóttir, S., Hjaltadóttir, S., Ólafsdóttir, U., Thorbjarnardóttir, B.,

Skaftadóttir, T., Sturkell, E., Jónasdóttir, E. B., Hafsteinsson, G., Sveinbjörnsson, H., Stefánsson, R., Jónsson, T. V.: Forecasting and Monitoring a Subglacial Eruption in Iceland, Eos Trans. AGU, *86*, 245, 2005.
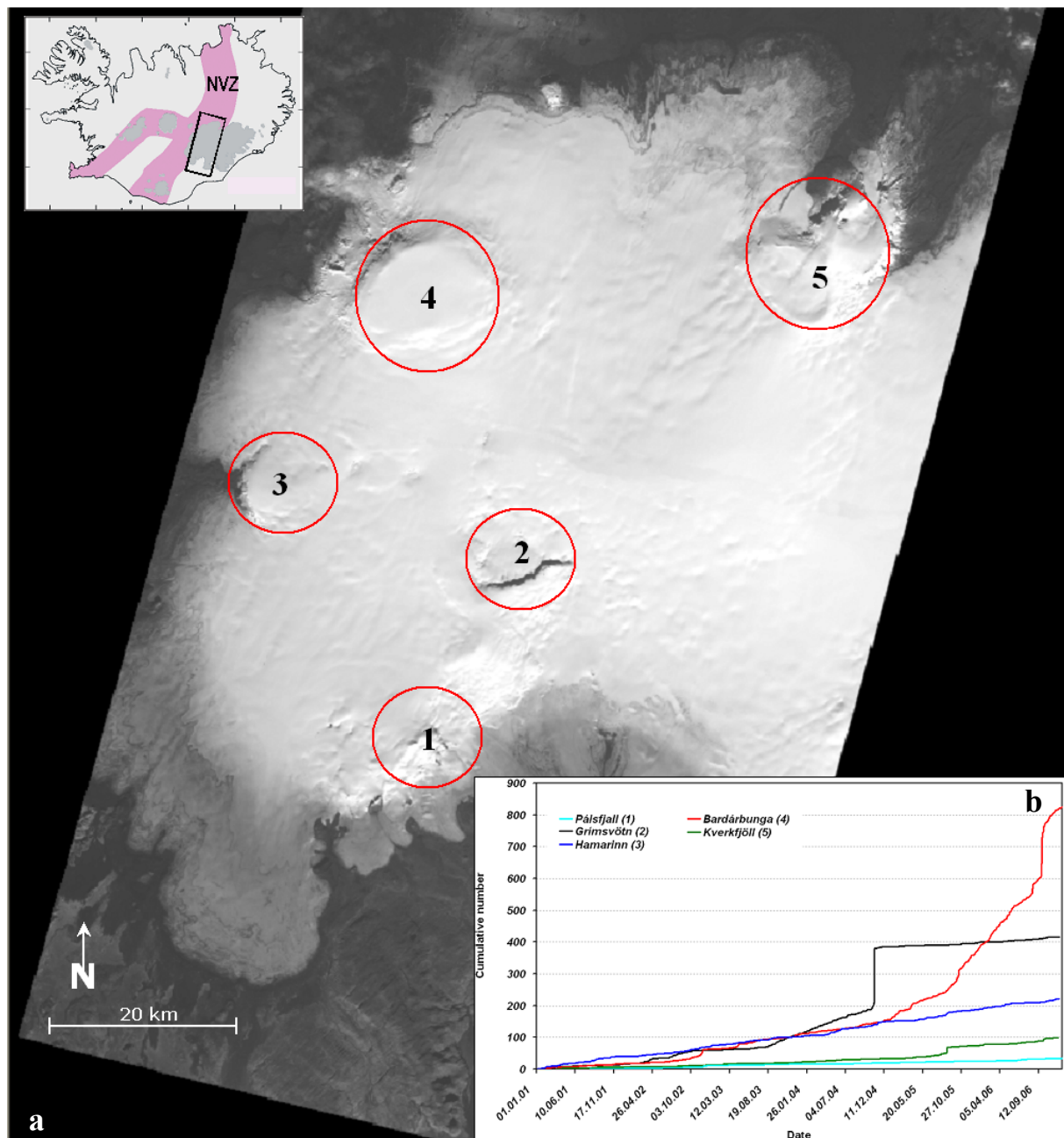
Figure 1. (a) ASTER-Mosaic (© NASA 2004) of the western part of Vatnajökull ice cap. Numbered red circles indicate the locations of subglacial volcanic systems. The most active volcanoes are the Grímsvötn (2) and the Bardárbunga-Veidivötn (4) systems. The insert map illustrates the geographic extent of Figure 1a and the Neovolcanic Zone (NVZ) crossing Iceland. (b) shows the cumulative number of earthquakes observed at the different volcanic centres (1-5) beneath western Vatnajökull from 01/01/2001 until 31/12/2006. At Pálsfjall (1), Hamarinn (3) and Kverkfjöll (5) no significant changes in activity are developed since 2001, whereas the 2004 eruption at Grímsvötn (2) is clearly reflected in the data. A prominent increase in seismic activity is pronounced at Bárdarbunga (4) since December 2004.
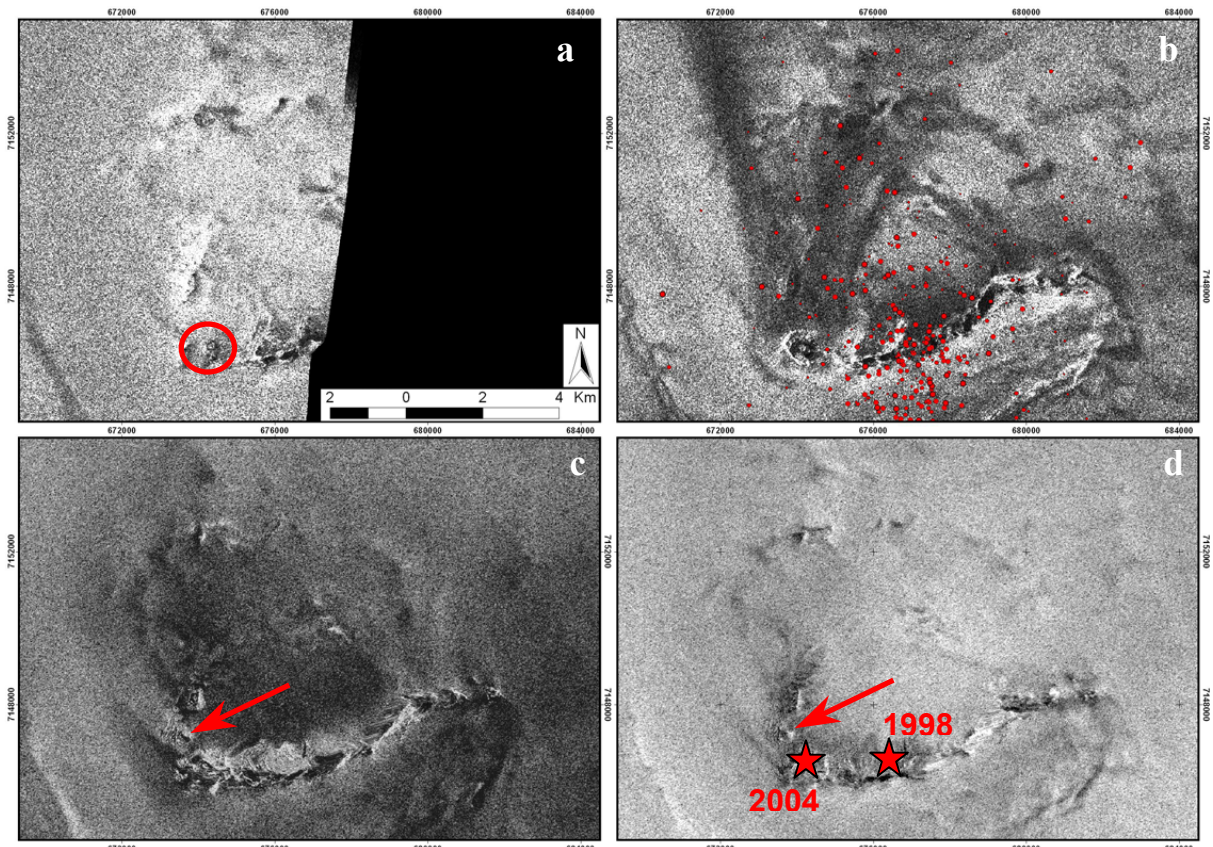
Figure 2. Important acquisitions of the ENVISAT-ASAR time series showing the Grímsvötn caldera. On 31/10/2004 (a) the eruption site inside the caldera (red circle) could be located in detail through the glacial ice cover about 35h prior to the eruptive phase due to the increased geothermal activity. The scene acquired on 13/11/2004 (b) seven days after the eruption shows the eruption site with the northerly deposited tephra fans. Locations of epicentres detected in 2004 (red dots, © Icelandic Meteorological Office) indicate the difficulty of an exact location of a potential eruption site under a glacier by the analysis of seismic data only. In the ASAR image acquired on 18/08/2005 (c) the new depression (red arrow) appears for the first time. It is although detectable on 02/12/2006 (d). Considering the locations of the eruption sites in 1998 and 2004 a westward migration of the activity along the ring fault of the caldera is evident.   © ESA 2004-2006
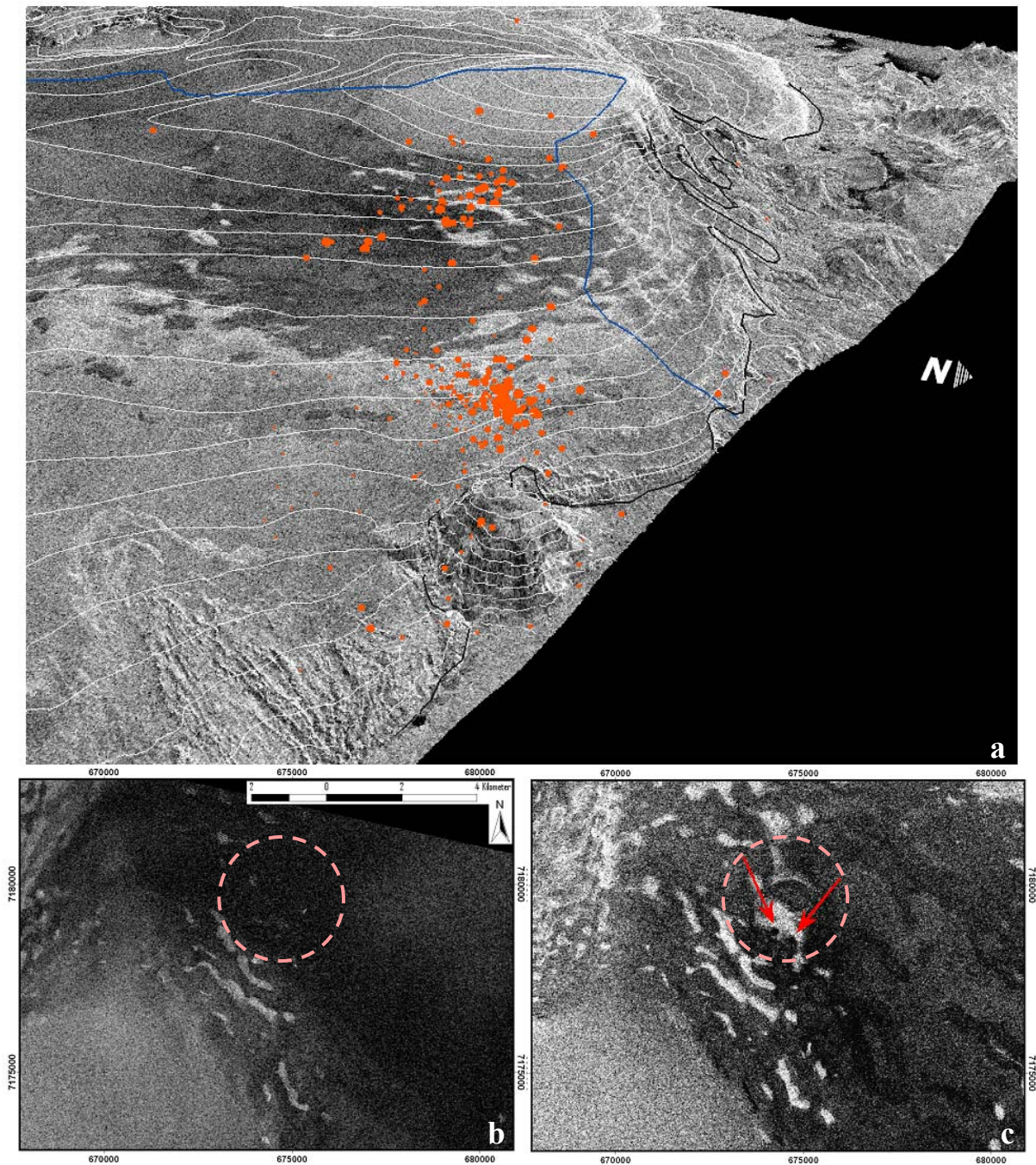
Figure 3. Recent activity at the northern slopes of Bardárbunga caldera. 3D-view (a) of the ASAR image 23/09/2006 including epicentres at Bardárbunga in 2006 (red dots, © Icelandic Meteorological Office) and the water divide girding the glaciated area (blue line) draining to the north via the river Jökulsá á Fjöllum. White lines indicate 50 m contour lines. Epicentres are distributed around to focal areas. Figure b (ENVISAT-ASAR 05/09/2006) shows the northern slopes of Bárdarbunga before the extensive earthquake swarm, starting on 23/09/2006 and lasting until 30/09/2006. The brighter features indicate crevassed areas. Simultaneous ASAR acquisition at the onset of the swarm activity on 23/09/06 (c) revealed the formation of two new ice depressions on the glacier surface. A future eruption at this location would trigger a jökulhlaup to the north via the river system Jökulsá á Fjöllum.

Acknowledgements

I am glad now for the opportunity to thank those people who supported me throughout this study by giving me new ideas, help and encouragement.

First of all I want to thank Dr. Ulrich Münzer from the Department of Earth and Environmental Sciences, Section Geology of the Ludwig-Maximilians-University for sparking my interest in doing research on Iceland. As the Principal Investigator (PI) of the ESA project ID 142, he gave me the great possibility to work within his group with the freedom to do those projects I wanted to do most. I have greatly benefited from his knowledge based on many years of research in Iceland and his talent and enthusiasm in finding solutions for occuring problems.

Further I would like to thank Ágúst Gudmundsson, Co-Investigator in the ESA project. He has been acting as our gateway to institutions, special data, knowledge and originalities of Iceland.

I have enjoyed the company and friendship of several diploma students of the Münzer group, Miles Taprogge, Julia Jaenicke, Florian Jäger, Sandro Martinis and the student apprentice Guðjón Eyjólfur Ólafsson. Many thanks for their various contributions and discussions. The numerous recreative football matches with Sandro will always be remembered.

I owe very much to Prof. Dr. Helmut Rott, Dr. Thomas Nagler, and especially Florian Müller from the Institute of Meteorology and Geophysics of the University of Innsbruck (Austria) for hosting me several times, sharing their outstanding knowledge about SAR and glaciers. The visits and discussions with them have always been highly productive and fruitful for me.

I am also very grateful to Dr. Johann Raggam and Dr. Karl-Heinz Gutjahr from Joanneum Research in Graz (Austria) for their help and advice with the RSG software package and a special training course on SAR processing. Karl-Heinz answered all my (sometimes silly) questions patiently during endless email conversations. I would not have been able to overcome some technical obstacles without that assistance.

I appreciate very much the eruption of the Grímsvötn volcano in autumn 2004, because this event brought me together with Dr. Christoph Mayer from the Commission of Glaciology of the Bavarian Academy of Sciences. He guided my way since then with lots of inspiration, practical help and endless time for discussions. This thesis wouldn't be what it is without his tremendous support.

I also owe special thanks to Dr. Oliver Spieler from the Mineralogy, Petrology and Geochemistry section at the Department of Earth and Environmental Sciences. He significantly increased my scientific knowledge on volcanic structures and processes and he always had an open ear not only for my scientific problems. Furthermore, his office is one of the best places for having a Coffee break with stimulating discussions on various topics.

Prof. Rocco Malservisi from the Geophysics section of the Department of Earth and Environmental Sciences deserves special thanks for his thoughtful comments and suggestions on several aspects of my work and for always being available for questions and discussions along my recent way in science.

I am grateful to Prof. Dr. Donald Dingwell (Department of Earth and Environmental Sciences, Section Mineralogy, Petrology and Geochemistry) that he spontaneously agreed to being the first referee of my thesis despite his huge workload. His opinion is of great importance to me.

Curriculum vitae

Personal:

Name:	Kilian Scharrer
Born:	10. September 1974 in Freilassing, Germany
Nationality:	German

Education:

since 01/2004   PhD student in Geology, Ludwig-Maximilians University, Title: Monitoring ice-volcano interactions in Iceland using SAR and other remote sensing techniques.

08/03   Diploma thesis: Surface morphology of the Mýrdalsjökull ice cap revealed by SAR remote sensing.
Diploma: Physical Geography, Remote Sensing, Geology, Botanic.

11/96-08/03   Geography diploma, University of Regensburg, final grade 1.1

08/95–07/96   basic military service

09/82–07/95   primary and secondary school qualification: "Abitur" (general qualification for university entrance), final grade 3.0

Professional Career:

since 01/2004   PhD student, Ludwig-Maximilians University, Munich.

05/00-03/02   Student assistant, Remote Sensing group, University of Regensburg.

09/01-11/01   Internship, Team SAR value adding, DLR (German Aerospace center) Oberpfaffenhofen.

09/97-10/97   Field work within the project "Natural rejuvenating of an alpine windfall" in Berchtesgaden national park.

Grants:

01/04   Doctoral scholarship of the Bavarian research foundation (DPA 37/04)